

ABSTRACT

Name: Thomas E. Liggett

Department: Biological Sciences

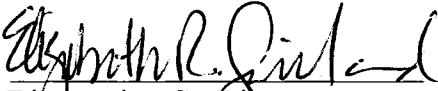
Title: *In vitro* Models for the Study of the Mechanisms of Damage in Age-related Macular Degeneration and Stargardt's Disease.

Major: Biological Sciences

Degree: Doctor of Philosophy

Approved by:

Date:


Dissertation Co-Director

11/20/07


Dissertation Co-Director

12/7/07

NORTHERN ILLINOIS UNIVERSITY

ABSTRACT

The retinal pigment epithelium (RPE) is interposed between the photoreceptor cells of the neural retina and the choriocapillaris, and lies on a bed of extracellular matrix called Bruch's membrane. Dysfunction in one of these components can cause a cascade of events that results in RPE and photoreceptor cell death, which causes permanent vision loss. The most debilitating vision loss occurs in the macular region due to its high concentration of photoreceptor and RPE cells and its role in central vision.

Mutations in the gene for the ATP-dependent binding cassette transport protein, ABCR, have been shown to result in a high accumulation of the autofluorescent pigment mixture, lipofuscin, within the RPE cells. The ABCR protein is located in the outer segments of the photoreceptor cells. Stargardt's macular dystrophy (STDG), retinitis pigmentosa (RP) and cone/rod dystrophy (CRD) are associated with mutations in this gene. Additionally, mutations are implicated in some forms of age-related macular degeneration (AMD).

Although AMD is a multi-factorial disease, the prolific accumulation of autofluorescent compounds in the RPE or in Bruch's membrane is a positive indicator for the disease. Clearly, understanding the mechanisms of the ABCR protein function and lipofuscin-mediated damage to RPE cells are the foundation of vision loss by retinal maculopathies.

The first part of the research presented in this dissertation describes the cloning, transfection and expression of the ABCR transporter protein that is often found defective in STGD patients and other retinal diseases. ABCR dysfunction leads to the prolific accumulation of lipofuscin in the RPE, which may in turn be related to the accumulation of age-related debris on Bruch's membrane. Therefore, a RPE cell line that mimics the *in vivo* state was isolated and characterized, including melanin pigmentation, ECM and differentiation. These cells were then used to determine the phototoxicity of lipofuscin and the lipofuscin precursor, A2PE. Photooxidative damage to RPE-challenged A2PE was performed and the lipophilic extracts analyzed. From these studies, the mechanisms that damage RPE cells are addressed, which facilitate the progression of AMD, STGD and other retinal dystrophies.

NORTHERN ILLINOIS UNIVERSITY

IN VITRO MODELS FOR THE STUDY OF THE MECHANISMS OF DAMAGE
IN AGE-RELATED MACULAR DEGENERATION AND
STARGARDT'S DISEASE

A DISSERTATION SUBMITTED TO THE GRADUATE SCHOOL
IN PARTIAL FULFILLMENT OF THE REQUIREMENTS
FOR THE DEGREE
DOCTOR OF PHILOSOPHY

DEPARTMENT OF BIOLOGICAL SCIENCES

BY

THOMAS E. LIGGETT

© Thomas E. Liggett

DEKALB, ILLINOIS

DECEMBER 2007

UMI Number: 3301638

INFORMATION TO USERS

The quality of this reproduction is dependent upon the quality of the copy submitted. Broken or indistinct print, colored or poor quality illustrations and photographs, print bleed-through, substandard margins, and improper alignment can adversely affect reproduction.

In the unlikely event that the author did not send a complete manuscript and there are missing pages, these will be noted. Also, if unauthorized copyright material had to be removed, a note will indicate the deletion.

UMI[®]

UMI Microform 3301638

Copyright 2008 by ProQuest LLC.

All rights reserved. This microform edition is protected against unauthorized copying under Title 17, United States Code.

ProQuest LLC
789 E. Eisenhower Parkway
PO Box 1346
Ann Arbor, MI 48106-1346

Certification:

In accordance with departmental and Graduate School policies, this dissertation is accepted in partial fulfillment of degree requirements.


Dissertation Co-Director

11/29/07
Date


Dissertation Co-Director

12/07/07
Date

ANY USE OF MATERIAL CONTAINED
HEREIN MUST BE DULY ACKNOWLEDGED.
THE AUTHOR'S PERMISSION MUST BE OBTAINED
IF ANY PORTION IS TO BE PUBLISHED OR
INCLUDED IN A PUBLICATION.

ACKNOWLEDGEMENTS

I owe an extraordinary amount of gratitude to my advisors, Dr. Elizabeth R. Gaillard and Dr. John Mitchell, for their constant support and advice over the years. They have helped me in many ways with some of the difficult situations of my graduate program. Additional recognition is owed to my committee members, Dr. Stuart Hill, Dr. Linda Yasui and Dr. Richard Hahin, for their time and effort. I would like to thank the faculty, staff and students of the Department of Biological Sciences and the Department of Chemistry and Biochemistry. I would specifically like to acknowledge Dr. Kenneth Gasser for his help in understanding the complexities of western blotting, Dr. Scott Grayburn for his advise on sequencing and cloning, Lori Bross for her assistance using the confocal microscope, and Dr. Tom Sims for supplying the RSGFP plasmid.

This research was funded in part by Fight for Sight, Prevent Blindness America, Midwest Eye Bank and Transplantation Center, Northern Illinois University Fellowship and Dissertation Completion Awards and by a grant from the National Eye Institute (NIH EY12344).

DEDICATION

In memory of T. Daniel Griffiths

To Mom and Dad, thank you for the enormous support that you have given me over the years and instilling in me the values and strengths to accomplish whatever I set my mind on

TABLE OF CONTENTS

	Page
LIST OF TABLES	ix
LIST OF FIGURES.....	x
 Chapter	
1. INTRODUCTION.....	1
Background	1
Anatomy of the Eye.....	10
Photoreceptor Cells	16
Retinal Pigment Epithelium	22
Bruch's Membrane	26
Choriocapillaris	27
Photoisomerization.....	28
Visual Cycle	31
Lipofuscin Production	34
ABCR	42
Retinal Dystrophies and Damaging Factors.....	45
Purpose	50

Chapter	Page
2. MATERIALS AND METHODS	54
Office of Research Compliance	54
Bacterial Media Preparation.....	54
Cell and Tissue Media Preparation	55
Sub-cloning of ABCR	56
Cell Membrane Preparation	60
Western Blotting	61
Dot Blotting.....	63
Sub-cloning and Expression of ABCR/ENT/RSGFP Fusion Protein	64
Microscopy of ABCR/RSGFP CHO Cells.....	64
Cell Fractionation of ABCR/RSGFP CHO Cells.....	66
Isolation and Characterization of Immortalized RPE Cells	66
Isolation of Primary RPE sheets.....	67
Extracellular Matrix Preparation.....	67
Reverse Transcriptase-PCR.....	67
Immunocytochemistry.....	68
Chromosome Preparation.....	72
Suspension Growth	72
³ H Emulsion Autoradiography	73
Repigmentation	74
A2PE Quantitation	74

Chapter	Page
A2PE Feeding	74
Irradiation Studies	75
Live Dead Analysis	75
Apoptosis Analysis.....	76
ES-Mass Spectrometry of A2PE-Fed Cells	76
 3. SUB-CLONING AND EXPRESSION OF pGENE/ABCR/ENT/V5/HIS.....	 77
Introduction	77
Results	84
Dot Blot.....	84
Western Blotting	89
Discussion	94
 4. PRODUCTION AND ANALYSIS OF pGENE/ABCR/ENT/RSGFP/HIS	 99
Introduction	99
Results	104
Confocal Microscopy	104
Cell Fractionation.....	104
Western Blotting	107
Discussion	107
 5. CHARACTERIZATION OF IMMORTALIZED RPE CELLS.....	 114
Introduction	114

Chapter	Page
Results	117
RPE Morphology.....	117
Reverse Transcriptase PCR	120
Immunocytochemistry.....	123
Transformation Tests.....	128
Discussion	133
6. MECHANISMS OF RPE CELL DEATH	139
Introduction	139
Results	141
Live Dead Analysis of A2PE-Fed Cells.....	141
Apoptosis Analysis of A2PE-Fed Cells	150
A2PE Analysis	155
MS of A2PE-Fed Cells.....	158
Discussion	158
7. CONCLUSIONS AND FUTURE WORK	162
ABCR.....	162
tRPE	164
Cytotoxicity	165
Conclusions	166
REFERENCES.....	167
APPENDIX: MISCELLANEOUS FIGURES	190

LIST OF TABLES

Table		Page
1	Primer characteristics used for the production and analysis of pGene/ABCR/ENT/V5/His.....	59
2	Primer characteristics used for the production and analysis of pGene/ABCR/ENT/RSGFP/His.....	65
3	Characteristics of primers used for reverse transcriptase polymerase chain reaction (RT-PCR) of tRPE Cells	69

LIST OF FIGURES

Figure		Page
1.1	Fundus photographs of the human retina	3
1.2	Vision loss caused by macular degenerations	8
1.3	Anatomy of the eye	11
1.4	Anatomy of the neural retina [48]	14
1.5	Major components of the eye involved in retinal maculopathies	17
1.6	Anatomy of a rod photoreceptor [48]	20
1.7	Visual transduction pathway [116]	29
1.8	Anatomy of the posterior retina	32
1.9	Visual cycle pathway [124]	35
1.10	Synthesis of A2E [142]	39
1.11	Proposed ABCR transport mechanism [123]	43
1.12	Reactive oxygen species	47
2.1	Schematic of the pGene/ABCR/ENT/V5/His construct	57
3.1	Plasmid maps	79
3.2	Diagrammatic representation of the mechanisms of the Gene/Switch system	82

Figure	Page
3.3 Agarose gel electrophoresis of the restricted and purified PCR product and pGene	85
3.4 Dot blot of transfected pSwitch CHO cells using different concentrations of mifipristone and probed by the α -V5 antibody	87
3.5 Dot blot to determine the expression levels of transfected clones using the α -V5 antibody	90
3.6 Western blots of concentrated and Ni/NTA purified ABCR fusion protein using α -ABCR antibody	92
3.7 Western blot of concentrated and Ni/NTA purified ABCR Fusion Protein	95
4.1 Schematic of the pGene/ABCR/ENT/RSGFP/His construct	102
4.2 Confocal microscopy of the transfected pSwitch clone B2 induced with 10 mM mifipristone for 16 hours	105
4.3 Stained SDS/PAGE of the cytosolic and membrane fractions from clone B2	108
4.4 Western blot of cells transfected with pGene/ABCR/ENT/V5/His compared to pGene/ABCR/ENT/RSGFP/His using the α -ABCR antibody for detection.....	110
5.1 Photographs of RPE cells.....	118
5.2 Agarose gel electrophoresis of the reverse transcriptase PCR reactions of different cell cultures under various conditions	121
5.3 Immunocytochemistry of tRPE cells expressing RPE-specific proteins.....	124
5.4 Immunocytochemistry of tRPE cells expressing cytoskeletal proteins	126
5.5 Zonula Occludins-1 (ZO-1) immunocytochemistry of tRPE cells grown on BCE-ECM using conditioned media	129

Figure	Page
5.6 Graphical analysis of tRPE transformation experiments	131
5.7 ³ Thymidine emulsion autoradiography of passage 102 tRPE cultures	134
6.1 Fluorescent photographs of tRPE cells that have taken up A2PE	142
6.2 Live/Dead photographs of RPE cells	145
6.3 Cell death of cultures with or without A2PE under various irradiation times.....	148
6.4 Apoptosis photographs of RPE cells.....	151
6.5 Types of cell death of cultures with or without A2PE under various irradiation times.....	153
6.6 ESI-MS spectra of A2PE suspended in methanol with 0.1% formic acid.....	156
6.7 ESI-MS spectra of A2PE isolated from irradiated RPE cells	159
A.1 Blast II alignment of the plasmid sequence (bold) compared to the expected sequence of pGene/ABCR/ENT/V5/His.....	191
A.2 MACAW alignment comparing the sequenced nucleotides to the expected sequence	193

CHAPTER 1

INTRODUCTION

Degeneration of the retina, and the resulting multiple retina disorders, can be caused by a variety of factors. A few of these have similar physiological characteristics due to a degeneration of the Retinal Pigment Epithelium (RPE) and photoreceptor cells. The resulting effect of RPE cell death can cause a progressive loss of photoreceptor function, which diminishes vision and eventually causes blindness. Stargardt's disease, Cone-Rod Dystrophy (CRD), Retinitis Pigmentosa (RP), Fundus Flavimaculatus (FFM), Sorsby's fundus dystrophy, Best's disease and Age-related Macular Degeneration (AMD) are all similar retinal dystrophies [1-4]. The research completed herein contributes to the growing body of knowledge elucidating the mechanisms of these diseases that leads to the progressive and eventual loss of vision.

Background

Retinal dystrophies are diagnosed by fluorescein angiography using a fluorescent dye or detected using a confocal laser-scanning ophthalmoscope. Fluorescein angiography allows the direct visualization of blood vessels exposed in

the retina. The blood vessels that grow into the retina are strongly visualized [2]. The choroidal blood vessels are below the retina and these vessels appear diffusely due to the RPE cells blocking the fluorescence. The fluorescence intensity increases in areas where RPE cells have died. Intense areas of autofluorescence can be visualized in the retina using the confocal laser-scanning ophthalmoscope. This fluorescence increases normally with age and as a result of pathological conditions. The intensity, location and size of the fluorescent granules determine the progression of the diseased state. Figure 1.1 is an image using a confocal laser scanning ophthalmoscope [5,6]. Picture A is the fundus autofluorescence of a normal eye and picture B is a diseased eye, with heavy fluorescence.

AMD is the leading cause of blindness in the United States and other developed countries. It affects over 30% of people over the age of 75 [7,8]. It was estimated in 2004 that 1.75 million people in the United States have AMD with a projected increase to 3 million by 2020 [9]. It is a multi-factorial disease that has been linked to smoking, diabetes, age, light, nutrition, immune status and heredity [7,8,10,11]. Smoking has been suggested to account for up to 32% of the cases of AMD [12].

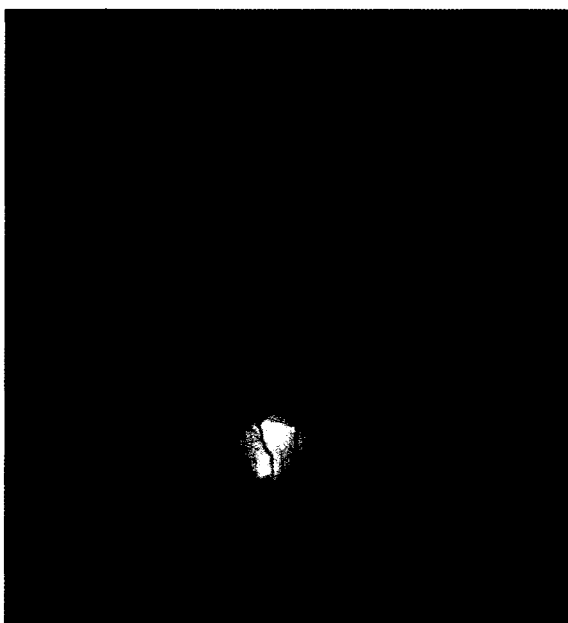
Clinically, age-related maculopathies have identifiable lesions in the retinal pigment epithelium (RPE) and Bruch's membrane, the presence of autofluorescent pigments called lipofuscin and the growth of new blood vessels. Many different classifications have been used to try to group individuals into categories based upon their pathology. Originally, senile macular degeneration was described in 1885 and

Figure 1.1: Fundus photographs of the human retina. A) Normal fundus [5]; B) Macular degeneration fundus [6].

B.



A.



disciform macular degeneration was determined to be a subset in 1926 [13].

Although these terms are still clinically used, the establishment of an international system separates AMD into two groups.

Early age-related maculopathy produces minor vision loss and changes in RPE pigmentation along with debris under the RPE [14]. Lesions in the RPE are small and whitish-yellow spots can be present. Additionally, atrophy of the RPE or increased pigmentation is often seen [15]. Late age-related maculopathy is characterized by severe vision loss and is termed age-related macular degeneration (AMD), previously known as senile macular degeneration. Symptoms include geographic atrophy (GA) of the RPE, choroidal neovascularization (CNV), pigment epithelium detachment (PED) and submacular disciform scar tissue [13].

Generally AMD is divided into two subclasses. The first type is dry AMD, which is also called atrophic or non-exudative AMD. Dry AMD is the same as GA without the presence of CNV. The second type is called wet AMD, also known as exudative or disciform AMD. Wet AMD is clinically the same as CNV. For clarity, only the terms GA and CNV will be used in this discussion to identify the two types of AMD.

A diagnosis of GA occurs when areas of loss of RPE cells and the overlying photoreceptor cells are seen. Autofluorescent deposits outside of the RPE are referred to as drusen. Large amounts of drusen, basal laminar and basal linear deposits between the RPE and Bruch's membrane and thickening of the membrane are observed [16]. Approximately, 85-90% of AMD cases have GA, of which there

is no known cure. GA manifests as discrete patches of vision loss that continue into central vision loss. CNV comprises the remaining 10% of the AMD cases. Choroidal neovascularization is characterized by blood vessel growth from the choriocapillaris through Bruch's membrane. Accumulation of blood or serous fluid beneath the RPE may result, causing PED [17]. Often the vessels grow through the RPE into the sub-retinal space. This growth causes permanent damage to the photoreceptors and scarring, both of which can result in blind spots [18]. Additionally, marked lipofuscin accumulation in the RPE occurs. CNV is temporarily reduced by non-invasive laser coagulation therapy that will destroy the blood vessels, but only 15% of CNV patients are candidates for this therapy [19]. The blood vessels do eventually grow back and the surgery must be repeated [20]. This process is controversial because lasers have been known to damage the retina and the potential effects of damage caused by this surgery are unknown. The remaining 85% have occult CNV where the blood vessels cannot be clearly identified by fluorescein angiography [17]. The newest forms of therapy are anti-VEGF (vascular endothelial growth factor) drugs that stop the blood vessels from growing further [13,21]. This treatment is very promising, but CNV is not diagnosed until the dystrophy has already progressed into RPE cell loss, and there is no known treatment to regain the loss in vision. Both GA and CNV are advanced stages of AMD.

Stargardt's Disease, originally documented in 1909, is characterized by a loss of central vision due to the loss of RPE cells in the macular area [22]. Stargardt's disease begins early in life with delayed dark adaptation and develops into blindness

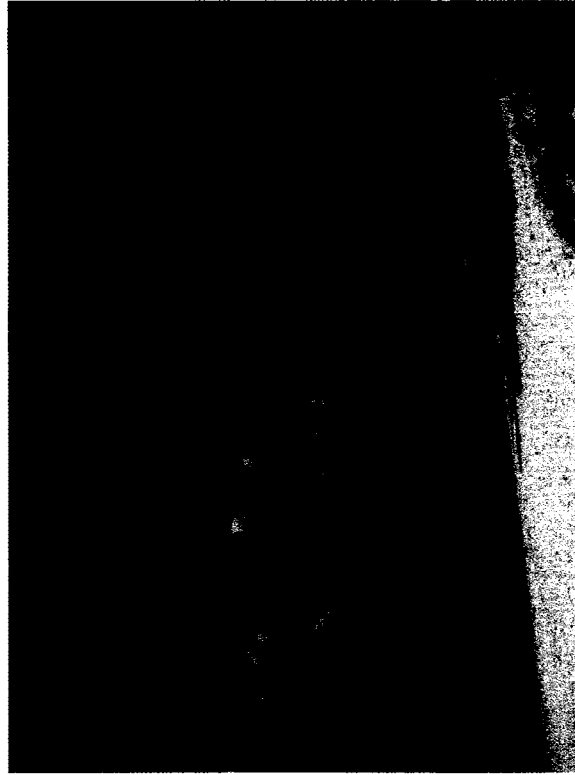
in the teenage years [23]. It is an autosomal recessive dystrophy caused by one of several mutations in the ABCR gene [24-26]. Approximately 1 in 10,000 individuals within the population have this disease [5]. It is characterized by an increase in the autofluorescent pigment mixture called lipofuscin, which is located primarily in the macula of the RPE and surrounding areas [27]. Increased lipofuscin accumulation appears to be associated with the progression of central vision loss (Figure 1.2A), which will then spread outward to the periphery. Figure 1.2B illustrates the vision of a normal eye for comparison. Fundus Flavimaculatus is considered to be a variant of Stargardt's disease that displays a later age of onset [28, 29].

Recently, studies have been published that show a higher incidence of AMD of grandparents of children with Stargardt's disease if the grandparent has one of the mutated alleles [1, 30]. It is speculated that mutations in just one of the ABCR alleles enhances an individual's chance of developing AMD by five times [31]. AMD is similar in etiology to Stargardt's disease where the prolific accumulation of lipofuscin occurs in Stargardt's disease, but happens much later in life, beginning around 50 years old [32, 33]. This shows a possible relationship between Stargardt's and AMD, but the connection between ABCR and AMD is under debate [24, 26, 34].

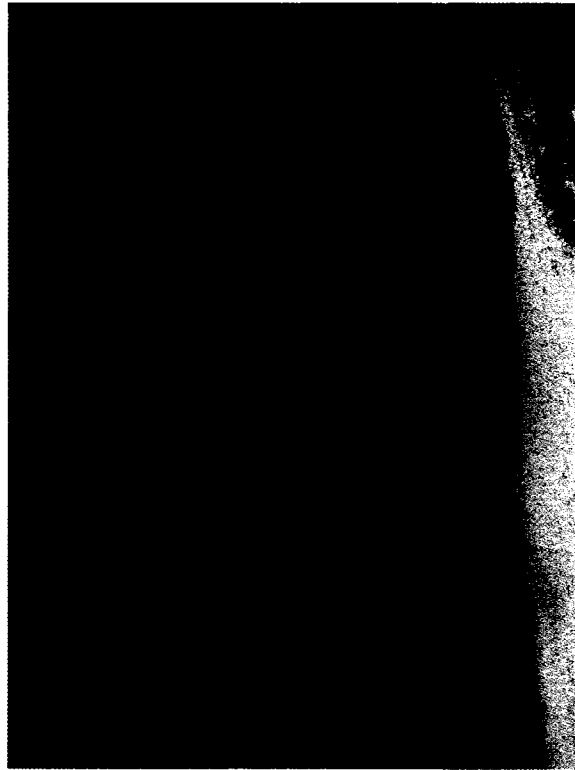
Both Stargardt's disease and AMD share many characteristics with other retinopathies; mutations in ABCR or one of the RPE-specific genes, RPE-65 and CRALBP, are found [4, 7, 35]. Cone rod dystrophy is an inherited autosomal recessive disorder that causes deterioration in the rods and cones [36]. Retinitis pigmentosa is an inherited disease that begins with night blindness because of the

Figure 1.2: Vision loss caused by macular degenerations. A) Macular dysfunction; B) Normal eye.

B.



A.



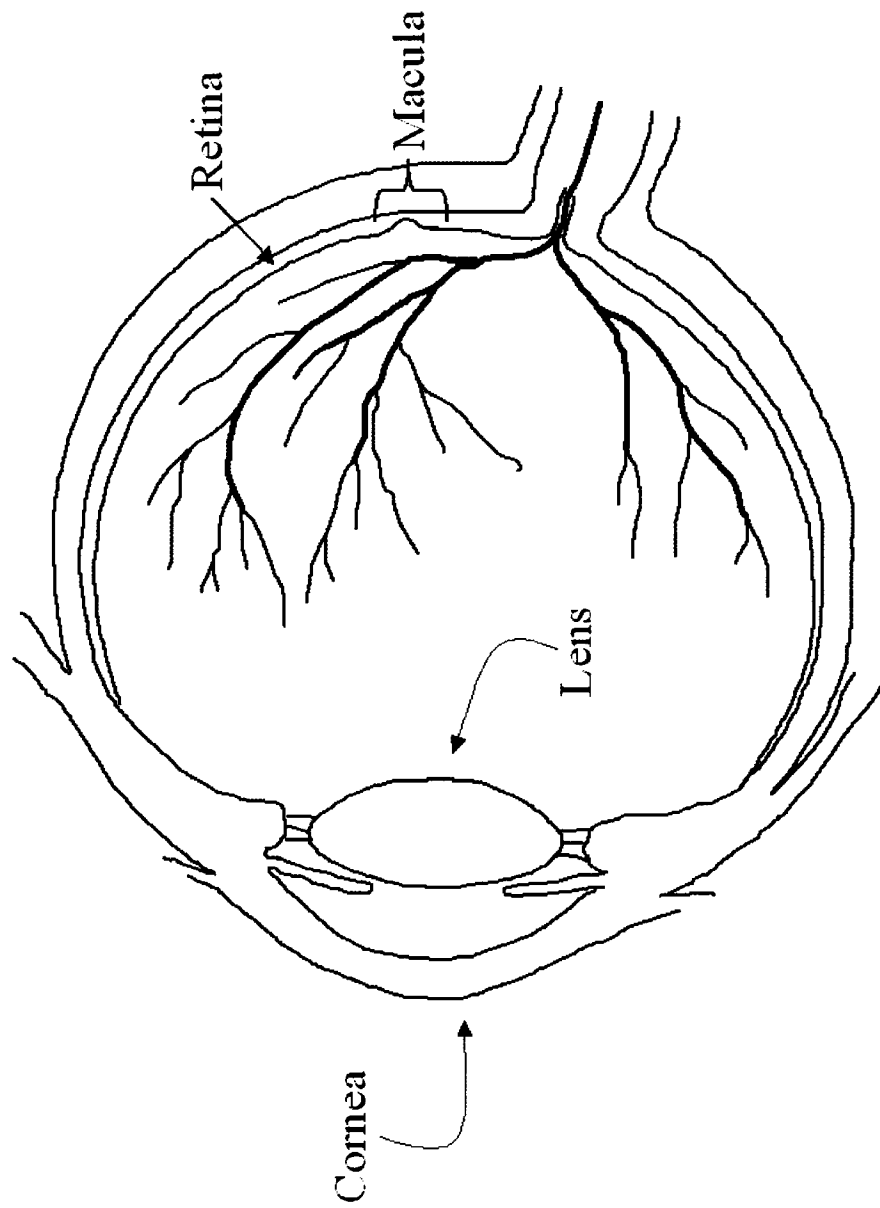
degeneration of rod photoreceptor cells. The disease progresses through a gradual loss of vision at the periphery and continues until only the central vision remains [37]. Best's disease and Sorsby's fundus dystrophy are defects with sub-RPE cell deposits. Best's disease displays a large accumulation of lipofuscin-like material between the RPE and Bruch's membrane. It is caused by mutations in the RPE-specific gene VMD2 [3, 38]. Sorsby's fundus dystrophy begins with night blindness and progresses into sub-foveal CNV around 40 years of age. Tissue inhibitor of metalloproteinases (TIMP-3) is mutated in these individuals [39]. TIMP-3 expression is altered in some AMD patients with GA [40].

Anatomy of the Eye

The eye is a complex organ consisting of tissues that function as filters, lenses, neural networks and other components. In order to understand retinal diseases and their physiology, the components of the eye, which are depicted in Figure 1.3, must be described along with their respective functions. The anterior and the posterior segments are generally treated separately.

Photons of light will initially enter the cornea. The cornea absorbs all photons having wavelengths that are less than 295 nm [41-43]. The convex characteristic of the cornea allows it to focus light onto the lens. Once light has passed through the cornea, it travels through the aqueous humor and is transmitted to the lens. The lens

Figure 1.3: Anatomy of the eye.

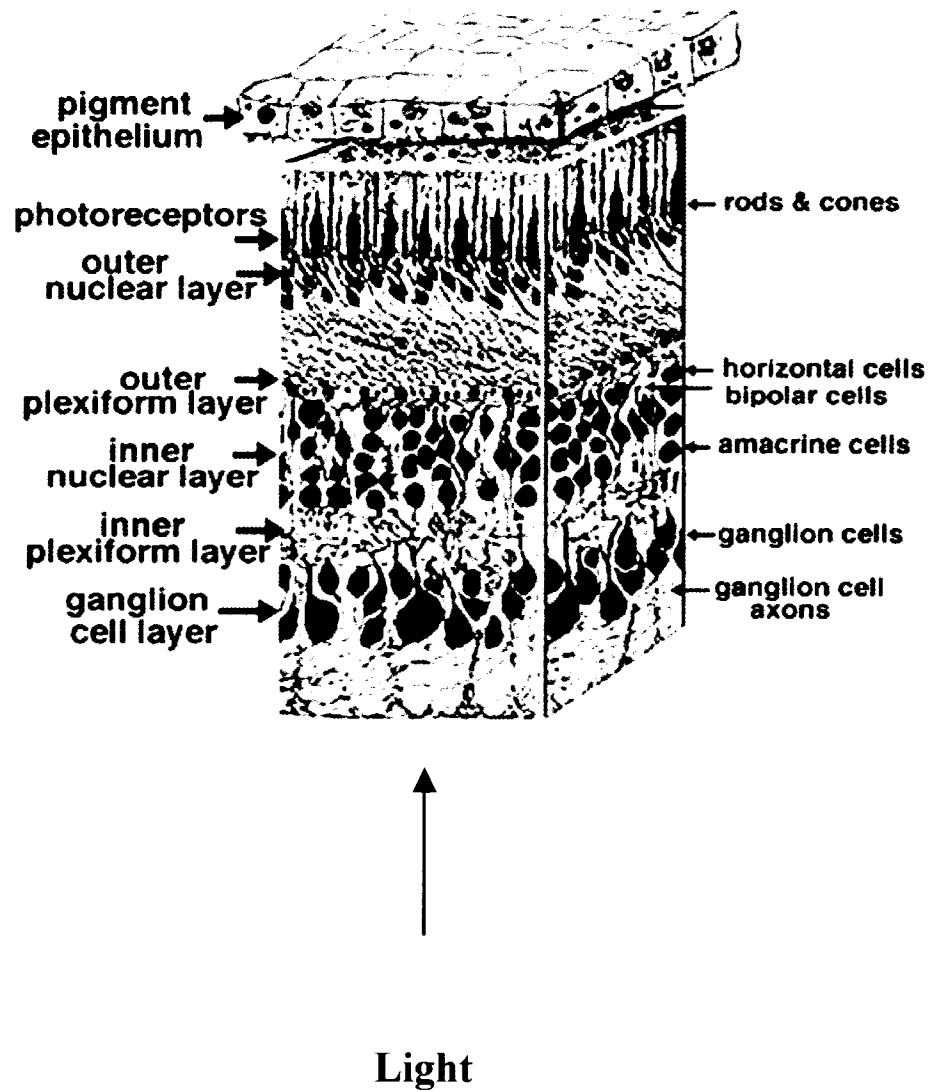


also absorbs photons of light between the wavelengths of 295 nm and 400 nm [41, 43, 44]. Consequently, only light between the wavelengths of 400nm to 700nm will actually reach the posterior part of the eye. Unfortunately, the lens does not always yield this protection throughout life. During the first decade of life, the lens is still in the process of development, which allows a small portion of the ultraviolet spectrum to pass through [41, 44]. Interestingly, lipofuscin accumulation begins in all individuals during the first decade of life and then the accumulation slowly declines for the next few decades [45]. The light exits the lens and is focused onto the retina.

The retina, choroid and sclera compose the posterior portion of the eye. The retina is a part of the forebrain that transduces light energy into an electrical signal. Topographically, the retina is divided into the macula and the posterior retina. The macula is a 3 mm diameter region of heavy pigmentation, and is surrounded by a 1 mm less pigmented region [46]. It is located approximately 5mm from the optic nerve [47]. Within the center of the macula is the fovea centralis, which has an area slightly over 2 mm² [46]. Because the majority of the light entering the eye is focused on the macula, this is the region of highest acuity vision.

The retina is a layer of cells that are generally divided into the inner retina and the outer retina. Figure 1.4 depicts the arrangement of cell layers of the retina. The inner retina is composed of ganglion cells and intermediary neurons (bipolar, amacrine and horizontal cells) [48]. The inner retina is responsible for processing information prior to sending it to the brain [49]. The outer retina is composed of the photoreceptor cells and the RPE. Interestingly, light must pass through the inner

Figure 1.4: Anatomy of the neural retina [48].



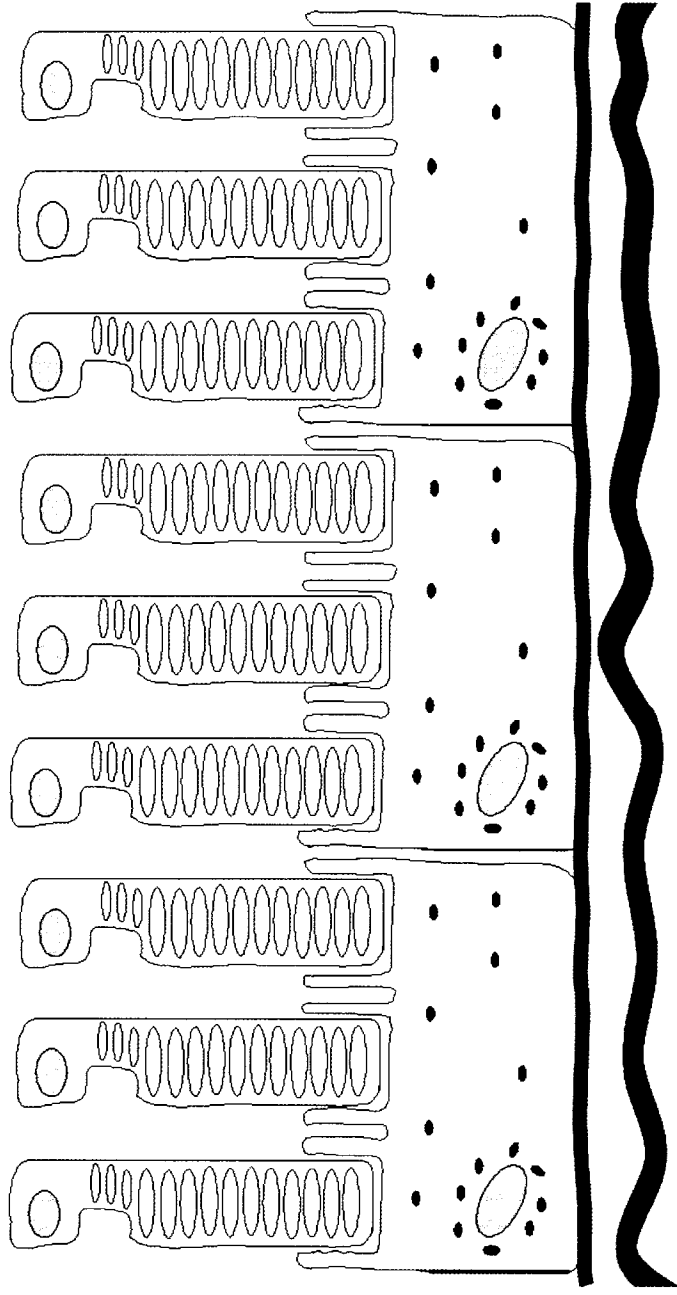
retina before reaching the photoreceptor cells. The photoreceptor cells absorb light and convert it into a chemical signal.

Figure 1.5 is a depiction of the anatomy of the four major components in the posterior eye that are affected by retinal maculopathies. The first component comprises the photoreceptor cells. The second component is the retinal pigmented epithelium (RPE) and is interposed between the photoreceptor cells and Bruch's membrane, which is the third component. The fourth component is the choriocapillaris, which supplies blood to the posterior retina. Each of these parts of the eye will be discussed in detail.

Photoreceptor Cells

There are two main classes of photoreceptor cells, rods and cones. Both rods and cones are neural cells that absorb photons of light. The cones are responsible for color detection and high acuity vision [49]. There are approximately 15,000 cones in the center of the foveal pit, which is totally devoid of rods [50]. Additionally, there are 200,000 cones in the remainder of the fovea [46]. Because of the intense concentration of cones, the fovea is considered to have the highest visual acuity. The number of cones diminishes drastically outside of the macula. The rods allow vision during dim light conditions, such as nighttime [51]. The peak density of rods is about 160,000 rods/mm², located in a ring around the fovea [52]. The concentration of rods diminishes towards the outer edge of the retina, but is still high when compared to the

Figure 1.5: Major components of the eye involved in retinal maculopathies.

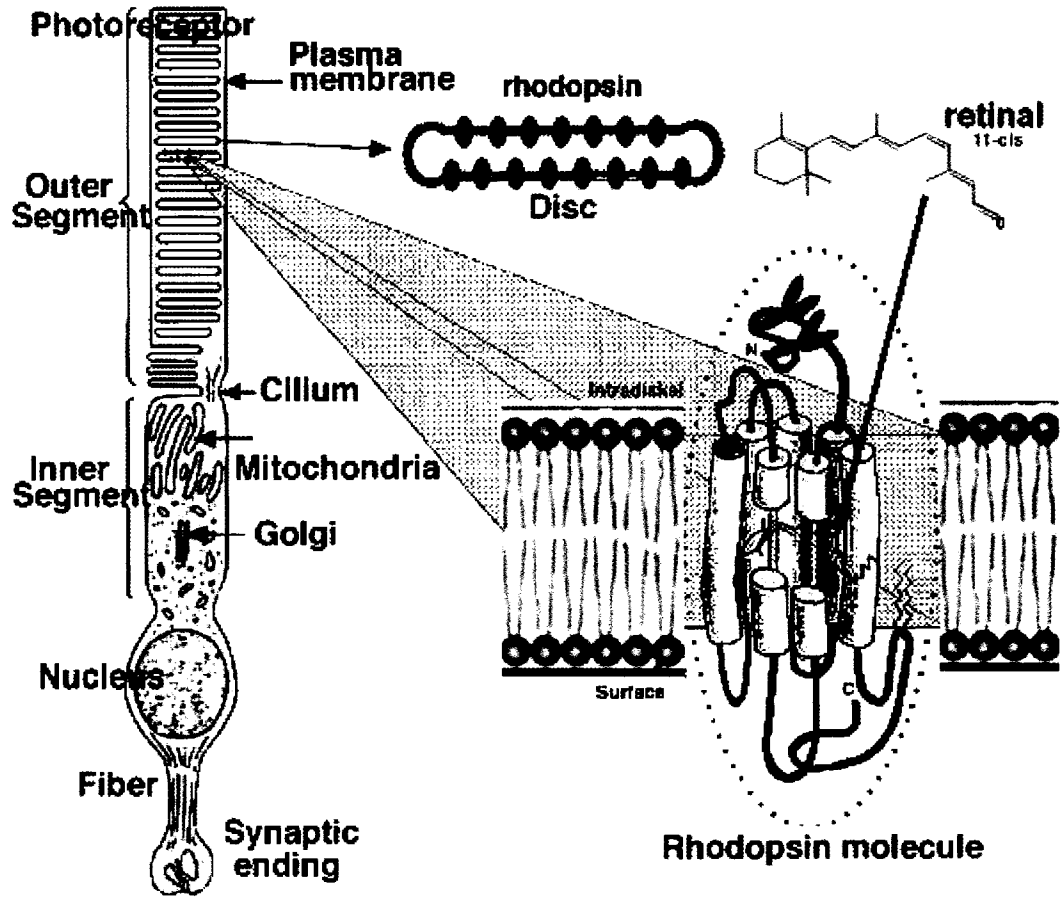


number of cones [52]. This is the source of peripheral vision. Due to the high concentration of rods and cones in the macula, small losses in the macular region can have a large impact on the vision of a person [2].

Although there are differences between rods and cones, their organization is generally similar. Rod photoreceptors have been studied quite extensively and will therefore be the only ones described. Each rod photoreceptor is composed of a synapse, a nucleus and an inner segment and outer segment separated by a cilium (Figure 1.6) [48]. The cilium is the only connection between the inner and outer segments and serves as a channel for molecules [51]. The base of the cilium contains numerous mitochondria in the inner segment. The Golgi, or myoid, portion of the inner segment is the location for the manufacture of most of the molecules used by the photoreceptor. Almost all proteins pass through the connecting cilium to the outer segment.

The rod outer segment is composed of a stack of approximately 1000 disc-shaped membranes [53]. Each disk has a double membrane and is separate from the plasma membrane. Disks originate from invaginations of the plasma membrane closest to the cilium. New discs are continually formed throughout life and displace older ones from the base of the stack towards the tips [51, 54]. The oldest disks at the tips are shed off at dawn and phagocytized by the RPE [51, 55]. This concept of continuous renewal is called molecular replacement, where the renewal of new disks is balanced with the shedding of old discs [51]. All of the proteins, carbohydrates and

Figure 1.6: Anatomy of a rod photoreceptor [48].



lipids in the disks follow this pattern of replacement. Each photoreceptor produces 10% of the outer segment each day, so the photoreceptors are considered to have the highest anabolic load of any cell in the body [49].

Each disk has a unique three-dimensional orientation where the lipids are longitudinally arranged and the proteins are aligned transversely in the outer segment [51, 54]. Although the outer segment is highly ordered, the proteins and lipids are not static, because the phospholipids in the rods contain a large concentration of highly unsaturated long-chain fatty acids. Phosphatidylcholine (PC) and phosphatidylethanolamine (PE) each account for 40% of the total phospholipid followed by 10% phosphatidylserine (PS) and 10% of other lipids [56, 57]. Approximately 32% of the PE fatty acids are docosahexaenoic acid (22:6) [57].

The major protein produced in rods is opsin. It is a seven-transmembrane G-linked protein. When the retinoid chromophore, 11-cis retinal, is bound, it is termed rhodopsin. The helices are oriented in the membrane disks so that light will optimally reach and excite the chromophores. Rhodopsin is dispersed throughout the disk, but excluded from the outer rim and incisures of the disks [58]. In contrast, the protein that is defective in Stargardt's patients (ABCR) is located exclusively in the outer rim and incisures [25, 59, 60].

Retinal Pigment Epithelium

The retinal pigment epithelium is a neural tissue that is of neuroectodermal origin and specifically originates from the outer layer of the optic vesicle [61].

During the embryology of the retina, the RPE cells secrete autocrine and paracrine growth factors for the proliferation, differentiation and chemotaxis of neural retina cells [62, 63]. Prior to birth, the RPE are fully differentiated and pigmented with melanin [63]. It is a cuboidal monolayer of cells that are post-mitotic with a variety of functions [64, 65].

Polarity

As in many epithelial cell types, the RPE is attached to and produces the extracellular membrane on the basal laminar side, which is a component of Bruch's membrane [66-68]. The apical side of the RPE cells has microvilli that are intercalated with the photoreceptor cells. These apical processes cover the distal 1/3 to 2/3 of the photoreceptors [65]. Intercellular tight junctions between RPE cells establish its polarity. The tight junctions form a circumferential ring around each cell, which aids in the blood-retina barrier. Many proteins have been exclusively isolated to the basal lamina or the apical portion of the cell [66, 69-72]. This allows selective transport of material from the choroid to the photoreceptor cells or to the interphotoreceptor matrix. RPE cells are responsible for producing the ion gradients in the interphotoreceptor space [69]. The tight junctions, along with the focal adhesions, allow a uniform monolayer of cells.

Melanosomes

The RPE are heavily pigmented with melanin, which is a unique feature of

this epithelium. Melanin in the RPE is a dense dark brown pigment known as eumelanin because of its low sulfur content [73]. It is produced in specialized lysosomes called melanosomes [74-76]. Over a dozen proteins are needed for melanization [76-78]. Although melanin is an amorphous high molecular weight substance, it is composed of only two colorless tyrosine derivatives, DHI and DHICA, which polymerize through a variety of bonds [73, 78, 79]. The RPE only produces melanin before birth, although some accounts have described melanogenesis in mammalian RPE cells in culture [61, 80-82].

The melanosomes are located in the apical portion of the cells, adjacent to the photoreceptor cells [61]. The functions of melanin are extremely diverse. Melanin broadly absorbs the light that passes through the photoreceptors in order to inhibit internal reflection [83]. The melanin also acts as an antioxidant and scavenger of free radicals--particularly superoxide ions, singlet oxygen and hydroxyl radicals--and can detoxify peroxides by quenching peroxyradicals [84, 85]. Melanin can sequester multivalent transition metals [61]. Additionally, drugs such as kanamycin, streptomycin and chloroquine derivatives have been shown to bind melanin [61]. Unfortunately, as individuals age, the number of melanosomes decreases [45, 86, 87]. Because of its important photoprotective effect, melanin will be re-addressed later in this chapter.

Phagocytosis

The RPE are integral in the survival of the photoreceptor cells. They secrete

paracrine growth factors and hyaluronan into the interphotoreceptor matrix. These are required for the survival of photoreceptor cells [69, 88]. The rod/RPE cell ratio is dependent upon location in the eye. The highest ratio is about 40 rods/RPE cell at the edge of the macula and decreases to about 20 rods/RPE cell in the periphery [89]. The cone/RPE ratio is even more dramatic with 30 cones/RPE in the fovea to 1 cone/RPE in the periphery of the eye [90]. The RPE cells are phagocytic and engulf rod outer segments and degrade the components [70, 91]. They will phagocytize approximately 10-15% of the outer segments per day [54]. Marshall has computed that a single RPE cell will phagocytize over 300,000,000 disks over a 70-year life span [53].

Phagocytosis by the RPE allows the elimination of wastes from the photoreceptor cells and the recycling of retinoids from the rod photoreceptors [92]. The RPE can also function to store excess vitamin A derived from the recycling process or from the diet [92, 93]. A RPE-specific protein, RPE-65, is novel in its ability to store vitamin A. The membrane-bound mRPE-65 helps recycle the retinoids and the cytosolic form stores excess vitamin A when synthesis is not required [94].

As a consequence of age, the numbers of RPE cells in the macula decrease [45]. Because the RPE cells are quiescent in the eye, neighboring cells expand instead of dividing. These RPE fulfill the functions of the dead RPE, which can cause an increase in the number of rods each cell must phagocytize [49]. The metabolic load of RPE cells increases naturally with age and is highest in the macula. The RPE cells are even considered more phagocytic than macrophages and have

extremely high levels of antioxidant compounds and enzymes, such as vitamin E, vitamin C, catalase, glutathione and superoxide dismutase [95]. When the RPE are no longer able to phagocytize the outer segments, the photoreceptor cells are affected. Accordingly, a mutation affecting the phagocytosis of outer segments in mice causes an accumulation of outer segment debris in the interphotoreceptor matrix and causes photoreceptor decline [96, 97].

Bruch's Membrane

Bruch's membrane is an extracellular matrix (ECM) composed of five layers: the basal lamina of the RPE, the inner collagenous zone, the elastic lamina, the outer collagenous zone and the basal lamina of the choriocapillaris [98]. ECM proteins have been shown to be integral in the differentiation, gene expression, proliferation, cell shape and survival of RPE cells [68, 99-101]. The major proteins that are secreted by the RPE are collagens, laminins, fibronectin and vitronectin. Over 12 types of laminin have been isolated and are expressed distinctly in different tissues that result in the different behaviors and morphologies of those tissues [63, 102].

RPE cells cultured on different substrates have exhibited a variety of phenotypes and gene expression profiles. Some of the substrates used were tissue-grade plastic, Matrigel, bovine corneal endothelial ECM, laminin, collagen, aged Bruch's membrane and different layers of Bruch's membrane [66, 100, 103-106]. Aged Bruch's membrane can have a detrimental effect on the differentiation and survival of RPE cells. CNV can potentially damage Bruch's membrane and expose

the collagenous layers to the RPE, resulting in cell death [104, 105]. These studies indicate that RPE cells require specific types of laminin for cells to differentiate and survive.

With normal aging, increased thickness, sub-RPE deposits and advanced glycation end products occur, especially in the sub-macular region [98, 107]. The sub-RPE deposits are believed to be formed from RPE cells under conditions where normal dispersal is dysfunctional. Histologically, the deposits, called drusen, contain apoptotic bodies of RPE cells, lipofuscin and ECM components [108, 109]. Drusen is correlated with an increase in volume of lipofuscin in the RPE [98, 108]. It is likely that drusen causes a displacement of the overlying RPE layer and acts by separating the RPE and the choriocapillaris, forming a hydrophobic barrier between the two tissues [13]. This separation further inhibits the transport of wastes and nutrients between the choriocapillaris and the RPE. In addition, stretching of the RPE cells can cause an alteration of the RPE-ECM interactions required for cell survival [101, 110].

Choriocapillaris

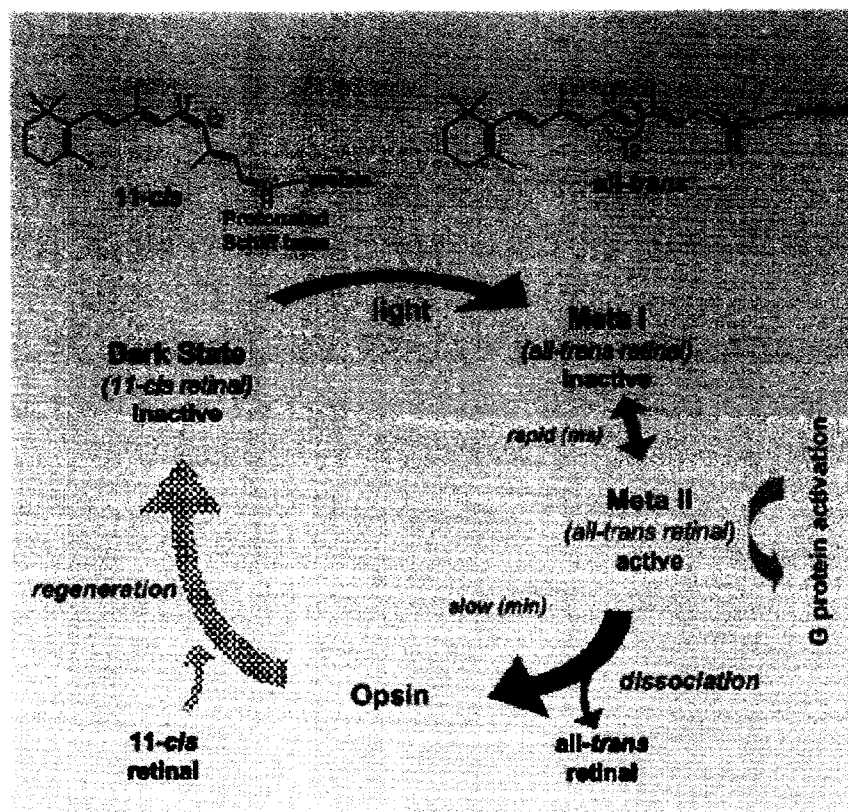
The choriocapillaris is a fenestrated capillary bed that is located posterior to Bruch's membrane. It supplies nutrients to the retina, and removes wastes, through the RPE cells. Additionally, the choriocapillaris supplies these cells with oxygen. Since the photoreceptors are avascular and both the RPE and the photoreceptors have a high metabolic rate, the choriocapillaris has a high oxygen tension, especially in the macular region [111]. It has been estimated that the concentration of oxygen is the

highest of any tissue, at 10%, and slightly lower than that of saturated blood, which is 15% [112, 113]. In advanced GA, the underlying vessels display shrinkage of the choriocapillary network [141]. A number of growth factors secreted by the RPE have been identified that stimulate CNV. RPE are hypothesized to secrete both angiogenic and inhibitory molecules for choroidal vascular cells [18, 114].

Photoisomerization

Rhodopsin is a photopigment that possesses a covalent linkage between 11-cis-retinal (11-cis) to the lysine 296 residue on helix 7 of opsin by a protonated imine group known as a Schiff base [115]. Upon absorption by a photon of light, the 11-cis chromophore undergoes conversion to all-trans-retinal (RAL), shown in Figure 1.7 [116]. The isomerization causes a twist in the chromophore-binding domain, and subsequent transmembrane reorganization to form metarhodopsin I through a series of intermediates [117, 118]. The activated receptor, Metarhodopsin II (MII), forms through a series of conformational changes in the receptor, deprotonation of the Schiff base, and alterations to the cytoplasmic surface [118]. Metarhodopsin II initiates the activation of the G-protein transducin to produce the phototransduction cascade that causes the photoreceptor to hyperpolarize [58]. The photoactivation of rhodopsin to form MII only takes milliseconds [58, 115]. The deprotonation of MI to form MII allows for a 10^7 -fold decrease in pKa of the chromophore-opsin complex,

Figure 1.7: Visual transduction pathway [116].



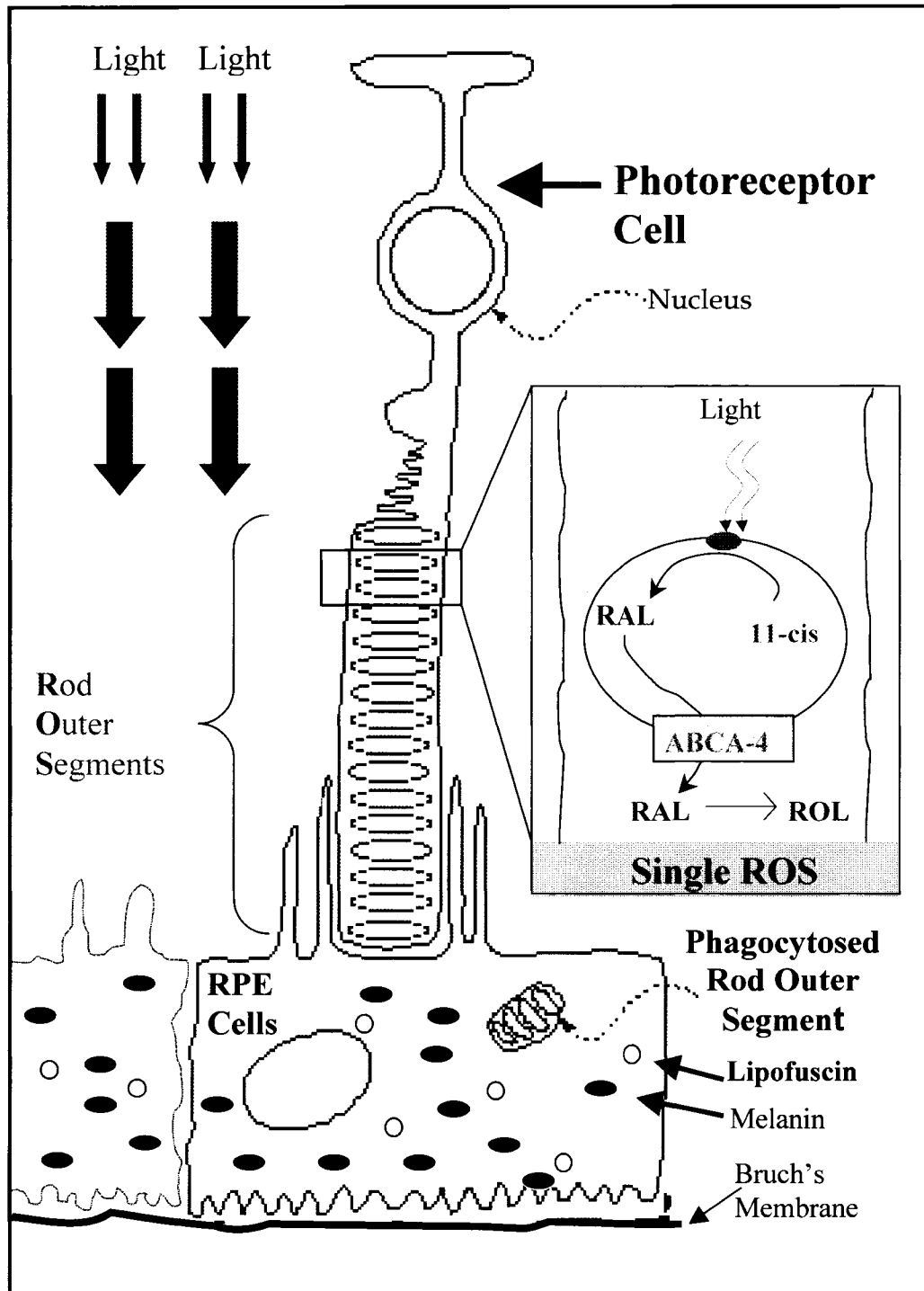
thereby allowing the spontaneous hydrolysis of RAL from opsin [119]. The opsin phosphorylates to activate it for binding another molecule of 11-cis retinal [120].

Visual Cycle

As discussed earlier, the photoreceptor cells and the RPE are intimately related. The photoisomerization described above takes place inside of the Rod Outer Segments (ROS), which are shown in the expanded box on the right side of Figure 1.8. The aldehyde on RAL is a highly reactive moiety and will react with lipids, proteins and nucleic acids [121]. The RAL must be converted into a less reactive form in order to inhibit damage to the photoreceptor cell. There are no enzymes that can effect this conversion of the RAL in the lumen of the rod outer segment, so it must be removed from the lumen to the cytosolic space. Transport of RAL is performed by the transmembrane protein ABCA-4, also known as ABCR or Rim protein [25, 59, 60, 122]. Once outside of the ROS lumen, the RAL is rapidly reduced into the relatively unreactive vitamin A, also called all-trans-retinol (ROL), by the enzyme all-trans-retinol dehydrogenase (all-trans RDH) [115, 123].

The re-isomerization of vitamin A occurs inside of the RPE cells. The ROS are phagocytized by the neighboring RPE cells, which will then bind with a lysosome to form a phagolysosome. The ROL is believed to be released prior to the phagocytosis of the ROS by an undiscovered mechanism. Since retinoids are

Figure 1.8: Anatomy of the posterior retina.

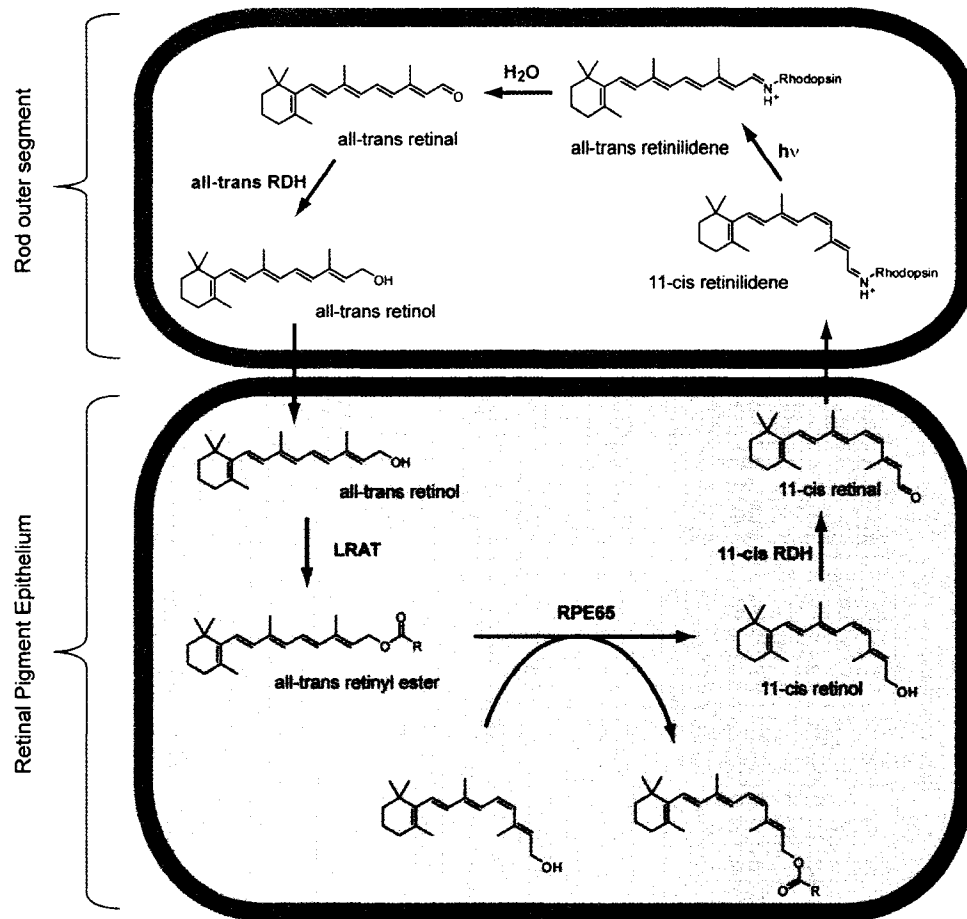


hydrophobic and chemically unstable, they are transported within and between cells by proteins. Figure 1.9 shows the retinoid cycle [124]. Within the RPE cells, the ROL is initially bound by the enzyme lecithin retinol acyl transferase (LRAT). This enzyme functions by transferring an acyl group from a phosphatidylcholine to produce all-trans-retinyl ester [115]. After the transesterification process, the ester is then bound to the protein RPE-65 [125]. The RPE-65 palmitoylates the ester and then transfers it to the enzyme retinyl isomerohydrolase [126, 127]. The function of the enzyme is to convert the all-trans-retinyl-ester to 11-cis retinol. Recently, studies have indicated that RPE-65 may have retinyl isomerohydrolase activity [127, 128]. Finally, the protein CRALBP binds the 11-cis-retinol, which gets converted back to the starting material 11-cis-retinal by 11-cis-retinol dehydrogenase (11-cis RDH) [4, 35, 129]. This is then postulated to be shipped back to the inner segments of the photoreceptor cells by interphotoreceptor retinoid binding protein, where it binds to opsin and finishes the retinoid cycle [130].

Lipofuscin Production

Lipofuscin, also known as “age pigment,” can be found throughout the body in post-mitotic cells such as neurons, cardiac myocytes, hepatocytes and the RPE. Concentrations of lipofuscin are an indicator of longevity, where higher concentrations are proportional to increased cellular age [131, 132]. It is characterized as a brown-yellow, acid-fast, electron-dense autofluorescent material

Figure 1.9: Visual cycle pathway [124].



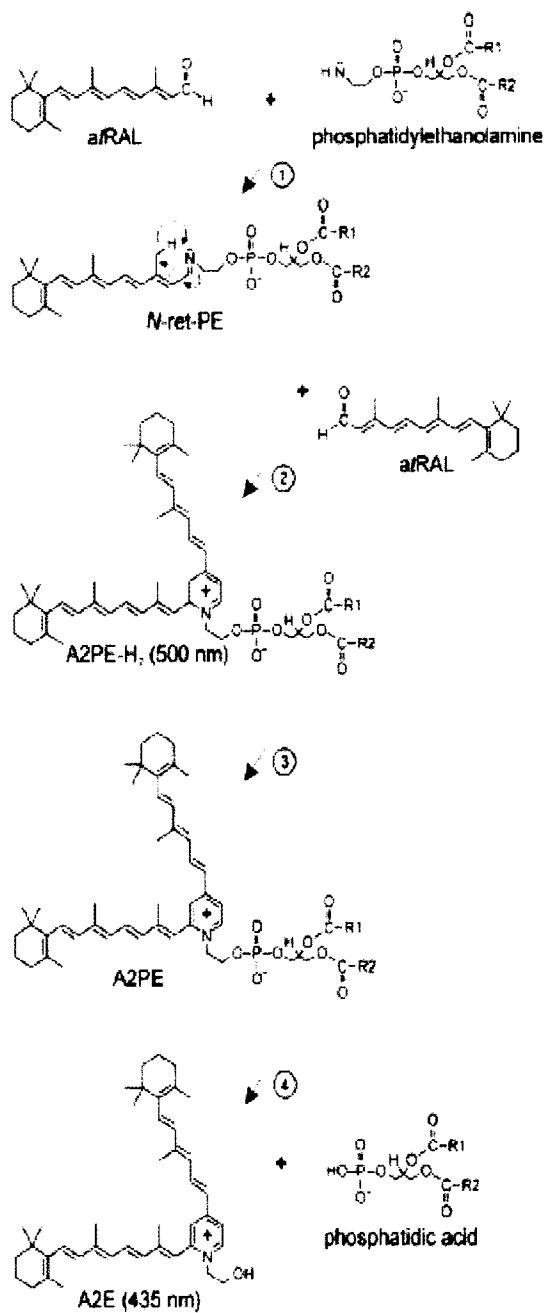
that is found exclusively in lysosomes [132, 133]. Two main hypotheses exist to describe the reasons for lipofuscin accumulation. The first explanation posits that small amounts of undegradable material accumulate over time in non-dividing cells, but get dispersed between the progeny of cells undergoing cell division [134]. The second one hypothesizes that a decline in lysosomal activity due to age causes a decrease in the efficiency of the degradation process [132]. Because of its amorphous nature, the etiology of lipofuscin remains a mystery. Experiments have shown that rats fed a diet deficient in the antioxidant vitamin E exhibit an increase in lipofuscin. The mechanism proposed by the authors of this study was that the extra lipofuscin resulted from the increase in oxidative stress associated with these tissues [135]. Cultures that have been grown under high oxygen concentrations have enhanced lipofuscinogenesis [136]. It is now established that the degradation of cellular components in lysosomes, a process known as autophagy, have been associated with lipofuscinogenesis, particularly with mitochondria that are high in reactive oxygen species [137]. In most post-mitotic cells, the accumulation begins at birth and increases linearly over time. This is not the case for RPE lipofuscin (RLF). In RPE cells, RLF accounts for 1% of the cellular volume during the first decade of life. The second decade shows a dramatic increase to 7-9% and remains relatively constant until approximately 50 years of age. The cells then begin to gradually increase RLF until the total cell volume occupied is 19% in individuals over 80 years old [45].

If lipofuscin is generated by incomplete digestion by lysosomes, then how are the actively phagocytic RPE cells affected? In some experiments, a reduction in the

amount of vitamin A (all-trans-retinol) fed to mice causes a reduction in RLF compared to mice fed a normal diet. Other experiments with RPE-65 knockout mice showed a decrease in lipofuscin fluorescence [138]. These studies indicate the importance of retinoids in RLF accumulation. In the pioneering work by Eldred and Katz, they were able to isolate ten different fluorescent fractions from chloroform:methanol extracts of RLF [139]. Further experimentation identified the predominant fluorophore as A2E, which was structurally identified as a bis-retinoid pyridinium salt [107, 140]. A second fluorophore was isolated and characterized as an isomer of A2E called iso-A2E [141]. These compounds are derived from two molecules of all-trans-retinal (ATR) and one molecule of ethanolamine as shown in Figure 1.10 [142]. Ethanolamine is found in the ROS as the major lipid, phosphatidylethanolamine (PE), along with ATR.

Similarities in the pathology of Stargardt's disease and AMD have led to the understanding of how A2E is formed in vivo. The reduction of ATR to all-trans-retinol (ROL) is the rate-limiting step in the phototransduction cascade and dependent on the protein ABCR. ROL absorbs UV light, which does not reach the retina. ATR absorbs light in the visible spectrum and becomes phototoxic. Under normal light conditions, an accumulation of ATR can photoreact to form a Schiff base with PE to form N-retinylidene-PE (NRPE) [57, 143]. In the *abcr*^{-/-} mouse model of Stargardt's disease, the buildup of ATR in the rod outer segments is greatly enhanced and an increase in lipofuscin was found in the RPE [144]. In other experiments comparing the *abcr* null mutant mice to Stargardt's patients, three intermediates in the

Figure 1.10: Synthesis of A2E [142].



biosynthesis of A2E were identified in the rod outer segments and RPE. These were NRPE, A2PE-H2, and A2PE [145]. A2PE-H2 results from the reaction of NRPE with another ATR to form the cyclic Schiff base. Normal mice showed no elevated accumulation of NRPE, A2PE-H2 or A2PE in the rods or RPE. Additionally, NRPE and A2PE were extracted from Stargardt's patients in the rod and RPE cells. Further evidence suggests that A2PE is formed only in the rod cells and then converted to A2E in the RPE by phosphate hydrolysis after phagocytosis [57]. This indicates that ABCR is responsible for detoxifying the photoreceptor outer segments by decreasing the concentration of ATR in the lumen of the ROS.

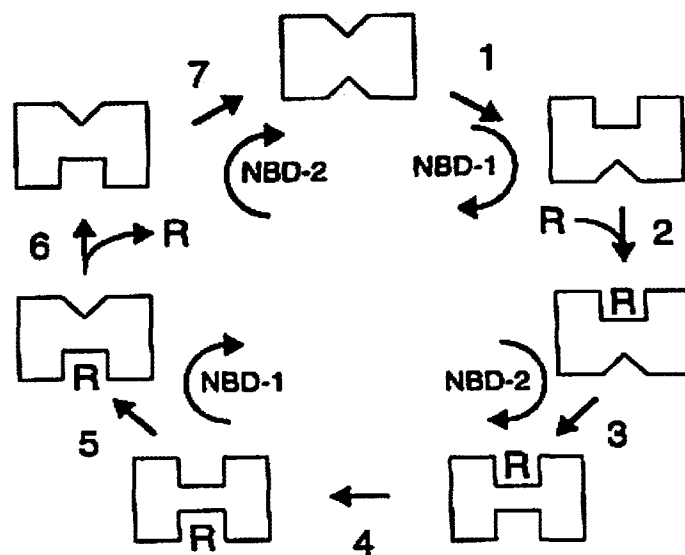
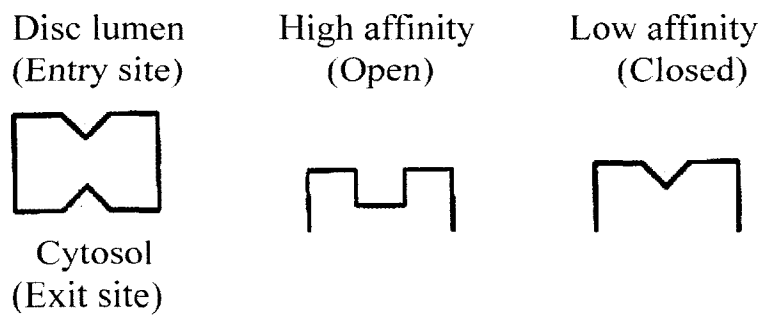
Lipofuscin is a complex mixture of modified proteins and lipids. Although A2E and several of its oxidation products have been characterized, Warburton et al. have identified RLF granules to be composed of 44% protein and 50% lipid [146]. The rod photoreceptors have a high concentration of polyunsaturated fatty acids (PUFAs), particularly docosahexaenoic (DHA). Membrane lipid peroxidation has been implicated in the formation of lipofuscin [147, 148]. DHA and other PUFAs are susceptible to free-radical-induced peroxidation in the presence of reactive oxygen species [149]. High concentrations of oxygen in the presence of light can induce peroxidation, which is why ROS have high concentrations of antioxidant molecules [150]. The peroxidation of lipids can result in further reactions with other lipids or the formation of Schiff bases with proteins [151]. These reactions can occur in the lysosomes in RPE cells.

ABCR

To help clarify the role of ABCR in the pathogenesis of Stargardt's disease and other retinal dystrophies, researchers have begun to investigate the mechanisms of its actions. ABCR is a member of the ATP binding cassette transporter superfamily [60, 152]. It is composed of a single polypeptide arranged in two tandem halves. Each half is composed of a transmembrane domain, a nucleotide binding domain (NBD) and a glycosylated extracytoplasmic domain [152-154]. ABCR is a highly abundant protein in the rod outer segments at approximately 3% of the total protein [25, 155].

Photoaffinity labeling indicates that ABCR specifically binds ATP and GTP and all-trans-retinal increases the ATPase activity in an uncompetitive manner [156]. Further studies have also indicated that NRPE can bind to ABCR [122, 144]. Sun and Nathans have proposed the mechanism of transport action by ABCR shown in Figure 1.11 [123]. The NBD-1 is required to activate the ligand-binding site from a low affinity to a high affinity state on the luminal side. NBD-2 functions in the same manner, but for the cytosolic side. The hydrolysis of both NBDs closes their respective sites. ABCR acts by flipping the substrate from the lumen of the rod outer segments to the cytosolic side using the hydrolysis of ATP [123, 145]. The alteration of binding and hydrolysis of ATP allows the transport of ligand to be unidirectional.

Figure 1.11: Proposed ABCR transport mechanism [123].



Retinal Dystrophies and Damaging Factors

With the knowledge of some of the components of lipofuscin and the process of how it is formed, a new understanding of the mechanisms of damage in retinal maculopathies can be attained. In Stargardt's patients, the connection between ABCR and lipofuscin accumulation is well established. This is not the case with AMD and other maculopathies. In addition to lipofuscin accumulation, a number of other mechanisms of damage are proposed for AMD, including inflammation, mitochondrial dysfunction, nutritional deficiencies, smoking, diabetes and phototoxicity.

Many experiments have shown that long-term exposure to visible light is a potential initiator of AMD damage, particularly blue light [7, 157, 158]. For example, rats maintained at higher light environments exhibit a decrease in photoreceptor density [159]. High oxygen concentrations may also contribute to lipofuscin accumulation and photoreceptor cell death [136, 159]. Both mitochondria and PUFAs have been implicated [150, 160]. The presence of light enhances the damage due to oxygen, both in vitro and in vivo. The combination of light and oxygen is termed photooxidative damage.

Oxygen acts as a double-edged sword. It is required for life as the terminal electron acceptor in the electron transport chain, yet it has the ability to generate reactive oxygen species (ROS) from mitochondrial inefficiencies. Atmospheric oxygen is a biradical where both electrons have parallel spins and it is referred to as

the triplet state. Activation of oxygen can occur through two distinct mechanisms. The direct absorption of sufficient energy to alter the spin on one of the unpaired electrons to produce singlet oxygen is a Type II reaction. The other process occurs through the reduction of oxygen through electron or hydrogen abstraction and is a Type I reaction [49, 113, 150, 161]. Figure 1.12 A shows some of the oxygen-derived metabolites and their respective half-lives. Type II reactions form singlet oxygen species, where type I reactions can form superoxide anion, hydrogen peroxide and hydroxyl radicals. ROS' have been observed to crosslink proteins, react with PUFAs to form peroxides and peroxy radicals (Figure 1.12 B) and even produce mutations in DNA [113, 150, 160-162]. Of all of the ROS', only hydrogen peroxide crosses membranes with any efficiency. Many compounds in the eye act as photosensitizers, i.e., absorb a photon of light to form an excited state that can then form ROS' or react directly with organic molecules [161]. Both ATR and protonated NRPE have the ability to cause photooxidative damage of ABCR, which then inhibits its function, resulting in a further increase in ATR and subsequent rise in lipofuscin accumulation [143, 163].

Studies with lipofuscin have shown that it is a generator of singlet oxygen, superoxide anions, hydrogen peroxide and lipid peroxides when irradiated with blue light [164-166]. Irradiation of A2E-challenged RPE cells causes a loss of cell viability, but this effect was blocked in oxygen-depleted medium [167, 168]. The mechanism of cell death was proposed to be apoptosis [169, 170]. Both lipofuscin granules and A2E-fed RPE cultures have also been shown to inhibit lysosomal

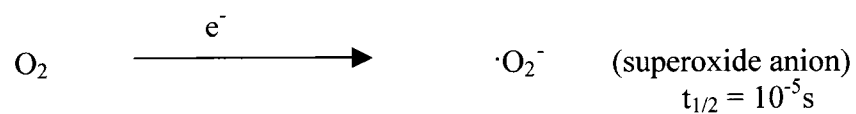
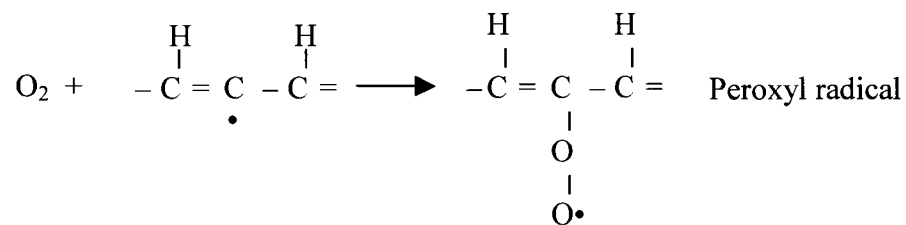
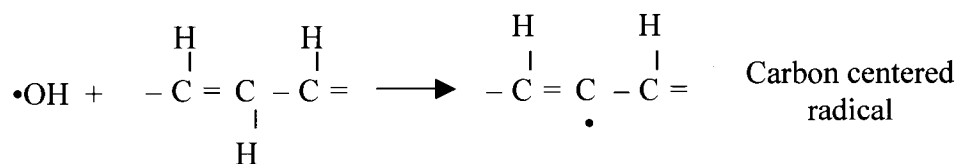
Figure 1.12: Reactive oxygen species. A) Type I and Type II mechanisms; B) Peroxidation reactions.

A.

Type II Reaction:



Type I Reactions:

**B.**

enzymes upon blue light irradiation [56, 171-173]. Due to its amphiphilic nature, A2E acts like a detergent and destabilizes lysosomal and other cellular membranes [56, 140, 171, 173, 174]. A2E will also undergo photooxidative changes to form highly reactive products [121]. Many of the oxidized A2E compounds isolated from lipofuscin have been reproduced in vitro upon blue light irradiation of A2E in the presence of oxygen [147, 175-178].

As previously discussed, melanin appears to be photoprotective to RPE cells by scavenging free radicals and ROS', inhibiting lipid peroxidation, absorbing light and binding multivalent transition metals. Other studies have shown the potential for its photocytotoxicity [73, 179-181]. There is a decrease in melanosomes with age and concomitant increase of complex particles [61, 74, 86, 87]. These complex particles are melanosomes encased in other material and are termed melanolipofuscins and melanolysosomes [45, 179, 182]. Macular RPE has higher concentrations of complex particles than non-macular areas. RPE of individuals over the age of 90 showed no pure melanosomes remaining [183]. Over decades, degradation of melanin polymers by hydroxyl radicals is proposed to alter the melanin structure [184, 185]. In essence, the photoprotective effect of melanin is likely to be altered over decades by phototoxicity in a similar fashion as lipofuscin.

AMD, Stargardt's disease and other retinal maculopathies are probably induced because of high levels of oxygen, light and PUFAs, primarily in the macula. There is likely a threshold level of damage that each RPE cell can sustain before cell death occurs. There are many hypothesized mechanisms as far as attaining the

threshold level, which include; age-related declines in RPE cells cause an increase in burden of phagocytosis, lipofuscin concentrations are highest in the macula and photoprotective agents such as enzymes, vitamins and melanin also decrease with age, thereby increasing the likelihood of ROS'. This further increases lipofuscin accumulation and, as a photosensitizer, induces more ROS'. Large accumulations of superoxide and lipofuscin have been observed to cause diminished RPE phagocytosis and likely result in photoreceptor death. In an attempt to remove the undegradable lipofuscin, it has been hypothesized that drusen deposits occur, which can cause further problems associated with nutrient deficiency and waste accumulation. Heredity, diabetes, smoking, and health throughout an individual's life will likely affect each individual's progression of lipofuscin accumulation.

Purpose

The ABCR protein plays a key role in processing photoreceptor pigments. We propose that mutations in the protein, whether genetic or photoinduced, cause increases in lipofuscin compounds, which leads to RPE cell death in retinal maculopathies. In this study, several tools have been developed that will allow the testing of this hypothesis. The compound that is predominant in individuals with mutations in the ABCR protein causes RPE cell death and becomes converted into known lipofuscin components.

To comprehend ABCR and its implications in disease, the protein's structure

and function must be established. Although research indicates that ATR and NRPE bind to ABCR, the binding site needs to be elucidated to determine the mechanisms of the protein's function. Binding sites are not simply a short string of amino acids, but are usually key amino acids that are in proximity to each other due to the protein's tertiary structure. Knowledge of the structure of the protein will produce a large amount of information about the function. Key mutations in the amino acid sequence can help to understand the dysfunction found in the genetic diseases, such as Stargardt's disease, RP and CRD. The issue is even more complex in AMD because ABCR seems to be very susceptible to photooxidative damage by ATR.

Prior to any biochemical analysis of a protein, an adequate supply of sample that can be purified and concentrated is essential. Since human tissue is difficult to obtain, dissection of animal eyes for the isolation of ABCR has to be performed, but it is cumbersome and time consuming. During the isolation process, ABCR could undergo potential photooxidative damage. It would be more advantageous to isolate the protein from transfected cells with cloned human ABCR. Because of the extensive post-translational modifications, the protein must be transfected in a mammalian cell line to produce a properly folded and functional protein.

Additionally, utilizing a selectable transfection system that is inducible allows *de novo* synthesis of the protein under controlled conditions. This cell system can then be used to understand ABCR in a cellular environment beyond biochemical analysis.

The first goal of this research was to isolate full-length human ABCR protein expressed in a selectable and inducible cell system. Accordingly, Chapter 3 presents

the work involved in inserting the unusually large gene into host cells and determining whether the protein was expressed. Human ABCR DNA was obtained and amplified by PCR. The PCR product was ligated into the pGene vector and transfected into pSwitch CHO cells. The cells were grown in medium that contained antibiotics to inhibit the growth of non-transfected cells. Confluent cultures were induced and the protein was isolated and purified by a Ni-NTA column. The protein was analyzed by dot blot and western blot with two different antibodies and a histidine probe.

The second goal was to determine the intracellular localization of the protein by expressing a fusion protein consisting of ABCR and green fluorescent protein (GFP). Chapter 4 utilizes the ABCR plasmid produced in Chapter 3. Also, a new plasmid construct was produced by the ligation of the ABCR plasmid with a GFP-PCR product. The new plasmid was stably transfected into new pSwitch CHO cells and induced. The cells were analyzed using confocal microscopy at various time points to detect the GFP fluorescence. Additionally, the fusion protein was isolated by cell fractionation, purified and subsequently analyzed by western blot. Multiple analyses were performed throughout both cloning processes to ensure sequence integrity so that downstream applications would not be affected.

Since ABCR dysfunction has been attributed to an increase in lipofuscin in the RPE, studies on the effects of this accumulation are required. Very little research on the cytotoxicity of lipofuscin has been performed due to its hydrophobicity and the lack of donor tissue. In an attempt to understand the effects of increased lipofuscin

accumulation, A2E has been used in its place.

Primary cell culture has been a useful tool in understanding the cytotoxicity of RPE cells. The lack of human tissue and the variation in genetics facilitated the need for established cell lines, but at the expense of an altered phenotype. Ideally, RPE cell lines should behave similar to their *in vivo* counterparts prior to any cytotoxicity studies.

The third goal of this project was to generate procedures for culturing a RPE cell line that behaves similar to *in vivo* cells. The work presented in Chapter 5 addresses the cell culture protocols for the establishment of a new cell line. The spontaneously immortalized cell line, herein called tRPE, was compared morphologically to RPE cells from the eye and from primary cultures. The tRPE cells were characterized by reverse transcriptase PCR and immunocytochemistry to determine the origin and degree of differentiation. Several transformation characteristics were tested to verify whether the tRPE was a transformed cell line. The final goal of this project was to expand the use of the tRPE as a model for AMD through cytotoxicity studies. More specifically, the phototoxicity of lipofuscin and A2PE was analyzed. Chapter 6 includes the analysis of RPE cells that had previously been fed A2PE and then irradiated. Analysis of the cells included live/dead assays, apoptosis assays and mass spectrometry to determine the alteration of A2PE into known lipofuscin components.

CHAPTER 2

MATERIALS AND METHODS

Office of Research Compliance

All work using DNA, plasmids, recombinant DNA and radioactive chemicals were presented and reviewed by the Office of Research Compliance (ORC). ORC number 140 was granted for the research entitled “Mechanistic Studies of Photooxidative Damage to the Human Eye.” All recombinant DNA work was performed in accordance with National Institute of Health protocols for research involving recombinant molecules [186].

Bacterial Media Preparation

Miller’s Luria-Bertani (LB) Broth (Fischer Biotech) was prepared according to the manufacturer’s directions and autoclaved, then stored at 4 °C. Miller’s LB Agar was prepared, autoclaved and placed in a 55 °C water bath to allow it to cool, but not solidify. The liquid agar was poured in 100 mm x 15 mm sterile dishes and then a Bunsen burner was used to flame the top of the liquid agar to remove any bubbles and to sterilize the top.

Where applicable, the agar was allowed to cool to 55 °C before the addition of ampicillin. A filter-sterilized solution of ampicillin (Sigma) in distilled-deionized water (dd-H₂O) was added to the agar solution to produce a final concentration of 100 µg/ml. The solution was mixed on a stir plate prior to pouring.

Cell and Tissue Media Preparation

The media known herein as DMEM with antibiotics was a mixture of high glucose DMEM (Gibco), 22.3 mM N-[2-Hydroxyethyl]piperazine-N'-[2-ethanesulfonic acid (HEPES) from Sigma, 8.8 mM sodium bicarbonate, and 1% antibiotic/antimycotic (Sigma). The pH of the solution was adjusted to 7.35 and then filter-sterilized. RPMI Media (Gibco) was prepared in the same manner as DMEM. pSwitch cell lines used a combination of DMEM and RPMI at a 1:1 ratio. For white light irradiation experiments, DMEM with 5.55M Glucose, HEPES, and sodium bicarbonate, but without phenol red and antibiotics, was used.

Conditioned media contained the same ingredients as DMEM with antibiotics plus 1 ng/ml basic fibroblast growth factor (bFGF), 50 ng/ml all-trans retinoic acid, 0.25 mM ascorbic acid, 100µg/mL Heparin, 10 ng/mL epithelial growth factor (EGF) and 1X ITS+3 Liquid Media supplement (Sigma).

Sub-cloning of ABCR

The pRK5/ABCR, which was kindly donated by Dr. Jeremy Nathans from Johns Hopkins School of Medicine [26], was transformed into supercompetent *E. coli* cells, isolated and characterized by restriction enzyme analysis. The ABCR gene was amplified using pRK5/ABCR as a template for the PCR with Pfu Turbo DNA Polymerase (Stratagene). The primers, ABCR-F and ABCR-R, were engineered to include new restriction sites and an enterokinase site at the C terminus. An experimental schematic is shown in Figure 2.1. All primers used for the subcloning of ABCR into pGene are given in Table 1, where the partial sequences are the portions of the primers that initially anneal to the template. PCR product was purified and a double restriction digest with Hind III and Not I was performed. The same digestion was performed on the pGene vector. Both samples were purified and the sticky ends of the PCR product and pGene were ligated together using Takara ligase.

Purified ligation product was transfected into electrocompetent *E. coli* cells and grown on ampicillin plates for selection. Colonies were isolated and the clones were analyzed for the presence of the plasmid by alkaline lysis using the method in Sambrook, et al. [187]. Positive colonies were grown and the plasmid was purified. PCR reactions were done to screen for the presence of a 1 kb segment within the ABCR gene with Taq Polymerase (Fisher), ABCR-IF and ABCR-IR. Additionally, PCR of the pGene/ABCR junction was performed with Front-F and Front-R to determine that the gene was in the correct orientation. Sequencing was performed

Figure 2.1: Schematic of the pGene/ABCR/ENT/V5/His construct.

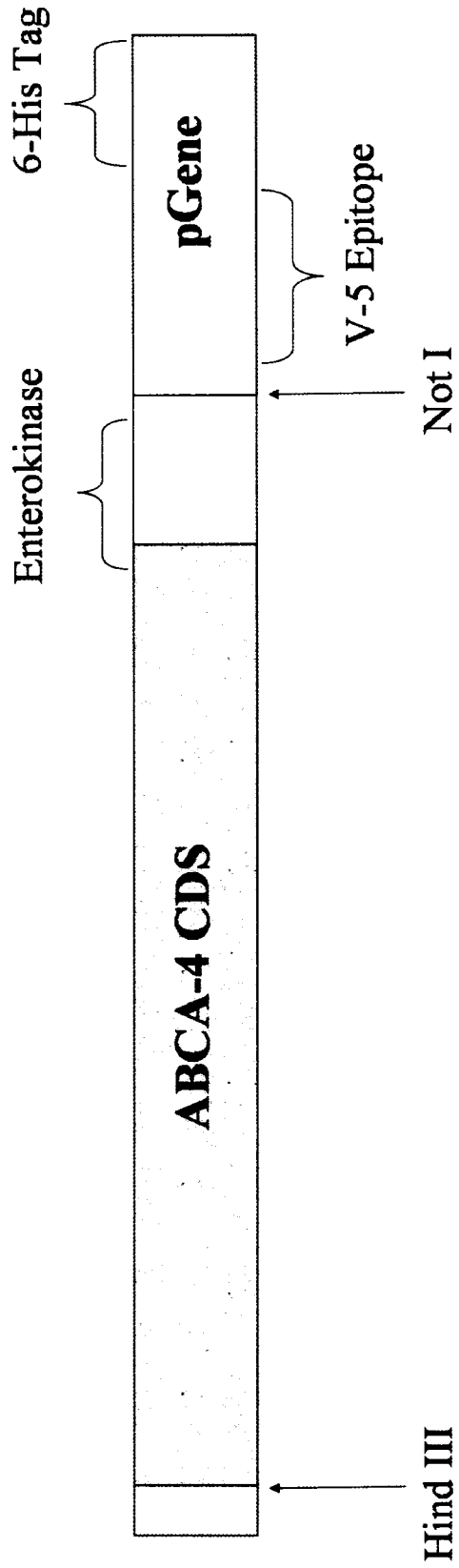


Table 1: Primer characteristics used for the production and analysis of pGene/ABCR/ENT/V5/His.

Primer Name	Sequence	Full or Partial	T_m (°C)	Length	G+C%
ABCR-F	ATTACCATGGGCTTCGTGAGACAG	Partial	58.9	24-mer	50.0
	CGGTGGAAGCTTATTACCATGGGCTTCGTGAGACAG	Full	72.9	36-mer	52.8
ABCR-R	TCCTGGGCTTGTCGACTG	Partial	57.2	18-mer	61.1
	GCATTTGCGGCCGCTTTATCATCATCATCCTGGGCTTGTCGACTG	Full	76	45-mer	53.3
ABCR-IF	CCTTACTCGAGACGCTCAAT	Full	57.3	20-mer	50.0
ABCR-IR	TCCATGCTGAAGAAGGTGTA	Full	55.3	20-mer	45.0
FRONT-F	ATCGGAGCTCGTTTAGTGAACCGT	Full	62.7	24-mer	50.0
FRONT-R	ACTGAGTCAGACAGGCCGATGTTT	Full	62.7	24-mer	50.0
REAR-F	ACAACATGCTCCAGTTCAGGTCT	Full	62.7	24-mer	50.0
REAR-R	GCATGCCTGCTATTGTCTTCCCAA	Full	62.7	24-mer	50.0

between the 3' end of ABCR and the 5' end of pGene to ensure that the V5 epitope and histidine tag were in frame with the PCR product using Rear-F and Rear-R primers. Dr. Scott Grayburn in the Department of Biological Sciences at Northern Illinois University performed all sequencing.

Linear plasmid was incorporated into pSwitch CHO cells with Lipofectamine 2000 (Invitrogen) and grown in RPMI/DMEM with 10% FBS, 100 µg hygromycin B/ml and 200µl of zeocin/ml to select for pGene positive clones according to manufacturers' protocols [188, 189]. Individual clones were isolated by cloning rings and subcultured.

Cell Membrane Preparation

Cells were placed in a hypotonic solution (10 mM NaCl, 1.5 mM MgCl₂, 1.63 mM CHAPS and 1x Halt Protease Inhibitor Cocktail [Pierce]) and briefly sonicated. The membrane fraction was isolated by centrifugation at 50,000 g for 2.5 hours at 4 °C. The cell pellet was resuspended in a buffer (20 mM Tris, 2% SDS, 10% Glycerol, 1% Triton-X 100 and 10% β-mercaptoethanol at pH of 7.4) and homogenized using a Dounce homogenizer. The solution was heated at 55 °C for 20 minutes and then was diluted ten-fold in phosphate buffer (50 mM sodium phosphate monobasic, 300 mM NaCl, 10 mM imidazole, protease inhibitor at pH of 8.0). The solution was concentrated using an Amicon Ultra regenerated cellulose 100 KDa molecular weight cutoff condenser for 24 hours at 4 °C until the total volume was reduced by 40-fold

[190]. Isolation of ABCR by the histidine tag was performed with Qiagen's Ni-NTA Spin Kit according to manufacturer's protocol [191].

Western Blotting

Concentrated cell membrane solution or molecular weight markers were pipetted into wells of 4-20% Tris-HEPES-SDS polyacrylamide gels (Pierce) in a Mini-PROTEAN II Electrophoresis cell (BioRad). SDS-PAGE gels were transferred to nitrocellulose using a BioRad transfer apparatus connected to a Lauda K-2/RD (Brinkman Instruments) refrigerated heat exchanger set at -8°C performed at 70 V for 7 hours in Dunn's transfer buffer (10mM NaHCO_3 and 3mM Na_2CO_3) with 1.4 μM SDS. The nitrocellulose was then blocked in SuperBlock (Pierce) with 0.05% Tween-20 (Surfacamps) for 1.5 hours.

Goat- α -ABCR

Primary antibody was diluted for a final concentration of 20ng/mL. Each membrane was incubated for 2 hours at room temperature and then rinsed with high salt TTBS (500mM NaCl, 10 mM Tris Base and 0.05% Tween-20 at pH of 7.6) for 5 minutes. Monoclonal donkey- α -goat HRP was diluted to a final concentration of 10 ng/mL in 10% SuperBlock in high salt TTBS. The membranes were soaked for 1 hour at room temperature while shaking and then washed in high salt TTBS 5 times at 10 minutes each with a final wash in PBS for 5 minutes.

Mouse- α -V5

Primary antibody was diluted to a final concentration of 10ng/mL. Each nitrocellulose membrane was incubated at 4 °C overnight using an orbital shaker. The membrane was washed using TTBS (10 mM Tris Base, 250 mM NaCl, 0.05% Tween 20 at a pH of 7.57) 2 times at 10 minutes each at room temperature. Goat- α -mouse HRP (Pierce) was diluted to a final concentration of 2ng/mL and incubated with the membrane for 1 hour at room temperature while shaking. The membrane was washed using the same protocol as the goat- α -ABCR, but low salt TTBS was used.

HisProbe-HRP

Nitrocellulose membranes were washed twice in TTBS after blocking in SuperBlock. Reconstituted HisProbe-HRP at a final concentration of 176ng/mL was used according to manufacturer's protocol [192].

Substrate

All washed membranes were incubated with SuperSignal West Femto Maximum Sensitivity Substrate per manufacturer's protocol [193]. Membranes were exposed to CL-XPosure Film (Pierce) until a signal developed.

Membrane Stripping

Probed nitrocellulose membranes were stripped with Restore Western Blot

Stripping Buffer (Pierce) to reprobe the same membrane. Optimization of the procedure was performed by testing under various conditions, such as substrate-only or secondary antibody incubation followed by substrate as per manufacturer's instructions [194].

Dot Blotting

Confluent transfected pSwitch CHO cells were induced with mifipristone (Invitrogen) under various concentrations and times. MOPS A solution (40 mM MOPS, 1 mM EDTA, pH of 7.2) was used to resuspend the cells to a final concentration of 2.3×10^7 cells per ml, and the solution was sonicated. Crude cell extracts were mixed with SDS loading buffer (1.05% SDS, 62.5mM Tris, 10% Glycerol, 137 mM NaCl, 1% Non-idet 40, 2 μ g/ml Aprotinin, 1mM PMSF, protease inhibitor [BioVision Inc], 1.5mM EDTA and 6% v/v β -mercaptoethanol) at a 1:1 ratio and then heated for 20 minutes at 55 °C. Immobilon P^{SQ} (Millipore) membrane was prepared according to manufacturer's protocols [195].

Equal volumes of crude extract were vacuum-adsorbed in a BioRad BIO-DOT Apparatus. The membrane was blocked with 10% non-fat dry milk (NFDM) on an orbital shaker for 1 hour. Proteins were detected with the α -V5 antibody as previously described.

Sub-cloning and Expression of ABCR/ENT/RSGFP Fusion Protein

All materials and methods for the production of pGene/ABCR/ENT/V5/His were followed identically, with the following exceptions. Red-shifted green fluorescent protein was amplified by PCR using pBIN 35 mGFP4 as the template. The plasmid was kindly donated by Dr. Tom Sims from the Department of Biological Sciences at Northern Illinois University. Amplification by PCR included new restriction enzyme sites engineered in the primers RSGFP-F and RSGFP-R. The sequences and characteristics for the primers used in the production of pGene/ABCR/ENT/RSGFP/His are given in Table 2.

Both the pGene/ABCR/ENT/V5/His plasmid and the RSGFP PCR product were cut with Age I and Not I restriction enzymes. The insert and vector were ligated together, purified and transformed into *E. coli* cells by electroporation. Rear-F and Rear-R were used as a PCR screen for the presence of RSGFP in the transfectants. Four sequences were performed using Rear-R, Rear-F, EGFP-SF and EGFP-SR to sequence the entire DNA from the 3' end of the ABCR construct to the 5' end of the pGene plasmid. Purified plasmid was linearized with Pvu I and transfected into pSwitch CHO cells.

Microscopy of ABCR/RSGFP CHO Cells

Approximately, 1.0×10^4 transfected CHO cells were cultured on sterilized glass cover slips (Gold Seal No. 1) in 6 well plates with hygromycin and zeocin. Each

Table 2: Primer characteristics used for the production and analysis of pGene/ABCR/ENT/RSGFP/His.

Primer Name	Sequence	Full or Partial	T_m (°C)	Length	G+C%
RSGFP-F	TTTGTATAGTTCATCCATGT	Partial	47.1	20-mer	35.0
	GCGCGGACCGGTTTTGTATAGTTCATCCATGG	Full	65.0	32-mer	53.1
RSGFP-R	AGTAAAGGAGAAGAAGACTTTTC	Partial	47.6	21-mer	33.3
	GAGGAAGCGGCCGCAAGTAAAGGAGAAGAAGACTTTTC	Full	65.3	36-mer	50.0
REAR-F	ACAACATGCTCCAGTTCAGGTCT	Full	62.7	24-mer	50.0
REAR-R	GCATGCCTGCTATTGTCTTCCCAA	Full	62.7	24-mer	50.0
EGFP-SF	AGGATCGAGTTAAGGGAATCG	Full	66.3	22-mer	50.0
EGFP-SR	GACTTCAGCACGTGTCTTGTAG	Full	61.5	22-mer	50.0

culture was induced with mifipristone for 16 hours and then the media was removed, followed by washing with PBS. Coverslips were placed on the slides and sealed around the edges with S/P Accumount 280 mounting medium (Baxter Scientific).

Each clone was viewed using a Zeiss Axiovert 100 Confocal microscope with a LSM 5 PASCAL laser modulator. A plan-neofluor 63x objective was used for all observations. The images were saved as LSM files and Image J was used to import files to save as tif files. Adobe Photoshop was used to overlay the pictures.

Cell Fractionation of ABCR/RSGFP CHO Cells

The Plasma Membrane Protein Extraction Kit (BioVision) was used for cell fractionation. The membrane and cytosolic portions were analyzed by SDS/PAGE and by western blotting according to previously stated protocols.

Isolation and Characterization of Immortalized RPE Cells

RPE cells were isolated and cultured by a modified technique described by Chang et al. [196]. Primary RPE cells were obtained from fresh calf eyes (Brown Packaging, S. Holland, IL) that were shipped on ice for a period of no more than two hours after extraction from the calf. Cells were grown in DMEM with 10% FBS with antibiotics at 37 °C and 5% CO₂.

Seven different primary explants were observed from the cultures and they were removed using cloning rings. Each of these clones was grown under low-

density conditions and a single colony was isolated from each, again with cloning rings.

Isolation of Primary RPE sheets

RPE sheets were isolated by a modified technique described by Ho et al. [106]. Exposed RPE cells were layered with 100 μL of 12% 175 Bloom porcine gelatin (Sigma) in a chilled eyecup. The eyecup was placed in a 4 $^{\circ}\text{C}$ cold room for 10 minutes to allow the gelatin to solidify. The RPE/gelatin was then placed on sterile glass microscope slides with the basal lateral side of the RPE towards the glass. The slides were then incubated at 37 $^{\circ}\text{C}$ for 5 minutes to melt the gelatin.

Extracellular Matrix Preparation

Bovine corneal Extracellular matrix (ECM) preparation was performed by a technique described by Campochiaro and Hackett [197]. Matrigel (BD Biosciences) was diluted 1:1 with DMEM without phenol red, antibiotics or FBS. The Matrigel/DMEM was layered onto chilled tissue-culture plastic at a ratio of 50 $\mu\text{l}/\text{cm}^2$ [198].

Reverse Transcriptase-PCR

RT-PCR was performed to determine whether the tRPE cells expressed specific mRNA that could identify them as originating from the RPE, since choroidal

melanocytes and other cells could have contaminate the cultures. Table 3 contains all of the primers used for reverse transcriptase PCR.

Total RNA isolation was done by guanidine isothiocyanate/Cesium Chloride Ultracentrifugation [199]. A phenol/chloroform purification followed with ethanol condensation [187]. The mRNA was isolated using Oligotex® (Qiagen) following manufacturer's protocol [200]. RT-PCR was performed using Sensiscript™ RT Kit [201] and HotStart*Taq* PCR Core Kit [202] all from Qiagen. Total cDNA from each sample was analyzed for the expression of each respective gene.

Immunocytochemistry

Passage 50 tRPE cells were grown on bovine corneal epithelium-derived extracellular matrix in 6-well plates and fed with conditioned medium. Three controls were used: one that had both antibodies, but no cells; another that had not been incubated with primary antibody; and the final control had not been incubated with secondary antibody.

Zonula Occludens-1

Confluent tRPE cultures were fixed in 4% paraformaldehyde, blocked with 3 % BSA (Sigma) for 1 hour and incubated with goat polyclonal α -ZO-1 (Santa Cruz Biotechnology) overnight at 4 °C while shaken. Cultures were twice washed in TTBS for 10 minutes and then incubated for 1 hour with a fluorescein-isothiocyanate (FITC)

Table 3: Characteristics of primers used for reverse transcriptase polymerase chain reaction (RT-PCR) of tRPE Cells.

Gene		Primer Sequence	Length	T _m (°C)	Annealing Temp	G+C %	Product size
CRALBP	forward	AGA ACT CTC CAG CTT CTA CCA GGA	24 bp	60.2	55 °C	50	301 bp
	reverse	AGC TTG GGA GGA GGA TGA CAT CTG	24 bp	59.8		50	
β-Actin	forward	TCA TGA TCG AGA CCT TCA ACA CCC	24 bp	60.3	55 °C	50	288 bp
	reverse	AGC AGA GCT TCT CCT TGA TGT CAC	24 bp	60.1		50	
RPE-65	forward	CCA GGG CTG CTG AGG TGG TTA ACA	24 bp	60	55 °C	50	278 bp
	reverse	GTG CCT GTC TCA CGA AGT ACG ATT	24 bp	60.1		50	
Vimentin	forward	ATG AAG GAA GAG ATG GCT CGT CAC	24 bp	59.9	57 °C	50	173 bp
	reverse	TCC AGA TTG GTT TCC CTC AGG TTC	24 bp	60		50	
Tyrosinase	forward	TAA CAG AAC CTG CCA GTG C	19 bp	52.7	60 °C	52.6	900 bp
	reverse	CTT TCT GTG CAG CGG GGT CCC CTA GA	26 bp	62.5		60	

conjugated bovine α -goat IgG (Santa Cruz). The monolayer was washed 3 times in TTBS and then covered in 1 mg/ml Hoechst 33285 in PBS for 15 minutes at 37 °C.

RPE-65

Cultures of differentiated tRPE cells were fixed in a 4% paraformaldehyde, washed 3 times in TTBS with 0.1% Triton X-100, blocked in 3% BSA and then incubated overnight while shaken at 4 °C with monoclonal rabbit α -RPE-65. The antibody was kindly donated by Dr. Rosalie Crouch from the Department of Ophthalmology at the Medical University of South Carolina [203]. The cells were washed 3 times at 10 minutes each in TTBS and then incubated with FITC-conjugated polyclonal donkey α -rabbit IgG (Santa Cruz). They were then washed 3 times in TTBS for 10 minutes each and Hoechst stain was added as described above.

Vimentin

Sub-confluent tRPE cells were permeabilized by freezing them for 2 minutes; the culture was then fixed with -20 °C methanol for 10 minutes and then washed 3 times with PBS for 5 minutes. Blocking was done with 3% BSA for 1 hour and then incubated overnight at 4 °C with Rabbit α -vimentin (Santa Cruz). The cultures were washed twice with TTBS before adding FITC-conjugated polyclonal donkey α -rabbit antibody (Santa Cruz) and allowing it to incubate for 1.5 hours. The culture was washed and the nuclei were stained in the same manner as the ZO-1 inoculation.

Pan-Cytokeratin

Confluent tRPE cells were permeabilized, fixed and blocked in the same manner as the vimentin immunocytochemistry culture. Rabbit α -pan-cytokeratin (Santa Cruz) was incubated at 4 °C overnight. The vimentin protocol was followed for the remainder of the experiment.

Bestrophin

The cultures were fixed in 4% paraformaldehyde for 20 minutes and then the cells were washed 3 times in PBS with 0.1% Triton X-100 at 10 minutes each. The cells were blocked with 1% BSA for 1 hour and washed twice with TTBS. Polyclonal rabbit anti bestrophin, which was kindly donated by Dr. Alan Marmorstein from the Cole Eye Institute [38], was incubated at 4 °C overnight. The cells were washed 4 times with TTBS for five minutes each wash. For the remaining steps, the vimentin protocol was followed.

Imaging

All cells were viewed with a Nikon Eclipse TS100 inverted fluorescent microscope with an OSRAM HBO Mercury Short Arc lamp. Four filter cubes were used. The CFP/dsR FRET filter cube had an excitation range of 426-446 nm and an emission range of 460-500 nm with a dichroic mirror cutoff at 455nm. The TRITC HQ filter cube had an excitation range of 530-550 nm and an emission range of 590-650 nm with a dichroic mirror cutoff at 565nm. The FITC HQ filter cube had an

excitation range of 450-500 nm and an emission range of 510-560 nm with a dichroic mirror cutoff at 505nm. The cells were imaged using a Nikon Cool-Pix camera at 3.5 megapixels attached to the microscope. Images were processed using Adobe PhotoShop.

Chromosome Preparation

Chromosome preparation followed protocols established by Griffiths and Carpenter [204]. Passaged cells were allowed to divide for 24 hours and then 0.5µg/ml colcemid and 0.5µg/ml vinblastin was incubated in the medium for 1 hour. Suspended cells were incubated in a 0.8% sodium citrate hypotonic solution, fixed in a 3:1 methanol/acetic acid solution and the suspension was dripped onto the slides at 30 inches and allowed to dry. Staining was done using Carrazi's Alum Hematoxylin. The chromosomes were counted using a Zeiss microscope with an attached CRT screen to amplify the image of each cell.

Suspension Growth

Approximately 3.8×10^5 tRPE cells and CHO-AA8 cells were incubated in 15 ml of DMEM plus 10% FBS and antibiotics using a roller drum apparatus (New Brunswick). A 0.5 ml sample of cells was counted in triplicate with a Coulter cell counter on days 0,1,5,7,9 and 11. The number of cells was compared to the initial cell counts.

³H Emulsion Autoradiography

Autoradiography was performed *in situ* by a modified technique described by Hopwood and Tolmach [205]. All protocols using radiation were approved by the NIU Radiation Safety Committee and in compliance with the Illinois Department of Nuclear Safety standards for protection against radiation.

RPE cells were grown to confluency in DMEM plus 10% FBS over the next 15 days. The plates were incubated with ³H thymidine for 4 hours at 37 °C. The medium was aspirated off of the cultures and the cells were washed twice with cold PBS. Next, 4% perchloric acid solution was added to the plates and placed at 4 °C for 4 days. The cells were fixed for 10 minutes in 3:1 methanol/acetic acid and allowed to dry overnight at 4 °C.

The cells were then overlaid with NTB-3 (Kodak) autoradiographic emulsion according to manufacturer's protocols [206]. The plates were placed in light-tight boxes placed at 4 °C for five days.

The plates were developed with KODAK D-19 developer, rinsed with ddH₂O and then fixed with KODAK Fixer for 3 minutes with a final rinse in ddH₂O. The plates were stained in Carrazi's Alum Hematoxylin (0.1% hematoxylin, 0.21 M Aluminum ammonium sulphate, 20% glycerol, 1.01mM Sodium iodate) for 15 minutes and then were rinsed. Each plate was coded to ensure that the experimenter had no bias. The number of heavily labeled cells for each coded plate was determined and compared to the total number of cells.

Repigmentation

Melanosomes were isolated from RPE cells from calf eyes by a technique described by Feeney-Burns [182]. The melanosomes were lyophilized and frozen until needed. The melanosomes were added to the media of confluent tRPE cells, as described by Boulton and Marshall, every 3 days for two weeks [207].

A2PE Quantitation

The A2PE was synthesized by Dr. L. B. Avalle. The samples were purified into different fractions by HPLC to ensure the purity of the sample and then dried under argon gas and placed at -80°C [208]. The different samples were dissolved in chloroform and a full-spectrum absorbance was taken using an Ocean Optics, Inc. S2000, spectrophotometer. Samples that had distinct absorbance at 335 nm and 457 nm were used for future experiments. The concentration of each sample was determined using an extinction coefficient of $33,000\text{ cm}^{-1}\text{M}^{-1}$, which is the extinction coefficient for A2E at 450nm. The samples were pooled together into one container for further experimentation and dried under Argon gas.

A2PE Feeding

In order to incorporate A2PE into the RPE cells gradually, A2PE (670 nM) in DMSO was added to 0.5 ml DMEM w/ FBS and thoroughly mixed in a sterile microcentrifuge tube, such that the final DMSO concentration did not exceed 0.5% of the total volume. This quantity was then fed to each well every four days to allow the

cells to uptake the A2PE. Controls were kept for this experiment by having wells that were fed from the sterile microcentrifuge tubes with only DMSO and DMEM. This daily process was repeated for a total of 4 feedings to give a total concentration of 7.37 mmol. The cells were allowed to incubate for a recovery period of 4 days in medium without A2PE.

Irradiation Studies

Philips 20 Watt Special Blue Bilirubin Bulbs (F20T12/BB) were used for all irradiations. To ensure that no UV is exposed to the cells, the cells were irradiated with the plastic lids on and covered with a ¼ inch Pyrex plate. The light was quantitated using a Li-Core Quantum sensor that detects light in the range of 400-700 nm. The total output of light from a fixed distance was determined to be 6.6 mW/cm². For all irradiations, the plates were placed at the same location to ensure that they received equivalent amounts of light.

Live Dead Analysis

Irradiated passage 7 ARPE-19 and passage 102 tRPE cells fed with A2PE were analyzed for cell viability. Initial experiments were performed using ethanol as a cytotoxic compound to determine the best concentrations of calcein AM and ethidium homodimer for RPE cells. The LIVE/DEAD Viability/Cytotoxicity kit (Molecular Probes) was used to determine the relative rate of death. Controls of A2PE cells that were not irradiated and cells that had no A2PE added were utilized.

Ethidium homodimer 1 was used at a final concentration of 0.5 μ M and Calcein AM was used at a final concentration of 1.5 μ M in PBS according to the manufacturer's protocol [209]. Hoechst 33258 was also used as a counter stain at a concentration of 1 mg/mL.

Apoptosis Analysis

Vybrant Apoptosis Assay Kit #2 (Molecular Probes) utilizing Alexa Fluor 488 annexin V/propidium iodide was used to determine apoptosis. The manufacturer's protocol was followed [210]. The same controls were used as the Live/Dead analysis. Additionally, Hoechst 33258 was used as a nuclear counter stain.

ESI-Mass Spectrometry of A2PE-Fed Cells

A2PE-fed RPE cells were trypsinized and released from the culture plates with a cell scraper. The solution was centrifuged to pellet the cells and resuspended in 2x ddH₂O and homogenized in a Dounce homogenizer. The solution was placed in a separatory funnel and 1x solution of chloroform/methanol (2:1) was mixed, shaken and allowed to settle. The organic soluble portion was removed and then dried under argon gas to remove all of the chloroform. The extract was resuspended in methanol with 0.1% formic acid and analyzed by LC-MS at a flow rate of 0.30 mL/min (Thermo Finnigan, LCQ Advantage Surveyor, ESI).

CHAPTER 3

SUB-CLONING AND EXPRESSION OF pGENE/ABCR/ENT/V5/HIS

Introduction

ABCR, which is also known as ABCA-4 or Photoreceptor Rim Protein, is a transmembrane protein found exclusively in the photoreceptor outer segments [123]. It belongs to the ATP-Dependent superfamily (ABC), which happens to be the largest of all gene classifications [154]. There are a number of genes in this group that have been found to cause disease in humans when mutated. Some examples and their respective diseases include CFTR, which causes cystic fibrosis, SUR, which causes unregulated insulin secretion, ABCA-1, which causes Tangiers disease, and MRPs, which aid in multi-drug resistance [211, 212]. All of the members of the ABC superfamily produce proteins that transport various molecules across a membrane and require energy in the form of ATP to translocate the molecules [213]. They are ubiquitous and have been found in every organism studied from bacteria to humans [214].

The ABCR model proposed by Bungert, et al. [152] is a protein composed of two similar ABC motifs. There are 2 transmembrane-spanning domains, which contain 6 transmembrane segments each that separate the exocyttoplasmic domains

(ECD) and the cytoplasmic domain [60]. The ECDs have 8 putative N-linked glycosylation sites, and a disulfide bond covalently links the 2 ECDs [152]. Each ECD faces the lumen of the rod outer segments. The cytoplasmic domain contains 2 nucleotide-binding domains (NBDs). Each NBD has the characteristic Walker A and B motifs found in all ABC proteins [153].

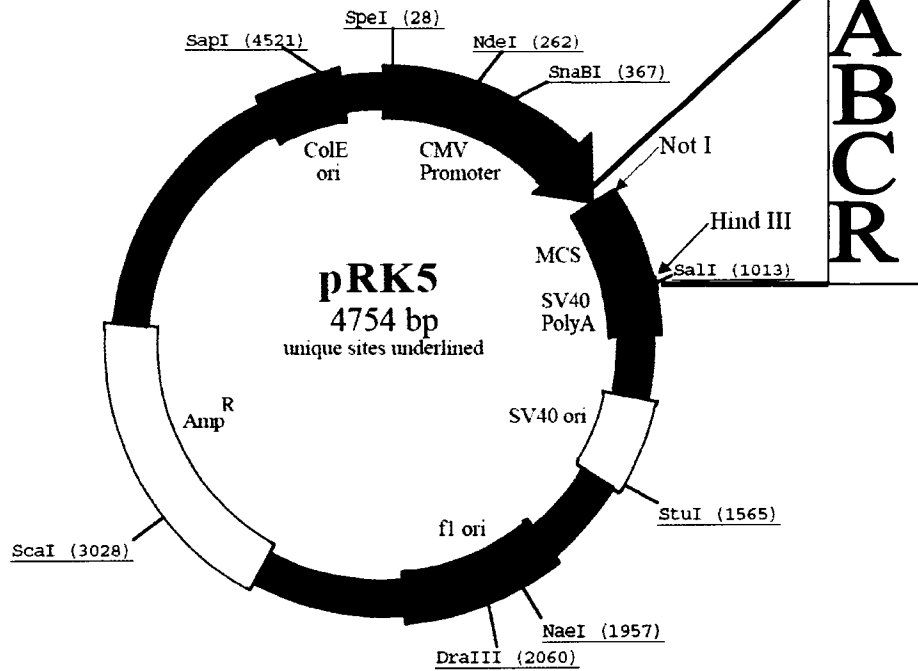
ABCR has been mapped to 1p22.1-p21 on the human chromosome and has a cDNA of 6,819 base pairs, which encodes a 2,273 amino acid protein [1]. The theoretical molecular weight was determined to be 256-kDa and the theoretical pI of 5.95 by ExPASy software [215]. Illing et al. have proposed that the apparent molecular weight of the protein is 220-kDa based on SDS-PAGE analysis [60].

The purpose of the research contained in this chapter was to isolate full-length human ABCR protein expressed in a selectable and inducible system. A mammalian cell line was needed to perform any post-translational modifications to the protein such as N-linked glycosylations, disulfide bond formation and to ensure proper folding to produce a functional ABCR protein. The ABCR cDNA was generated by Sun and Nathans [26] and placed in the pRK5 plasmid with a Not I restriction site on the 5' end of the gene and a Hind III restriction site on the 3' end, as seen in Figure 3.1A [216].

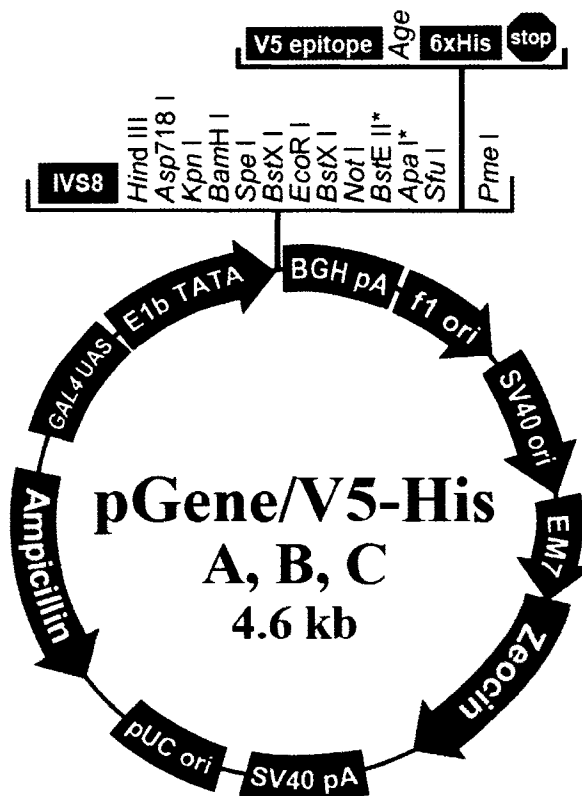
Sub-cloning was done in order to incorporate a 6x histidine fusion tag and an enterokinase site in the new protein. The enterokinase site will allow extraneous amino acids, from the V5 epitope and histidine tag, to be cut from the ABCR fusion protein so that the protein can be studied biochemically in its native form. The

Figure 3.1: Plasmid maps. A) Plasmid map for pRK5 with inserted ABCR [216]. B) Plasmid map for pGene/V5/ His with expanded multiple cloning site (MCS) [188].

A.



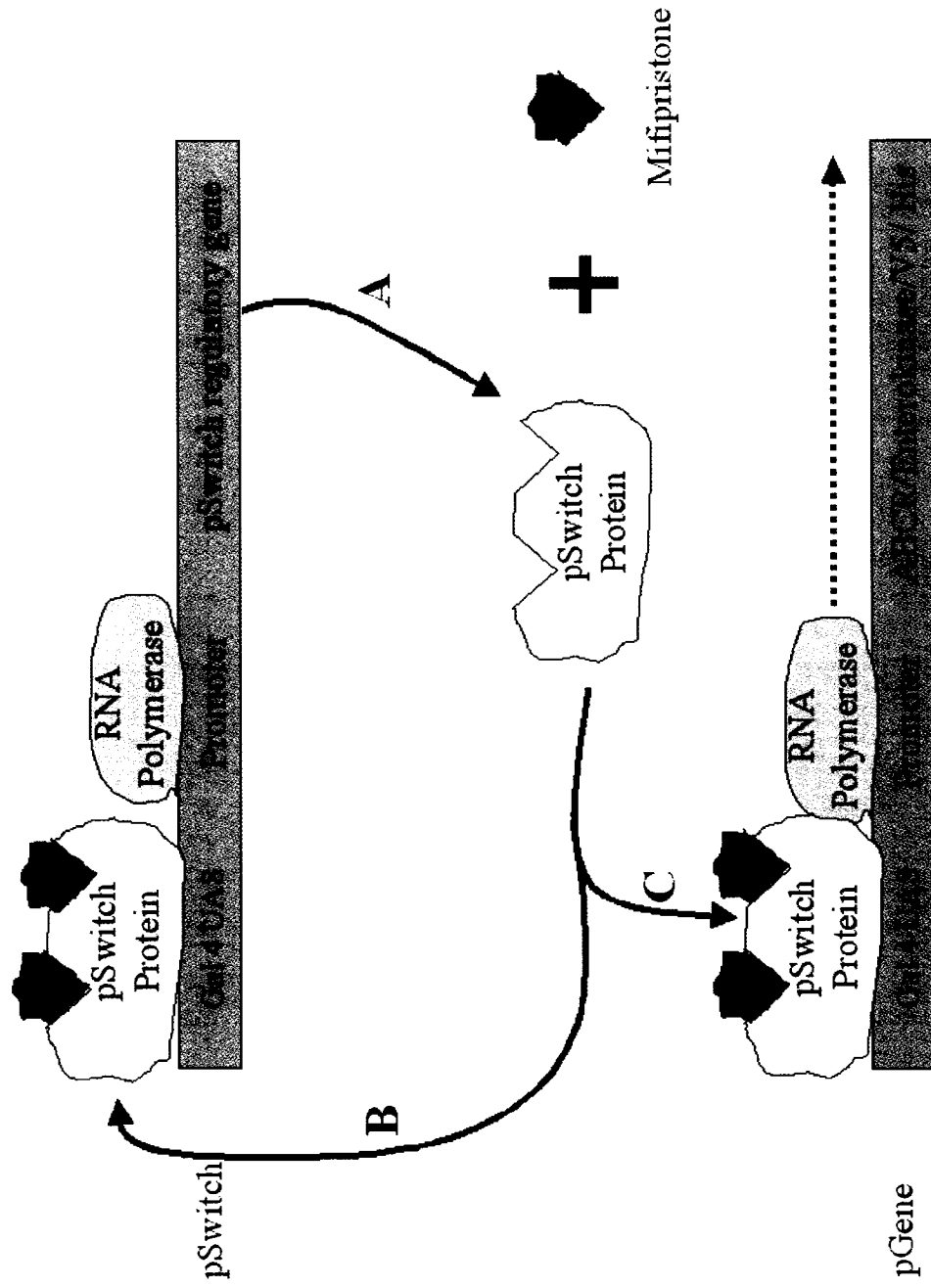
B.



enterokinase site will also allow for specific removal of ABCR from nickel nitrilotriacetate acid (Ni-NTA) columns. New restriction sites were engineered because the pGene plasmid has the Hind III upstream of the Not I site (Figure 3.1B), which is opposite for the pRK5 vector. The reversal of the sites is necessary for the correct orientation of the cDNA in the new vector.

The GeneSwitch system was used because it has a tightly regulated expression and has multiple selection controls. It contains two plasmids, pGene and pSwitch. The pSwitch plasmid was already transfected into CHO cells, and contains a hygromycin resistance gene. The pGene plasmid contains a zeocin resistance gene. So, the transfection of CHO cells is not transient. In addition, mifipristone is used for protein expression. Figure 3.2 is a diagrammatic representation of the mechanisms of this system. The top linear box represents the pSwitch plasmid that was transfected by the supplier. The lower linear box represents the pGene plasmid. The pSwitch produces the regulatory protein in extremely dilute concentrations constantly, as shown in path A. When mifipristone is added to the cells, it binds in a bimolecular fashion to the apoprotein and activates it [217]. The activated pSwitch protein can bind to the nuclear binding site on the pSwitch plasmid and cause a substantial increase in expression of the pSwitch protein as seen by path B. This acts as a positive feedback mechanism. Path C is activated by the addition of mifipristone, which binds to the pGene plasmid and begins expression of the inserted gene.

Figure 3.2: Diagrammatic representation of the mechanisms of the GeneSwitch system.



Results

The ABCR was amplified by PCR using the pRK5/ABCR as a template. Restriction digestion, with Hind III and Not I, of both the ABCR PCR and pGene were performed individually and then purified by agarose gel electrophoresis (Figure 3.3). The two components were then ligated and transformed into *E. coli* cells. A total of 72 clones showed preliminary positive results after analysis by an alkaline lysis experiment of each of the colonies. A PCR screen of the internal portion of ABCR yielded 13 positive clones. One clone was selected and the nucleotides between the 3' end of ABCR and the 5' end of pGene were sequenced. BLAST II analysis was used to compare the sequenced nucleotides, highlighted in bold, against the expected sequence (Appendix Figure A.1). Linearized plasmid was then transfected into pSwitch CHO cells and subsequent colonies were isolated. The clones were maintained in hygromycin and zeocin until needed.

Dot Blot

Five trials were set up to determine the optimal induction time and concentration of mifipristone. Figure 3.4 shows the dot blot of the five trials using the anti-V5 antibody, which was located on the carboxyl end of the fusion protein. Clearly, as the concentration of mifipristone was increased and added in multiple increments, there was an increase in the signal intensity. At the time and

Figure 3.3: Agarose gel electrophoresis of the restricted and purified PCR product and pGene.

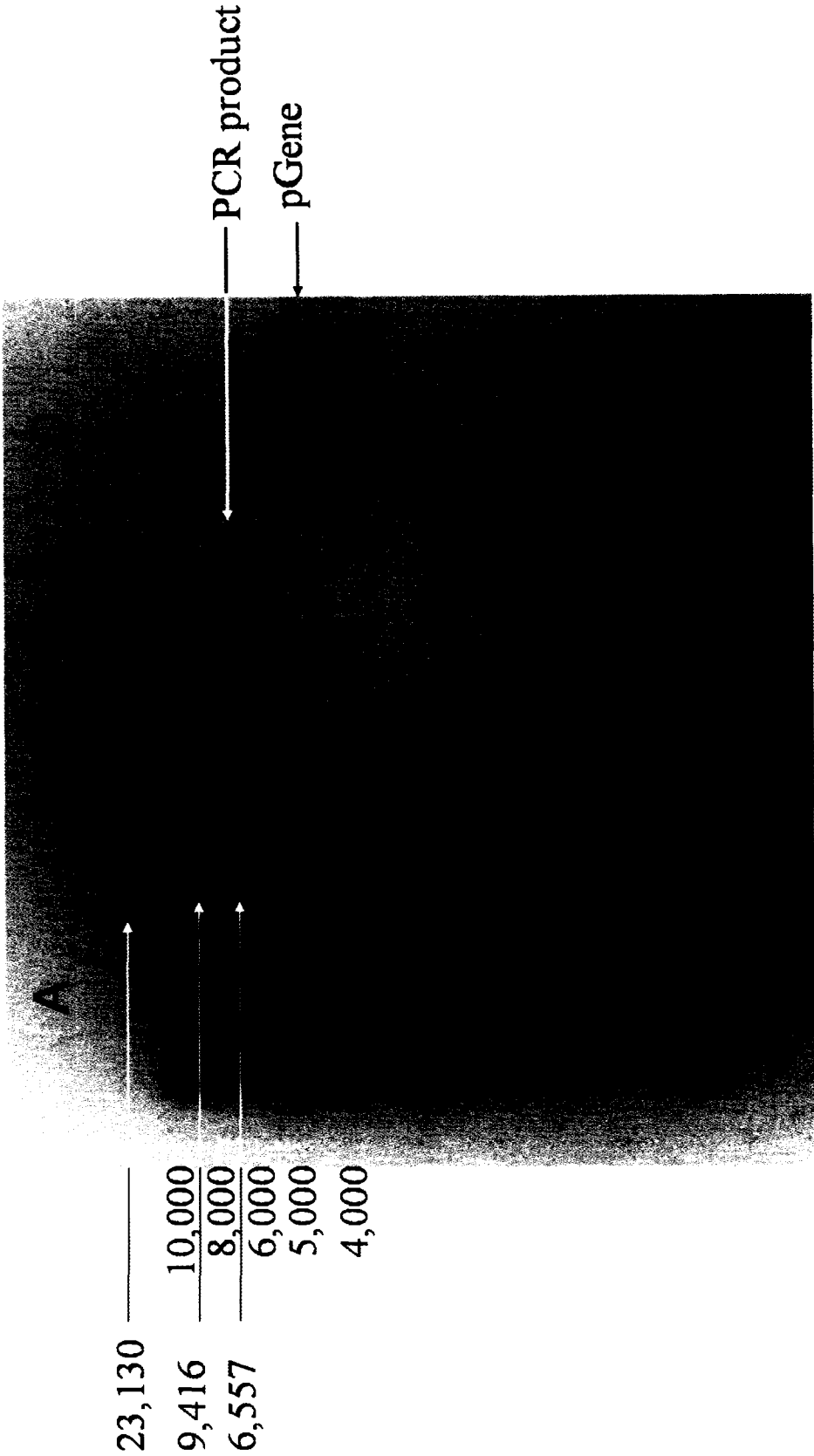
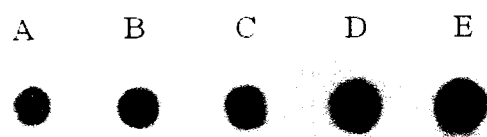


Figure 3.4: Dot blot of transfected pSwitch CHO cells using different concentrations of mifipristone and probed by the α -V5 antibody. Spot A was a sample induced with 1X mifipristone for 24 hours where X was equal to the concentration suggested by the manufacture [217]. Spot B was the same number of cells induced with 1X mifipristone for 48 hours. Spots C, D and E were induced twice, once at the beginning and again after 24 hours. Spot C was induced initially with 1X and again with 1X mifipristone solution and the cells were trypsinized at 48 hours after induction. Spot D was initially induced with 2X mifipristone and again with a 2X solution and the cells were trypsinized at 52 hours. Spot E was initially induced with a 2X solution and again with a 3X solution and the cells were removed at 52 hours.



concentration used for spot E, there did not seem to be any appreciable cell death by cell detachment (data not shown). The concentration and time used for slot E was used for the remainder of the experiments.

To analyze the presence or absence of ABCR in each of the different clones, dot blots were performed. Also, this experiment was utilized to determine the relative levels of expression for each of the different clones that were isolated (Figure 3.5). Only slight amounts of signal were observed in control B. By comparison, the different clones that were induced had a variety of expression levels of the gene. The number for each clone corresponds to the concentration of DNA that was used to transfect the cells. There was an apparent pattern amongst the clones where the ones with the higher DNA concentration (20A –20 D) showed better expression, but this could also be due to their slower growth rate.

Western Blotting

Western blotting was performed to answer the question of whether the protein was observed at the correct MW. Figure 3.6 was a western blot using α -ABCR IgG for detection. Molecular weights were marked to the left of the membrane. Arrow A points to the band that corresponds to the correct MW of the protein. An additional signal was observed at a much lower molecular mass. This protein band with an apparent MW of about 60 KDa was greatly enriched by chromatographic steps designed to purify the cloned ABCR construct. Additional studies were performed to determine whether this band actually represented the product of the ABCR gene

Figure 3.5: Dot blot to determine the expression levels of transfected clones using the α -V5 antibody. Control A was a culture of non-transfected cells that were induced with mifepristone. Control B was a culture transfected with the pGene/ABCR/ENT/V5/ His plasmid that were not induced. The numbers above each set of spots refer to their clone number.

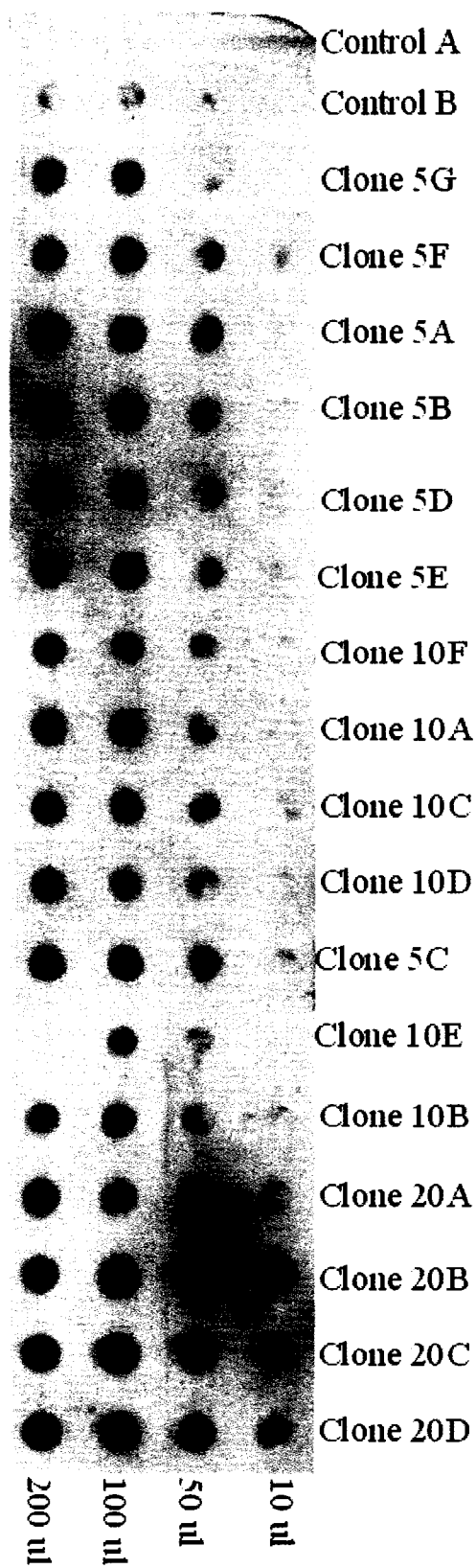
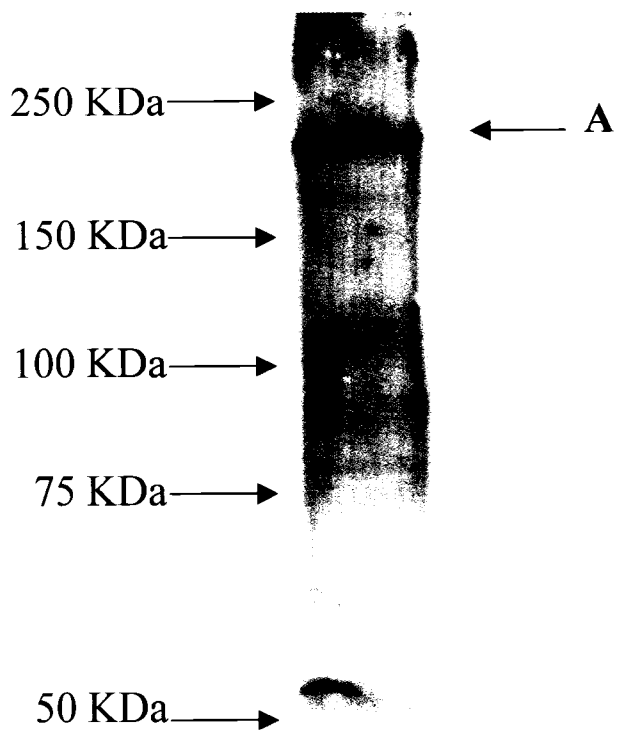


Figure 3.6: Western blot of concentrated and Ni/NTA purified ABCR fusion protein using α -ABCR antibody.

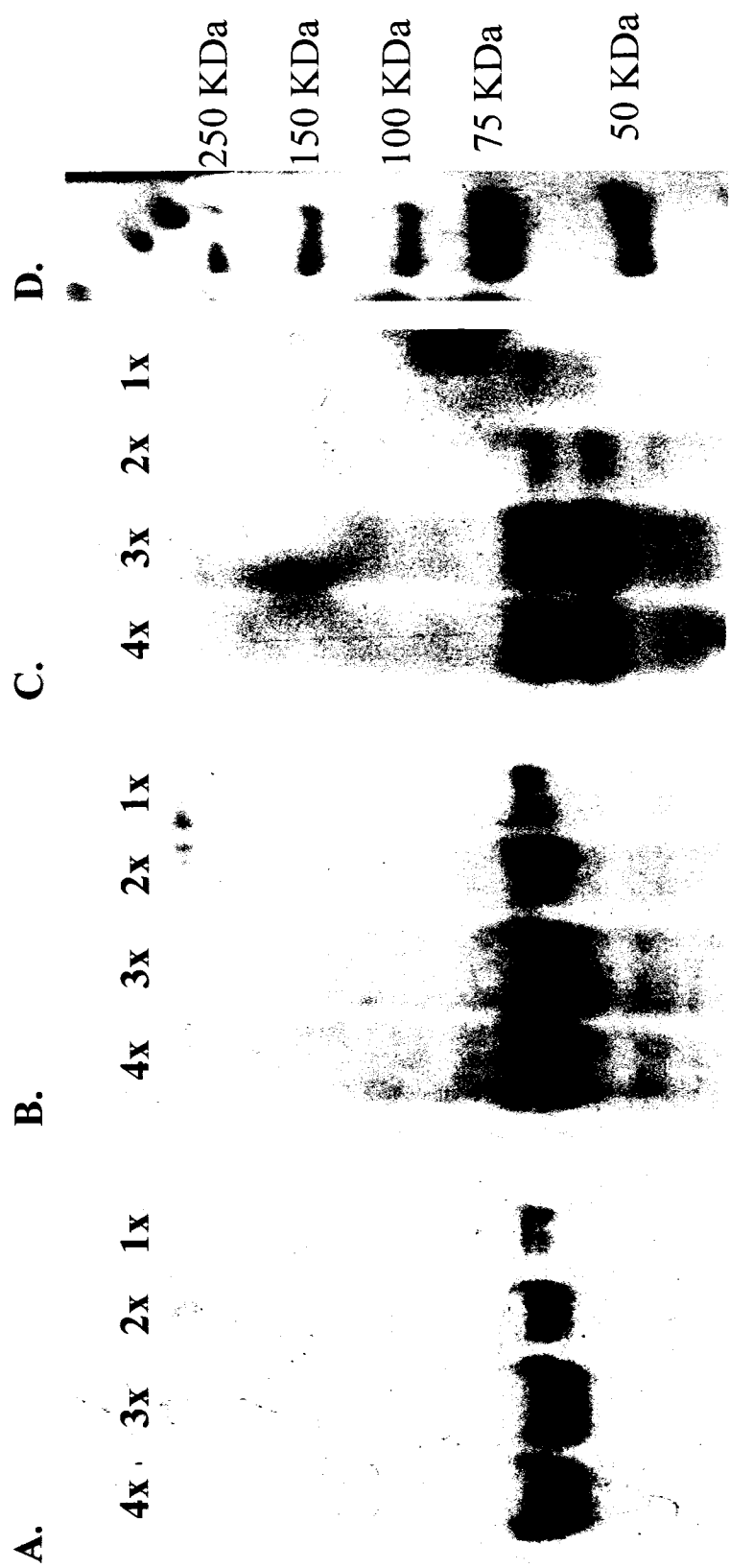


migrating abnormally due to unusual protein conformation. Figure 3.7 shows the western blots using three different probes on the same membrane. The α -ABCR antibody detects the amino (N) terminus of ABCR. This lower band was then identified using two other detection systems on the C terminus, which were α -V5 antibody and a histidine probe. Antibodies to ABCR and V5 along with a histidine probe detected the protein in the same location on the same membrane in a concentration dependent manner. To ensure that the Restore Western Blot Stripping Buffer was performing properly, western blots were conducted on separate membranes and all immunoreacted to the probes (data not shown).

Discussion

The detection of ABCR was confirmed by multiple experiments. The addition of mifipristone caused a concentration-dependent increase in the immunoreactivity with an antibody to the V5 epitope, where control cells showed little or no reactivity. The protein was isolated using a Ni-NTA spin kit, which binds to the 6x tag on the C-terminal end of the protein. Although a very small number of mammalian proteins can potentially bind to the Ni-NTA column, this mixture was separated by SDS-PAGE. When the purified protein was analyzed by western blot, the full-length protein was detected using an antibody to the N-terminus of the ABCR protein. The observed MW is the same as the literature MW for human ABCR transiently transfected into HEK cells [26, 60].

Figure 3.7: Western blots of concentrated and Ni/NTA purified ABCR fusion protein. A) α -ABCR antibody; B) α -V5 antibody; C) HisProbe; D) MW markers. Four different concentrations of protein were used and labeled above each lane. Membranes B and C were the same membrane as part A, which were stripped and reprobed. In membrane A, a strong signal appeared around 75 kilodaltons in a concentration-dependent fashion, which bound to the N terminus. Membrane B conferred similar results using the α -V5 antibody, which bound the V5 epitope that was located on the carboxyl (C) terminus of the protein. His-Probe in membrane C also had a band at the same location on the membrane.



The detection of the protein by western blot resulted in some unexpected results. A lower molecular weight protein was detected with all three probes, including probes that were immunoreactive to the putative N-terminus and the C-terminus. All of the probes localized to the same band on the membranes. These western blots were performed on cell homogenates that were enriched for the recombinant protein by using the Ni-NTA spin column. Additionally, small proteins should have been eliminated from this preparation by filtration using a concentrator with a 100 KDa MW cut-off. It is not obvious, then, why much of the ABCR gene product appeared to migrate as a smaller protein even though the full protein seemed intact.

Although this is speculative, the process of solubilization might have produced two conformations of the protein: one that was totally linear and another that was partially denatured. Since glycosylations have been shown to inhibit binding of SDS [218], the 12 transmembrane domains could have folded upon each other due to their vicinity to each other. The conditions for solubilization, although successful, still need to be optimized to totally denature the protein.

Purified ABCR has been isolated from bovine rod outer segments [60, 122, 156] using a sucrose density gradient. Additionally, human ABCR has been cloned into HEK cells, but the protein does not contain a tag for isolation and is transiently expressed [26, 60]. Both methods require the isolation of the protein using immunoprecipitation.

The expression system used for the generation of our ABCR fusion protein is

an improvement over previous published methods. The GeneSwitch system utilizes antibiotic genes for the stable transfection of the plasmid. The new protein was engineered to contain a histidine tag and an enterokinase site on the C-terminal end. The incorporation of these two components, and using a stable transfection system, provides a more convenient technique for the isolation and purification process to study the protein in future experiments.

In summary, dot blots showed that the cells were inducible with mifipristone and that multiple cell lines contained ABCR protein. Two unique bands have been characterized by western blot from purified ABCR solutions. One band was at the correct MW for the full-length protein and another band was observed at a much smaller MW. The smaller MW band was intense and probes reacted to opposite ends of the protein.

CHAPTER 4

PRODUCTION AND ANALYSIS OF pGENE/ABCR/ENT/RSGFP/HIS

Introduction

In photoreceptor cells, the ABCR protein is associated with the membranous disks of the rod outer segments [60]. These membranous disks are located between the inner segments and the plasma membrane. The disks do not actually bind to the plasma membrane and are considered lysosomal [59]. To date, there have been no reports of photoreceptor cells grown in culture; therefore, ABCR must be isolated from cells removed from animal eyes. One of the most widely used procedures used to isolate the protein is a pull-down assay using an anti-ABCR antibody attached to a solid matrix in a separatory column followed by extraction. During the process, denaturation and abnormal interactions in the hydrophobic transmembrane domains can alter the protein. Sun and Nathans were the first to transiently transfect cultured cells and isolate the protein in a similar manner [163].

In photoreceptor rod cells, ABCR has a very distinct location at the rims of the outer segments [25]. Other cell types are not likely to have the same genetic programming in order to form the requisite extended membranous disks. So, it is not clear where we might expect to find ABCR that is expressed in non-photoreceptor

mammalian cells. Three possibilities exist for the final location of the protein. These are in lysosomal membranes, in plasma membranes or secreted into the medium. Knowledge of the location is important to determine the isolation conditions for the protein (i.e., detergent concentration, cell lysis, refolding options). A green fluorescent fusion protein expressed in cells is often used to determine the location and trafficking of the protein and an attempt was made to use this technique to identify the location of expressed ABCR.

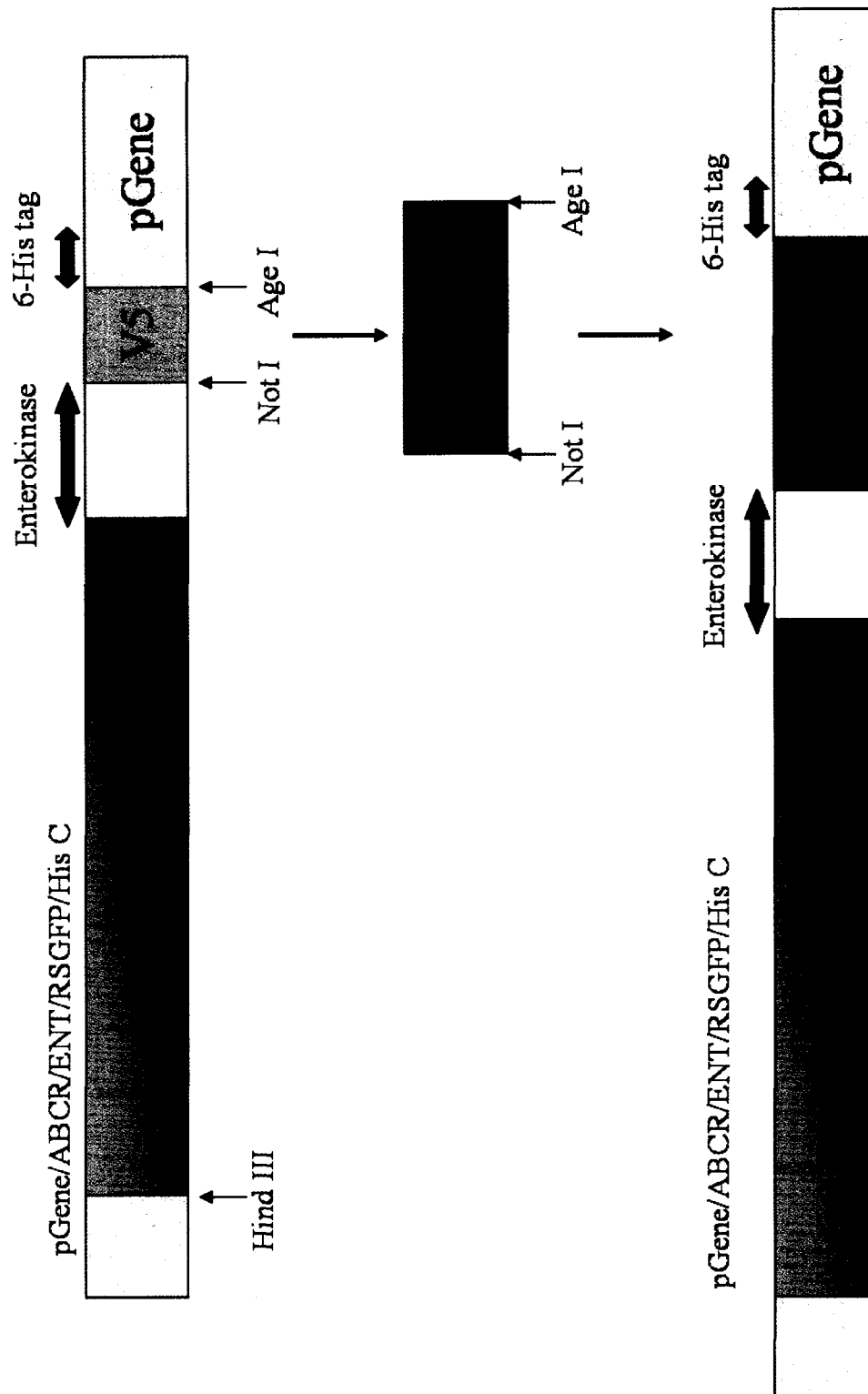
Green Fluorescent Protein (GFP) is a spontaneously fluorescent protein that was isolated from the jellyfish *Aequoria victoria* [219]. The protein does not require cofactors, substrates or other cellular interactions, so it functions in both *in vivo* and *ex vivo*. It is a 238-amino-acid protein with a molecular mass of 28.3 kDa [220]. Commonly, it is used as a reporter in cells and organisms to determine expression levels, cell lineage or localization of proteins. Purified GFP absorbs light maximally at 395 nm and to a lesser degree at 475nm and it has an emission maximum at 509 nm [221]. The stability of the emission is dependent upon alterations in the amino acid sequence [222].

Enhancement of the signal was found through site mutations in three key amino acids (V163A, M153T and F99S), which produced the “cycle three” mutant. These mutations produced a hydrophobic domain within the protein, which altered the protein’s folding to produce a more soluble form of the GFP protein [223, 224]. The protein has been designated as smGFP to differentiate it from the wild-type GFP. This three-cycle mutant inhibits aggregation of the protein [223]. In both *E. coli* and

CHO cells, the aggregation of wild-type GFP is cytotoxic [223, 224]. Higher levels of expression cause increased concentrations to be produced to amplify the signal. One additional mutation, S65T, has been shown to cause an enhanced red-shifted GFP (smRSGFP). This mutation shifts the excitation wavelength 83 nm towards the red part of the spectrum to 488nm, while retaining the same emission spectra [224, 225]. This allows the utilization of FITC filters commonly found in confocal microscopes and fluorescent inverted microscopes. The red-shifted protein removes the absorption below 450 nm so that a dual fluorescence can be used with another dye or protein. The fluorescence intensity of the red-shifted GFP is a 6-fold increase over the wild-type protein [224]. GFP has been utilized as a protein tag for multiple proteins and retains its intrinsic fluorescence when expressed as a fusion protein on both the N and C terminal ends [221, 222, 226].

The question of the cellular location of the ABCR protein expressed in our CHO cells was addressed by expressing a fusion protein containing ABCR and smRSGFP. The smRSGFP was subcloned from the pBIN 35 mGFP4 plasmid [226]. Figure 4.1 is a schematic showing the experimental design of the different components of the new plasmid where the top picture is the vector and the RSGFP is the insert to produce the new plasmid (lower picture). The new fusion protein still retained the 6-His tag and was designated pGene/ABCR/ENT/RSGFP/His.

Figure 4.1: Schematic of the pGene/ABCR/ENT/RSGFP/His construct.



Results

RSGFP was cloned into pGene/ABCR/ENT/V5/His to replace the V5 epitope. Four sequences were performed to generate the complete nucleotide sequence from the 3' end of ABCR through the 5' histidine tag. The sequences were aligned using MACAW alignment software and are found in appendix Figure A.2. Transfected pSwitch CHO cells were selected for the presence of the new plasmid with the antibiotic zeocin, and induced with mifipristone.

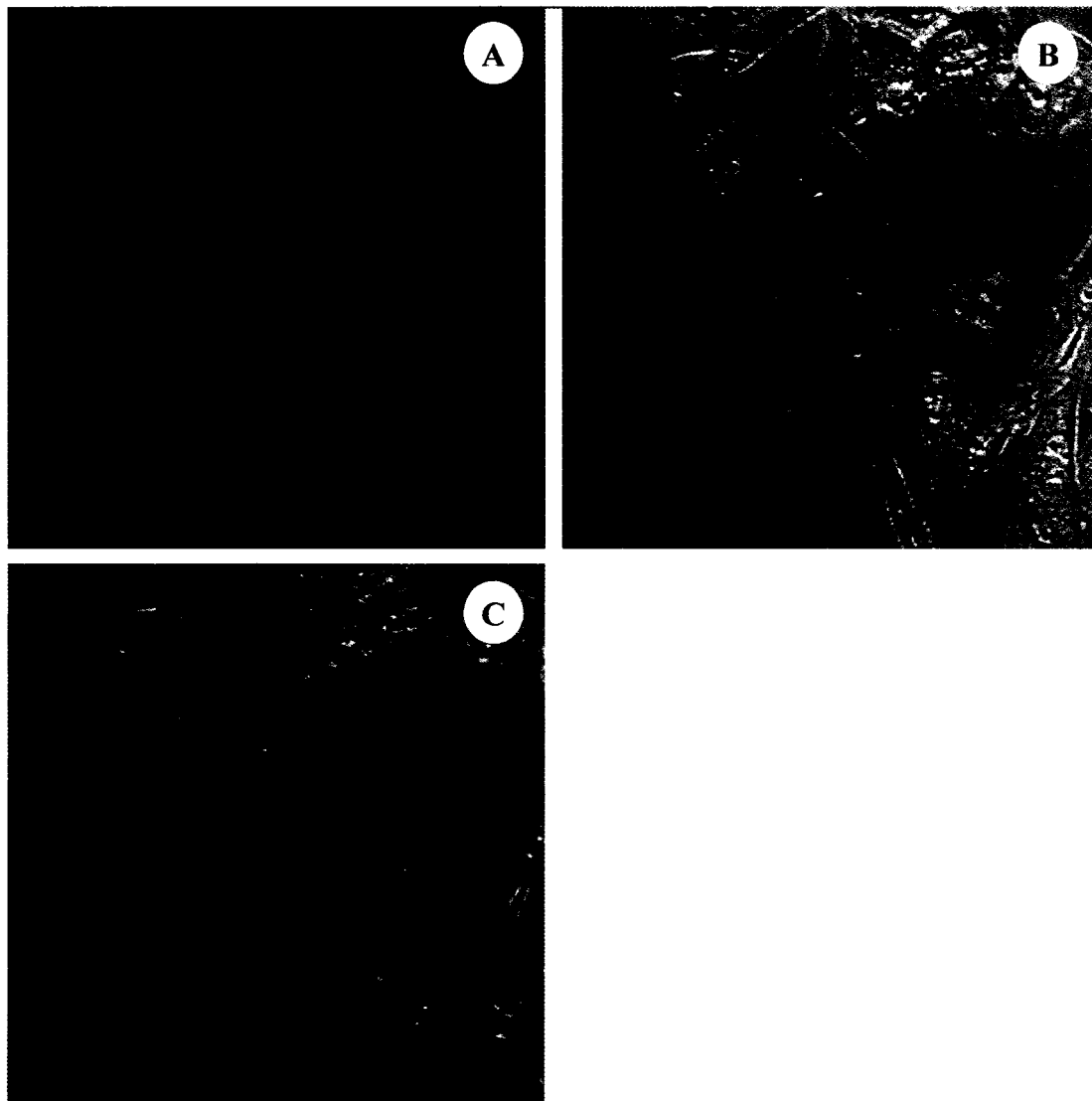
Confocal Microscopy

The confocal microscope was used in fluorescence mode to aid in the detection of clones that had high expression of the fusion protein. Figure 4.2 shows the presence of a signal. The ABCR/RSGFP appears to be extranuclear and punctate, rather than diffuse, in the cell cytoplasm. This distribution would suggest that the ABCR/RSGFP construct is membrane-associated or in membrane areas within the cytoplasm. Images were compared to cells that were not induced and cells that were induced but had no plasmid transfected. Both of these showed negligible signal (data not shown).

Cell Fractionation

Whole-cell homogenates were separated into nuclear, cytosolic and membrane portions and each fraction was purified by a Ni-NTA spin column. These fractions

Figure 4.2: Confocal microscopy of the transfected pSwitch clone B2 induced with 10 mM mifepristone for 16 hours. A) FITC-only picture; B) Phase contrast picture; C) FITC photo overlayed on top of the phase contrast.



were analyzed by SDS/PAGE to determine if the protein could be observed at the proper molecular weight in the membrane fraction and not the other fractions. The nuclear fraction in lane C (Figure 4.3) shows no bands. In lane B, the cytosolic fraction shows virtually no band at 250 kDa and a lower band around 75 kDa that was less intense when compared to the membrane fraction in lane A.

Western Blotting

A western blot was performed to compare the MW of the ABCR/RSGFP protein to the ABCR protein from Chapter 3. The purified ABCR/RSGFP in lane A of Figure 4.4 shows an increase in MW of approximately 30 kDa in comparison to ABCR, shown in lane B. This difference in MW is approximately the mass of RSGFP alone.

Discussion

Since CHO cells do not contain the membranous structure found in the retinal rod cells, it is of interest to determine the cellular location of ABCR in these transfected cells, as this would suggest how this unusual protein is being processed by the host cell. *In vivo*, the ABCR protein is found located in the disks of the rod outer segments. The protein is generally never located in the plasma membrane. Experimentation using GFP fusion proteins is a common practice for the

Figure 4.3: Stained SDS/PAGE of the cytosolic and membrane fractions from clone B2. A) Membrane fraction. B) Cytosolic fraction. C) Nuclear fraction.

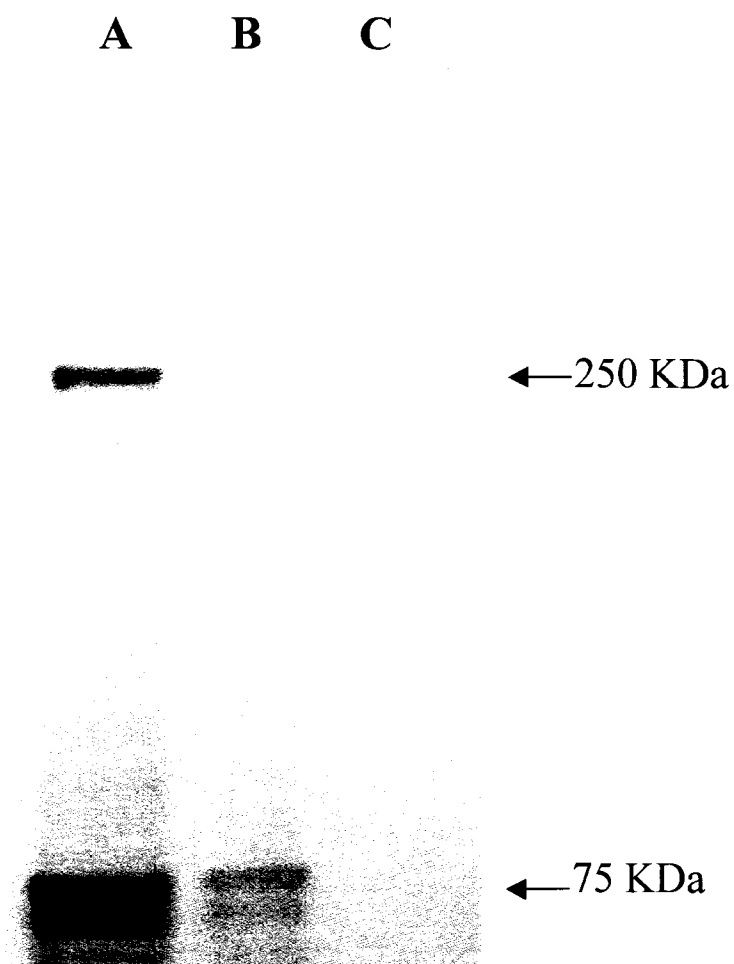


Figure 4.4: Western blot of cells transfected with pGene/ABCR/ENT/V5/His compared to pGene/ABCR/ENT/RSGFP/His using the α -ABCR antibody for detection. A) ABCR/RSGFP. B) ABCR.



determination of a protein's location. Yet, there are no accounts of a GFP fusion protein with ABCR in CHO cells.

The ABCR/RSGFP protein is likely to be membrane bound, but the exact location of the protein remains to be determined. Fluorescence of the transfected CHO cells shows the expression of the ABCR/RSGFP, and the pattern of fluorescence appears to be non-nuclear. Problems with the refractive index of the coverslip caused a lack of alignment between the fluorescent image and the phase contrast image, so no further analysis was possible. Further experiments need to be performed in confocal mode to establish if the fluorescence is in membrane-bound vesicles. The cell fractionation experiment shows protein at the correct MW in the membrane fraction only, which further establishes that the protein is not localized to the nucleus. A small amount of lower MW band in the cytosolic fraction may be due inefficient separation of the fractions.

It is likely that the CHO cells expressed full-length ABCR/RSGFP, but further experiments are needed for this confirmation. The cell fractionation experiment shows the protein at the correct MW. The correct full-length MW was estimated by using the addition of the literature values for ABCR and RSGFP. SDS/PAGE does not identify the bands present, but, because the purification technique was based upon the 6x tag located on the C-terminus, the presence of the band at the correct MW is compelling evidence to justify that the protein is full-length.

Additionally, the protein was analyzed by western blot using the α -ABCR antibody that detects the N-terminus. Although the high MW band was not detected,

there was sufficient evidence that enhances the conclusions about the SDS/PAGE.

As discussed in Chapter 3, the lower MW band appears to be full-length protein that has migrated faster. Since the ABCR/RSGFP was compared to purified ABCR from Chapter 3, the same conclusions can be made about the bands on the western blot.

The ABCR/RSGFP protein was approximately 30 kDa greater than the ABCR, which is the approximate mass of RSGFP alone. The RSGFP portion of the fusion protein is located on the C-terminus, and it was visualized by fluorescence. When all of these experiments are together, it is very likely that the protein is full-length. Because hydrophobicity, glycosylation and high MW inhibit transfer of proteins during a western blot, different transfer conditions will be needed to visualize the ABCR/RSGFP at the correct MW.

These experiments indicate that the protein is membrane bound, but whether it is localized in the plasma membrane or in membrane-bound vesicles remains to be determined. It is likely that the CHO cells expressed the full-length fusion protein and slight modifications in technique are needed to show this to be definitive. The presence of the protein in the membrane means that the CHO can generate the proper post-translational modifications. The RSGFP marker makes the isolation of the protein more efficient, because non-denatured fractions can be visualized for the presence of the fluorescence and the protein can be quantitated.

CHAPTER 5

CHARACTERIZATION OF IMMORTALIZED RPE CELLS

Introduction

The retinal pigment epithelial (RPE) cells have a variety of functions in the eye. Many of these functions, such as phagocytosis of the outer segments, secretion of paracrine growth factors and visual recycling, are requisite for photoreceptor survival. Therefore, the survival and the optimal functioning of the RPE is vital. Numerous retinal diseases have a similar etiology involving the damage of RPE cells. Cell culture has become an important tool to study normal and degenerative stages of RPE tissue.

Traditionally, cell culture experiments were performed from retinal tissue explants that have a poor rate of attachment and proliferation. At low passage numbers, many changes have been observed in cultured RPE cells, such as a loss of basal infoldings, loss of RPE-specific proteins, depigmentation and shortening of the apical microvilli [64]. Since a limited number of differentiated cells were obtained per eye, multiple eyes were pooled together. The diversity of genetics from different donors caused variation from one experiment to the next. This variation in donor source encouraged the development of new methodologies.

Immortalization of rat RPE cells by SV40 was performed to produce the RPE-J cell line, and the spontaneously immortalized BPEI-1 rat cell line allowed multiple experiments to be performed with the same genetic makeup [38]. But, immortalization by the large T antigen of simian virus has been shown to produce cells with altered differentiation and gene expression [227, 228]. SV40 immortalization still undergoes M2 crisis and telomerase is required to overcome the constraints of senescence [229]. Additionally, BPEI-1 has been shown to have characteristics that are transformed and, therefore, are undifferentiated [230].

A spontaneously immortalized human RPE cell line called D407 and a human telomerase immortalized RPE have become available [231]. The D407 cells were shown to have altered gene expression, a diminished capacity to phagocytize rod outer segments and have a trisomy chromosome number [232].

Recently, the human cell line ARPE-19 was established. It was a spontaneously arising cell line that was isolated from a 19-year-old subject. It had been determined to have a high proliferative capacity, but a limited life span [233]. Fetal human RPE cells normally senesce around 35 population doublings, and adult cells are expected to have a greatly diminished lifespan. The lowest passage number available is 5, at which time the cells are already depigmented [234].

Due to a lack of human tissue, variation in genetics and dedifferentiation of existing cell lines, there is a need to establish new cell lines. The normal physiological state of RPE cells remains unclear. Many mechanisms such as how RPE cells promote photoreceptor and choroidal vascular survival, inhibition of

proliferative vitreoretinopathy and the internalization of photoreceptor outer segments are only beginning to be understood. Additionally, the various retinal diseases each need unique tissue culture models that display the characteristics found *in vivo*.

Culture conditions such as extracellular matrix, pigmentation, and growth factors all have an influence on the degree of differentiation and epithelial shape [235]. Once the physiology of RPE cells and their interactions with external factors are understood, then tissue could be grown for future transplantation to replace diseased RPE.

The goal of this research was to generate procedures for culturing a RPE cell line that behaves similar to *in vivo* cells. The results discussed herein focus on the characterization of a spontaneously immortalized bovine RPE cell line, called tRPE, that was isolated from a primary RPE explant. The morphology of the cells has been determined on a variety of extracellular matrices and has been compared to *in vivo* characteristics and primary RPE cells. To determine whether the cells were of RPE origin, the expression of RPE-characteristic genes and proteins was examined by reverse transcriptase PCR (RT-PCR) and immunocytochemistry. Studies to establish whether or not the cells were transformed have been performed. Experiments to repigment the tRPE cells were completed and its effect on the morphology of the culture was observed.

Results

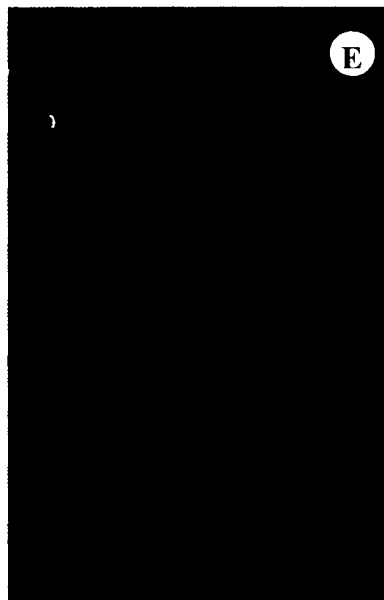
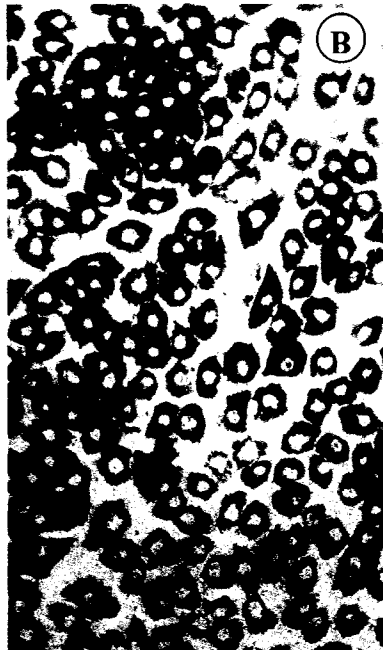
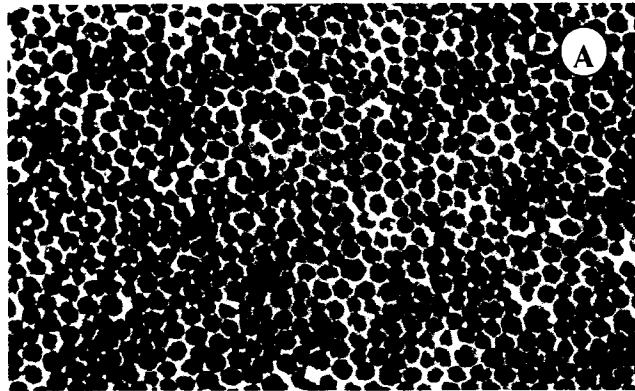
RPE Morphology

Primary RPE cells were isolated using the gelatin isolation protocol as an indicator of the *in vivo* morphology. The morphology of these cells was used as a comparison for the optimal outcome for the RPE cell tissue cultures. The RPE cells were hexagonal in shape and densely pigmented throughout (Figure 5.1 A) as observed by phase contrast microscopy. It should be noted that even the center of the cell contained pigment covering the nucleus.

Primary cells that were trypsinized had attached to tissue culture plastic dishes generally within one week. Proliferation of the cells generally began one to two weeks after attachment. The cells increased in size by approximately four-fold and the shape of each individual cell became polygonal (Figure 5.1 B). The nucleus was visible with melanin localized in a perinuclear arrangement. When the cells were at passage 5 (Figure 5.1C), they were totally devoid of pigment, but still retained the epithelioid morphology. The nucleus was indented and was visible by phase contrast microscopy. Cultures were maintained to approximately 35 passages before they senesced.

A new RPE cell line was generated from calf eyes that were dissected and grown on tissue culture plates. Seven primary RPE cell explants were isolated by cloning rings and grown under low-density conditions. Colonies were reisolated to generate pure cultures. The cells were allowed to become confluent and then

Figure 5.1: Photographs of RPE cells. A) Melanotic RPE *in vivo* morphology. B) Photograph of a confluent passage 1 primary melanotic RPE culture with the inset as a close-up. C) Photograph of passage 9 primary RPE cells displaying a polygonal morphology. D) Photograph of passage 102 tRPE cells repigmented by feeding them melanosomes with the inset as a close-up to visualize the individual granules. E) Photograph of confluent passage 102 tRPE cells grown on bovine corneal endothelial extracellular matrix (BCE-ECM).



passaged. Of these clones, only one produced a cell line that surpassed the 50 population doublings and eventually was passaged to over 150 population doublings. This cell line was designated as tRPE. They have the ability to become repigmented (Figure 5.1D) after feeding the cells isolated and purified melanosomes, and yielded the same morphology as the pigmented primary cells. The control cells 3T3, HeLa and UV61 did not take up the melanosomes (data not shown).

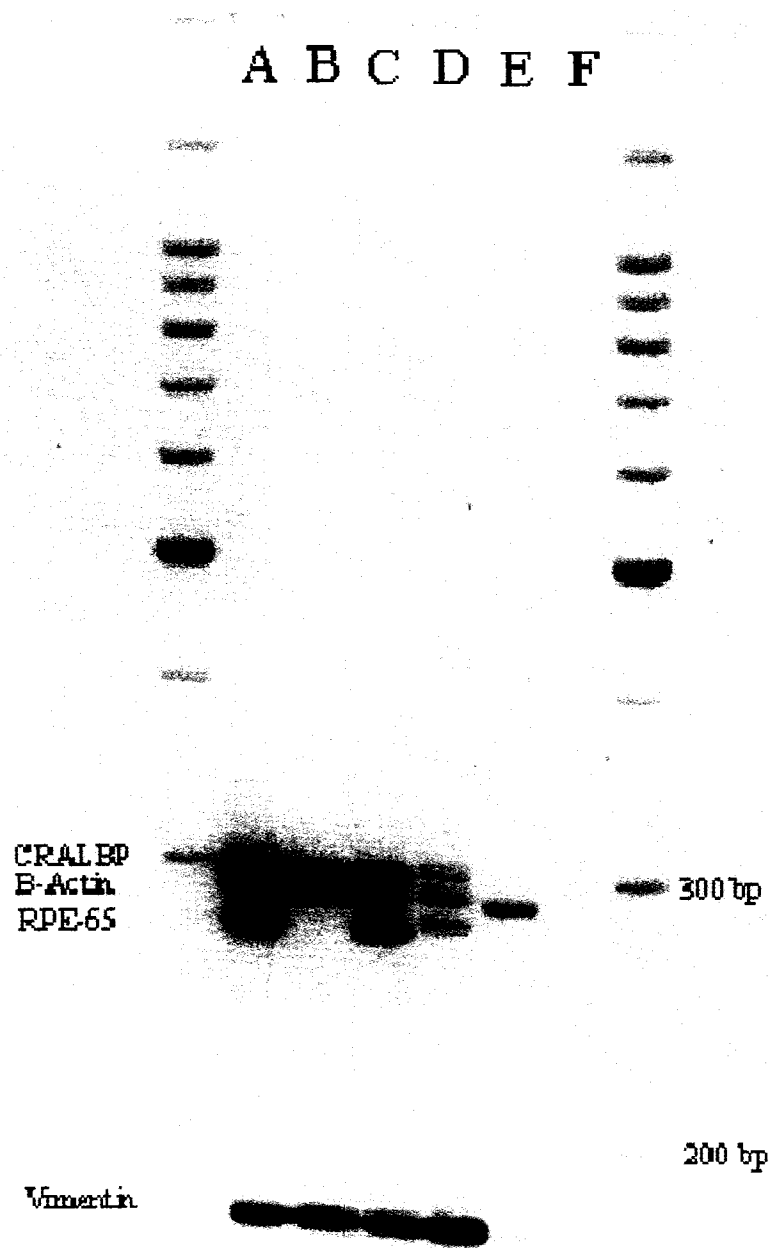
The tRPE cells grown on top of BCE-ECM (Figure 5.1 E) more closely resemble the primary cell morphology when compared to Matrigel or tissue-grade plastic. They were flat, polygonal and did not grow as dense as the RPE cells grown on Matrigel or plastic.

Reverse Transcriptase PCR

RT-PCR was performed to detect the expression of four genes. Since other cell types can contaminate cultures from crude dissection, the RPE-characteristic genes, RPE-65 and CRALBP, were used as markers for the identification of RPE cell origin. Additionally, both RPE-65 and CRALBP expression are diminished *in vitro*, so they were also used as markers for RPE differentiation. Expression of β -actin was used as a quantitative marker, since it is a ubiquitous housekeeping gene. Finally, vimentin is expressed in cultured RPE cells.

The cells freshly extracted from the eye express all four genes as shown in Figure 5.2. (lane A), but, after passage on plastic, the cells lose expression of the RPE-65 (lane B). The tRPE cells regained the expression of RPE-65 when grown on

Figure 5.2: Agarose gel electrophoresis of the reverse transcriptase PCR reactions of different cell cultures under various conditions. Molecular weight markers are located on both sides with the size on the right. The location of each gene's PCR is located on the left. A) RPE cells extracted from the eyecup; B) Passage 5 primary cells grown on plastic for two months in normal DMEM media; C) Passage 50 tRPE cells grown on BCE-ECM for two months in conditioned media; D) Passage 50 tRPE cells grown on plastic for two months in conditioned media; E) Control using CHO cells; F) Control using no DNA polymerase in the PCR reactions.



the combination of extracellular matrix and in conditioned medium (lane C). When the tRPE cells are grown on plastic and conditioned medium, the expression of RPE-65 remains, but at reduced levels (lane D). The CRALBP and β -actin signal was also reduced, while vimentin expression was high. These results show that the combination of BCE-ECM and conditioned medium are required for the tRPE cells to express RPE-characteristic genes that are found *in vivo*.

Immunocytochemistry

Expression of two RPE-specific genes was analyzed. RPE-65 was immunolocalized in tRPE cells (Figure 5.3A) throughout the cells. Ma et al. have shown that a Sf9 cell line transfected with a plasmid-containing recombinant human RPE65 will have a distribution throughout the cell when detected with an anti-RPE65 antibody [236]. The other RPE-specific protein analyzed was bestrophin (Figure 5.3B). There was heavy localization of the protein seen towards the periphery of the cells. The protein was also seen as less intense on the interior, but the intensity could have been diminished because it was not within the same focal plane.

Cytoskeletal proteins were also analyzed. Figure 5.4 A illustrates a tRPE culture that showed positive immunoreactivity to the anti-vimentin antibody. The red fluorescence shows a radiating pattern from the nucleus that was Hoechst counterstained in blue. Most of the cells stained intensely for vimentin. Additionally, the tRPE expression of pan-cytokeratin is seen in Figure 5.4B. The cells had a more

Figure 5.3: Immunocytochemistry of tRPE cells expressing RPE-specific proteins. A) RPE-65 immunocytochemistry of tRPE cells grown on BCE-ECM using conditioned media. Green was a photo of the FITC filter cube showing the localization of RPE-65 and overlaid was the blue photo using the DAPI filter cube showing the nuclear counterstain Hoechst 33258. B) Bestrophin immunocytochemistry of tRPE cells grown on BCE-ECM using conditioned media. Green was a photo of the FITC filter cube showing the localization of bestrophin and overlaid was the blue photo using the DAPI filter cube showing the nuclear counterstain Hoechst 33258.

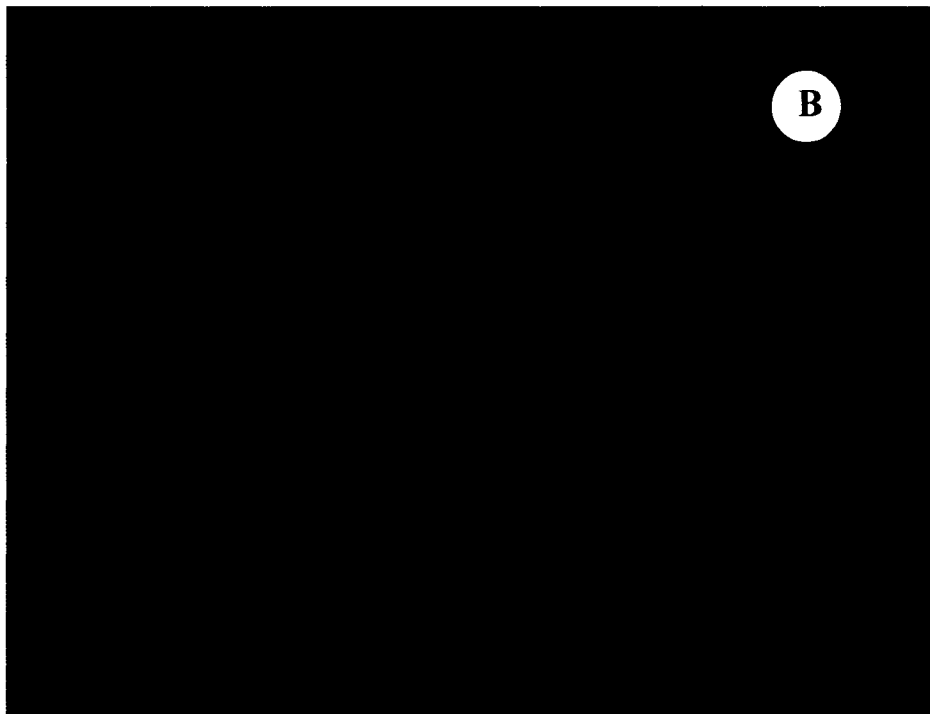
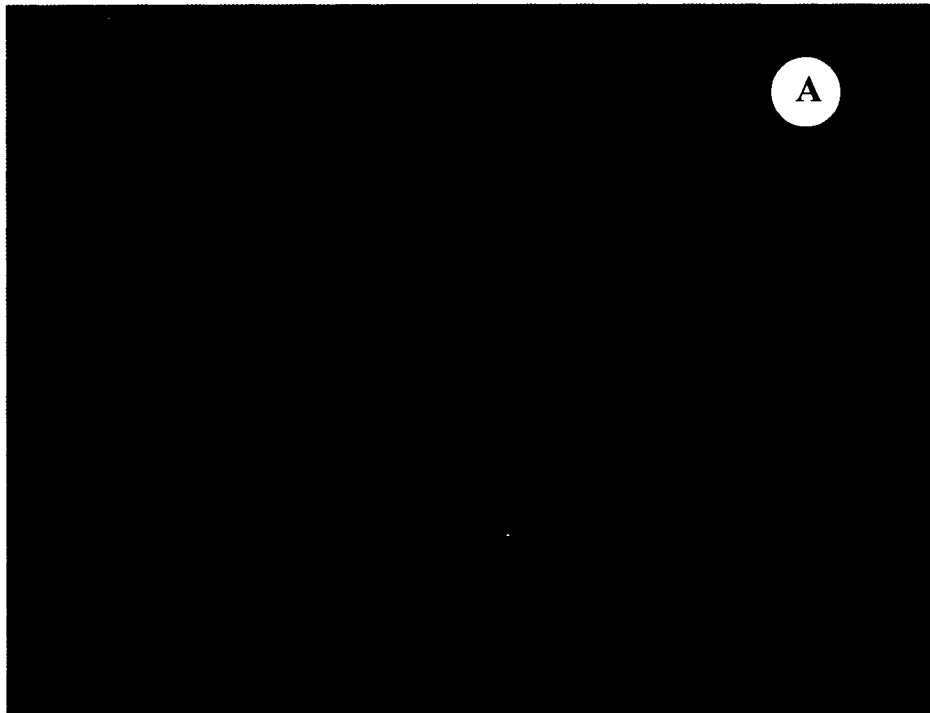
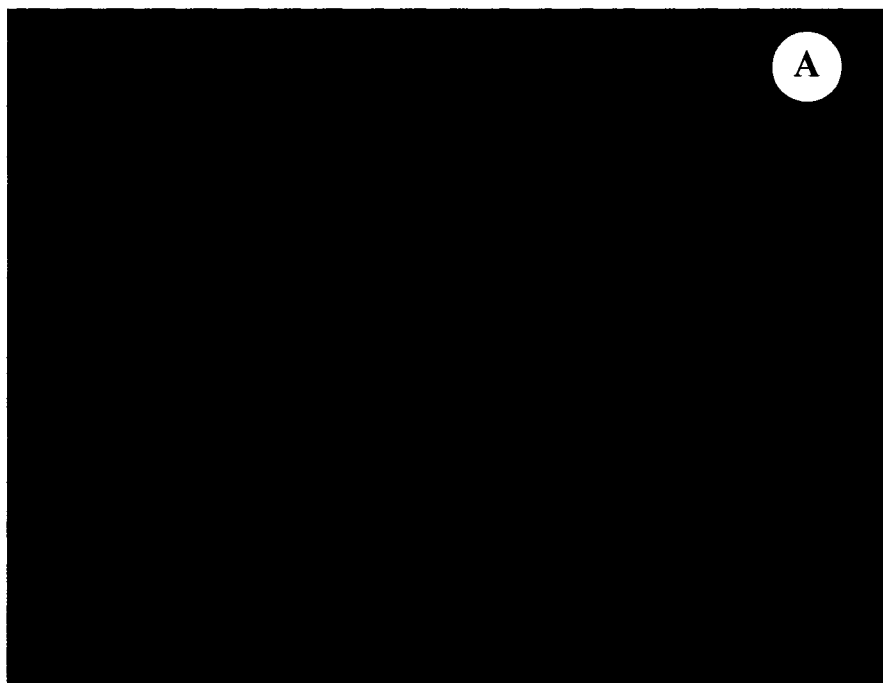


Figure 5.4: Immunocytochemistry of tRPE cells expressing cytoskeletal proteins. A) Vimentin immunocytochemistry of tRPE cells grown on BCE-ECM using conditioned media. Red was a photo of the TRITC filter cube showing the localization of vimentin and overlaid was the blue photo using the DAPI filter cube showing the nuclear counterstain Hoechst 33258. B) Pan-cytokeratin immunocytochemistry of tRPE cells grown on BCE-ECM using conditioned media. Green was a photo of the FITC filter cube showing the localization of the cytokeratin and overlaid was the blue photo using the DAPI filter cube showing the nuclear counterstain Hoechst 33258.



intense fluorescence that was localized around the nucleus and fingerlike extensions that radiated outwards.

Additionally, the expression of zonula occludins (ZO-1) was determined as a marker for the formation of epithelial tight junctions. Figure 5.5 shows that the cellular location of the protein was in a hexagonal shape on the periphery of the cells. All experiments were negative for the three controls as described in Chapter 2.

Transformation Tests

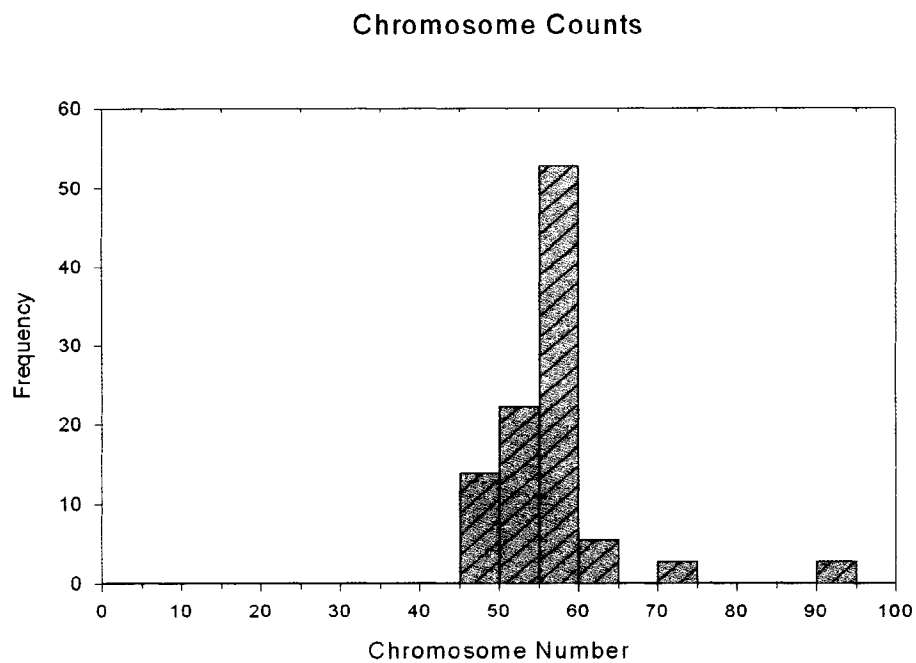
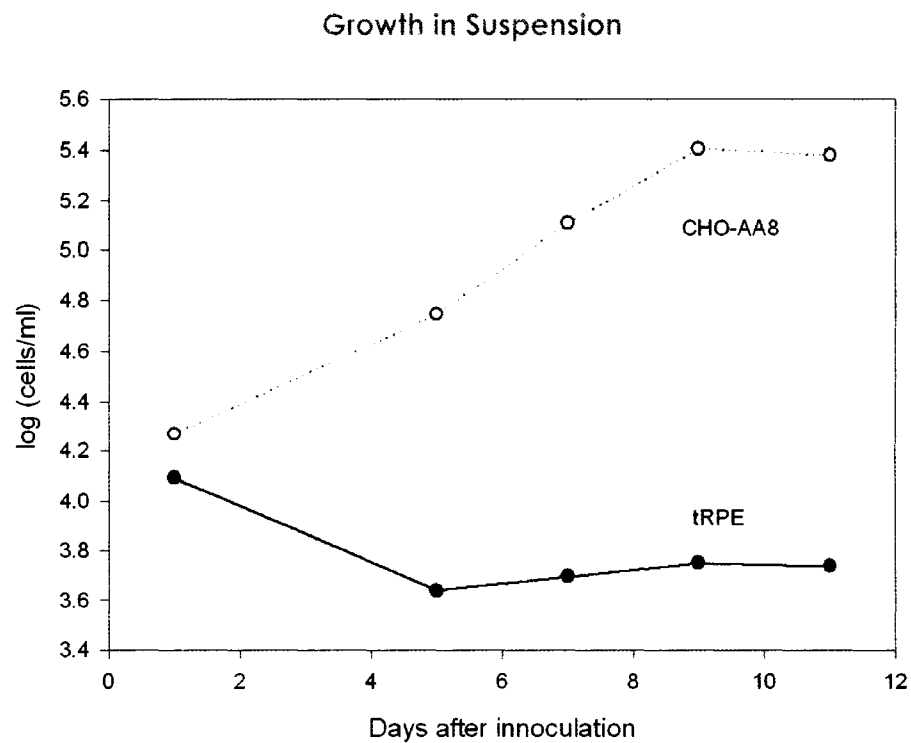
Initially, the tRPE cells were thought to be spontaneously immortalized because they had no foci formation after the cells became confluent. Generally, as cells increase in passage number, they have the ability to become transformed due to mutations accumulating in their DNA. Specific tests were done to establish that the tRPE cells were not transformed even at population doubling 102. Additionally, the experiments would also show that the cells still retained specific characteristics of a differentiated state.

Chromosome counts of the tRPE varied only slightly from the normal diploid number of 60 [237], which is indicative of non-transformed cells (Figure 5.6A). All of the chromosomes were telocentric except for two and many of the chromosomes were small. It was believed that counts that were less than 60 chromosomes arose from the loss of chromosomes during the fixation process while hypotonic cell solutions were dropped onto the slides.

Figure 5.5: Zonula Occludens-1 (ZO-1) immunocytochemistry of tRPE cells grown on BCE-ECM using conditioned media. Green was a photo of the FITC filter cube showing the localization of ZO-1 and overlaid was the blue photo using the DAPI filter cube showing the nuclear counterstain Hoechst 33258.



Figure 5.6: Graphical analysis of tRPE transformation experiments. A) Frequency of chromosome counts of passage 102 tRPE cells (n=63). B) Growth curves of passage 102 tRPE cells compared to CHO cells grown in suspension cultures.

A.**B.**

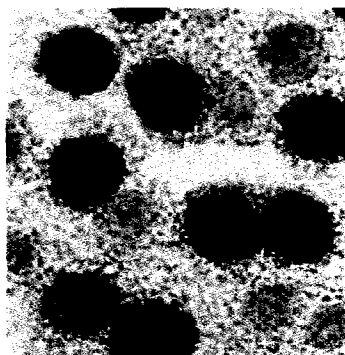
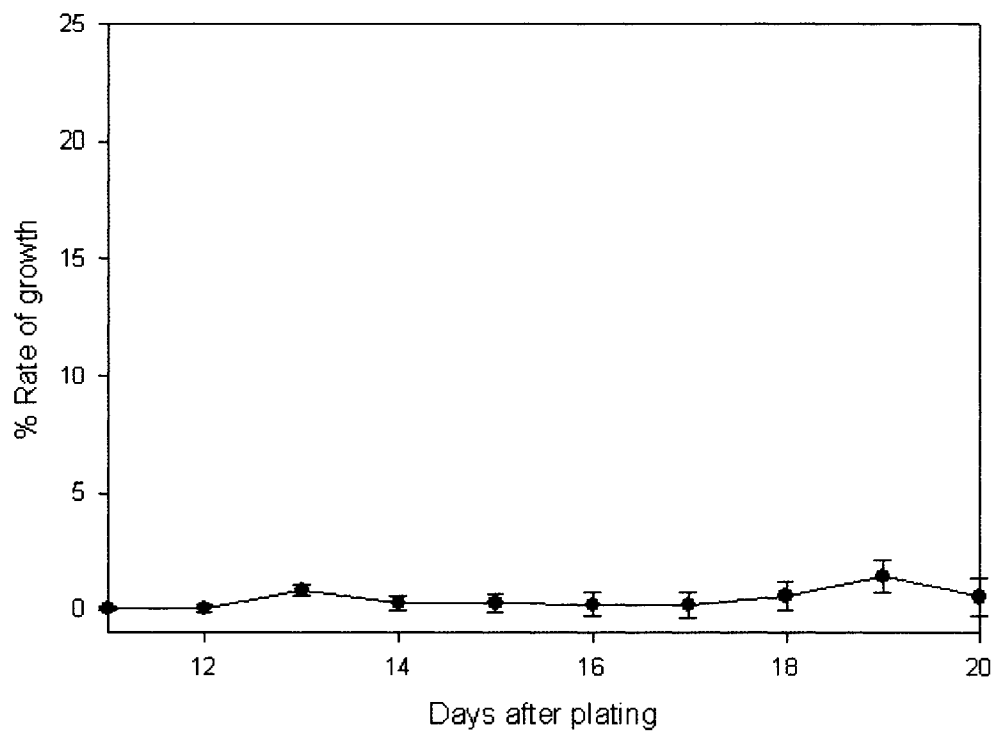
Growth of cells in a roller drum apparatus inhibits cells from attaching to the sides. Epithelial cells require some substrate, whether an ECM or tissue culture plastic, to attach in order to survive [197]. Transformed cells can become anchorage-independent. The graph in Figure 5.6B compares the tRPE cell line to CHO-AA8. It is clear from the graph that the tRPE cells did not divide in culture; in fact, their cell number rapidly declined after initial incubation. The CHO-AA8 cells continued to grow until they reached a steady state.

The ^3H thymidine emulsion autoradiography assay can be used to determine the total percentage of cells that are dividing in a given time. Since transformed cells generally have a faster rate of proliferation than untransformed cells, the assay is also an indicator of whether the cells are transformed. The cells that took up the thymidine generated a high density of silver grains around the nucleus of the cell after exposure to the emulsion (Figure 5.7A). The number of cells that had silver grains were compared to the total number of cells in a given area. The graph in Figure 5.7 B shows that a maximum of 1.5% of the total cells had divided, but most time points generated values less than 1%.

Discussion

The tRPE cell line had similar morphological characteristics as the passaged primary cells. Although the tRPE were never observed to have a hexagonal morphology, they were polygonal. Because ECM is integral in the differentiation of

Figure 5.7: 3 Thymidine emulsion autoradiography of passage 102 tRPE cultures. A) Photomicrograph of cells showing the presence of silver grains over the nucleus; B) Percentage of cells incorporating 3 thymidine at various times after plating.

A.**B.****Pulse termination growth curve**

RPE cells, two types of ECM were used to determine the optimal matrix material. Growth of RPE cells on BCE-ECM and Matrigel has been established and used by many investigators [99, 103, 197, 235, 238].

Morphologically, tRPE cells and primary cells grown on BCE-ECM were epithelioid. When Matrigel was used, the cells were elongated and disorganized. Matrigel did not seem to inhibit the proliferation of RPE cells. Based upon morphological characteristics, BCE-ECM was a better substrate for tRPE cells. Other researchers have shown that primary RPE and other RPE cell lines grow better on BCE-ECM than Matrigel [99, 103]. Growth on BCE-ECM has been shown to produce an increase in CRALBP expression [197].

Addition of growth factors was attempted as a mechanism to increase the differentiation of RPE cells. Although serum-free media has been established for RPE cultures, the cost and time for preparing it prohibited its use [71, 238]. Some of the ingredients were supplemented into the DMEM media as a cost-effective approach. The supplementation of the media was a requirement to fully differentiate the tRPE cells in order to determine if they produced RPE-specific proteins. RPE-65 expression is rapidly lost in cells that have been cultured without any external signals [239, 240].

Multiple groups have confirmed that cultured RPE cells will express ZO-1, RPE-65, and CRALBP under specific conditions [112, 197, 241, 242]. The RPE-characteristic genes and proteins RPE-65, CRALBP, and bestrophin were expressed in the tRPE cell line using the combination of BCE-ECM and conditioned media.

Both vimentin and cytokeratin immunolocalization will show a strongly staining perinuclear cage-like structure surrounded by profuse finger-like projections extending out from the nucleus [67]. Cytokeratins are intermediate filaments that function in structural integrity and differentiation of epithelial cells [243]. Immunocytochemistry showed that most of the cells were positive for vimentin and cytokeratin, but not all. The tRPE cells were reactive against antibodies to both proteins in a typical pattern of the cytoskeletal network.

Long culture conditions are needed to form adherens junctions in RPE cells [241, 242]. These form an adhesion belt around each cell [243]. Tight junctions provide structural integrity and cell-to-cell signaling between epithelial cells. ZO-1 immunofluorescence shows that the tRPE cells form adherens junctions, and a nearly hexagonal structure.

The tRPE cells are spontaneously immortalized after being passaged up to 150 population doublings. Growth beyond 100 population doublings is considered immortal. The cells did not have the ability to grow in the lack of serum or under low serum conditions and did not form foci (data not shown), which are two other characteristics of transformed cells.

Bovine cells have a normal diploid chromosome number equal to 60 [237]. All of the autosomes are telocentric except the X and Y chromosomes, which are metacentric [244]. Transformed cells have been shown to be aneuploid or heteroploid [245]. Most of the chromosomes that were counted were within the 55-60 range with many at 60 chromosomes.

Growth studies of cells in suspension or soft agar were performed to determine whether the cells were anchorage-independent and exhibited the loss of contact inhibition [246]. The tRPE cell numbers dramatically decreased at the beginning of the experiment, indicating they require a substrate to attach.

Pulse labeling was performed to confirm that the cultures stopped or slowed down proliferation after confluence, a process called density-dependent inhibition of cell growth [247]. The number of dividing cells was never greater than 1.5%, with most times being less than 1%. Comparatively, actively dividing tRPE cells were expected to have a rate of labeling around 25%. Transformed cells could show up to 50% of cells labeled with ^3H -thymidine. The tRPE cells did not exhibit significant cell division at confluency.

From the results, it appears that the tRPE is a stable RPE cell line that demonstrates many features of primary RPE cells, and therefore they can serve as a valuable tool in RPE research. They are an improvement over the current ARPE-19 cell line because they are immortal and, therefore, do not senesce. Additionally, the tRPE cells do not have transformation characteristics, such as those found in the D407 and BPEI-1 cell lines.

CHAPTER 6

MECHANISMS OF RPE CELL DEATH

Introduction

The main predictor of longevity in post-mitotic cells is the lack of accumulation of lipofuscin granules [131]. Lipofuscin is an amorphous heterogeneous mixture of unknown compounds that are lipid-like materials, protein deposits and generally insoluble debris [137, 146]. It can account for up to 30% of the cytoplasmic volume [45]. In RPE cells, lipofuscin is believed to be an accumulation of undegradable compounds from the byproduct of phagocytosis of photoreceptor outer segments combined with autophagocytosis [137, 138, 248]. Some of the compounds in the RPE resemble oxidized polyunsaturated fatty acids and proteins that are commonly seen in lipofuscin throughout the body [161, 249]. Other components have characteristic fluorescence spectra that resemble retinoids [139, 249, 250]. A portion of the fluorescent material within the RPE is a mixture that resembles both melanin and lipofuscin. This material has been termed melanolipofuscin and may be a better indicator of AMD than lipofuscin [45, 181].

The chloroform extract of human RPE lipofuscin is composed of over 10 types of fluorescent material [139, 149, 170]. This lipofuscin has an excitation

maximum of 365nm and a peak emission of 590nm [182]. The only fully characterized components of the fluorescent chloroform extract have been the bis-retinoid Schiff base, termed A2E, and several of its oxidation products [137, 176]. A2E is derived from the conversion of A2PE located in the photoreceptor cells [57, 141, 145].

Because lipofuscin can absorb light in the visible spectrum, studies have been performed to attempt to understand its potential for phototoxicity. In the *abcr -/-* model of Stargardt's disease, a prolific accumulation of A2E was evident [144]. Since Eldred and Lasky have evaluated lipofuscin and determined the chemical structure of A2E, a number of cytotoxicity studies have been performed with A2E [140, 141, 145]. A2E has been shown to have detergent-like properties and interact with lipid membranes [18,140, 169,173, 174]. It also impairs lysosomal activity, but does not inhibit lysosomal enzymes [171]. Other researchers have shown A2E to induce blue-light-mediated apoptosis [169, 170]. Most of these effects have been attributed to the amphiphilic nature of A2E, although Wang et al. have shown reactive aldehyde and ketone oxidation products [121]. Additionally, A2E is highly oxidized when irradiated in the presence of oxygen both *in vitro* and *in vivo* [147, 167, 176].

Although A2E studies have been quite useful in understanding the compound, there has been controversy whether its effects *in vitro* are exaggerated when conclusions are interpreted with respect to AMD [166, 251]. Primarily, the controversy centers around whether A2E produces the effects at physiologically

relevant concentrations, and whether A2E is the predominant fluorophore [146, 165, 215, 252, 253].

The hypothesis of this dissertation was to determine whether mutations in ABCR causes an increase in lipofuscin compounds, which leads to RPE cell death. The tRPE cell line was used to determine if it was a suitable model for AMD through cytotoxicity studies. The focus was directed towards A2PE-fed RPE cells irradiated with blue light. Cell cultures were analyzed using the LIVE/DEAD assay and an apoptosis assay. Additionally, the cellular extract was analyzed by mass spectrometry to determine if the A2PE was altered in the cells, and if it was converted into the major lipofuscin component, A2E.

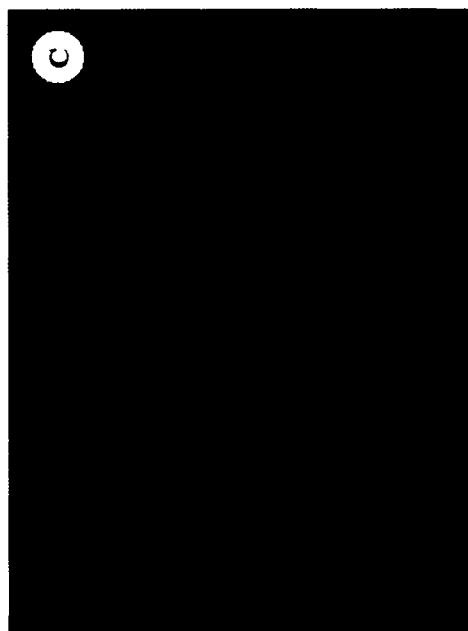
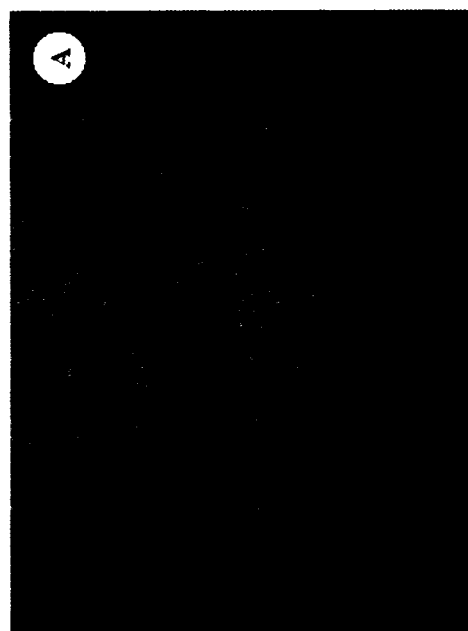
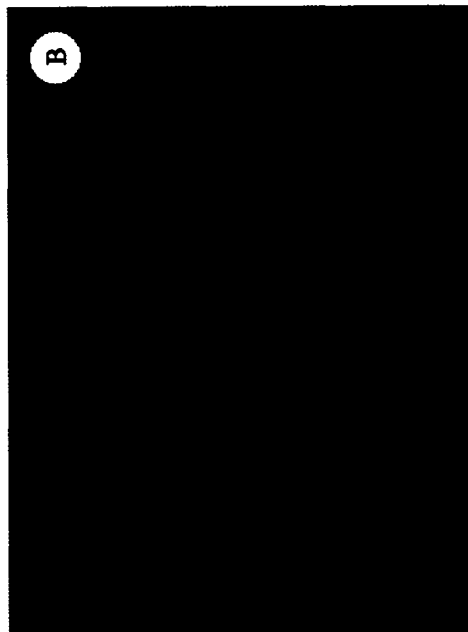
Results

ARPE-19 and tRPE cells were fed A2PE in small quantities over a period of 2 weeks to reduce toxicity induced by rapid uptake of the compound. The cells were kept in the dark during the experiment and fed under the conditions of low intensity yellow light. Figure 6.1 pictures a sample of the tRPE cells that had taken up the A2PE. The particles appear punctate and arranged in a perinuclear fashion in all figures.

Live Dead Analysis of A2PE-Fed Cells

Does A2PE affect the survival of RPE cells? The Molecular Probes

Figure 6.1: Fluorescent photographs of tRPE cells that have taken up A2PE. A) Phase contrast microscopy image; B) FITC filter cube image; C) TRITC filter cube image.



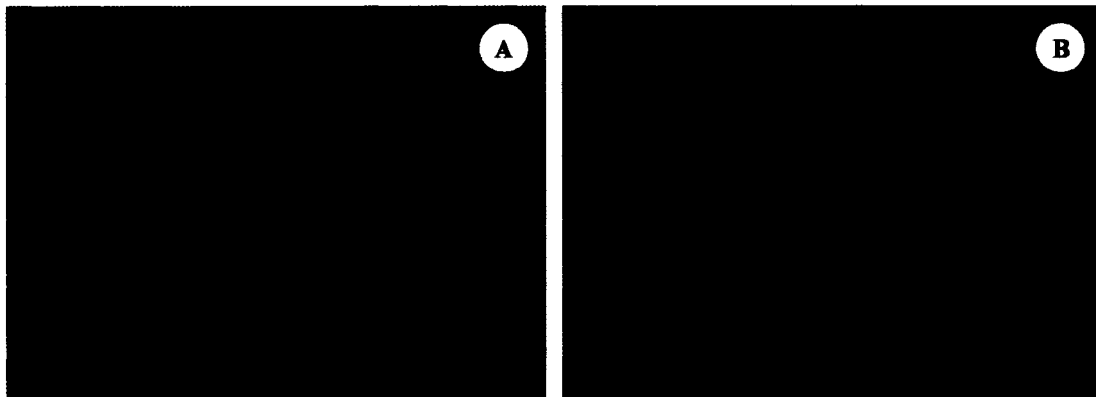
Live/Dead kit allows for the quick and easy determination of cell fate. Some of the cells converted the calcein AM to calcein (Image A), indicating their viability. Other cells had died and incorporated the ethidium homodimer (Image B). Panel 1 in Figure 6.2 depicts ARPE-19 cells that were irradiated for 6 hours and then analyzed. For comparison, cells that were not irradiated are shown in Panel 2. To determine if the tRPE cell line would compare to the ARPE-19 cells, the tRPE were only irradiated for 4 hours yet they showed the same response as the ARPE-19 cells (Panel 3). Hoechst staining (Panel 4, Figure C), which shows all nuclei, was performed for all experiments to be used to count the total numbers of cells. The phase contrast microscopy image (Panel 4, Figure D) of the irradiated culture in panel 1 shows that the cells were rounded up and not attached to each other, which is indicative of dying cells for epithelial cultures. Additionally, there was an orange/yellow hue to the cells.

Individual photographs were scored for the number of dead cells compared to total cells to quantitatively assess the effects of A2PE, light, time and cell type. The data for the different conditions were compiled in a graph shown in Figure 6.3. Blue light exposure alone (yellow bars) was not toxic to either cell line. Additionally, A2PE incorporation under dark conditions (red bars) does not affect the viability of either cell line. Clearly, A2PE incorporation causes the cells to become immediately sensitive to irradiation with blue light, as seen by the cross-hatched bars. The tRPE cells may have an elevated sensitivity when compared to the ARPE-19 cells.

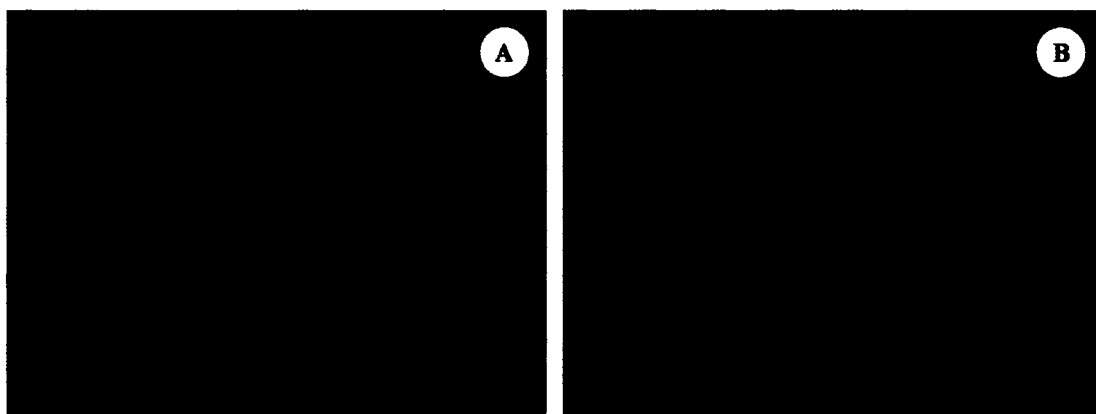
Additionally, one experiment was performed to determine if the RPE cells could

Figure 6.2: Live/Dead photographs of RPE cells. A) The calcein AM is converted to the highly fluorescent calcein by an intrinsic esterase in live cells, which is shown using the FITC filter cube; B) Ethidium homodimer enters dead cells through damaged membranes and the fluorescence is seen with the TRITC filter cube; C) DAPI filter cube showing the fluorescence of the Hoechst 33258 nuclear stain; D) Phase contrast microscopy. Panel 1: A2PE-fed ARPE-19 cells irradiated for 6 hours. Panel 2: Unirradiated control ARPE-19 cells without A2PE. Panel 3: A2PE-fed tRPE cells irradiated for 6 hours. Panel 4: Same exposure as panel 1.

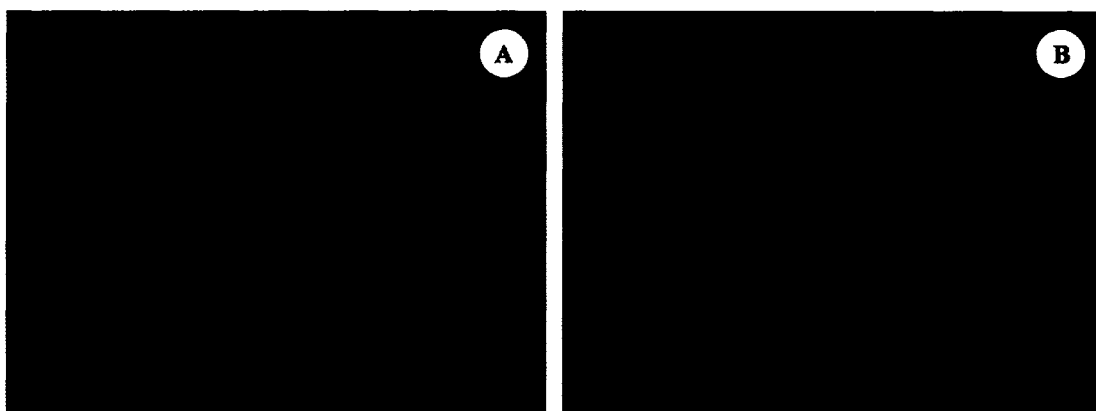
Panel 1



Panel 2



Panel 3



Panel 4

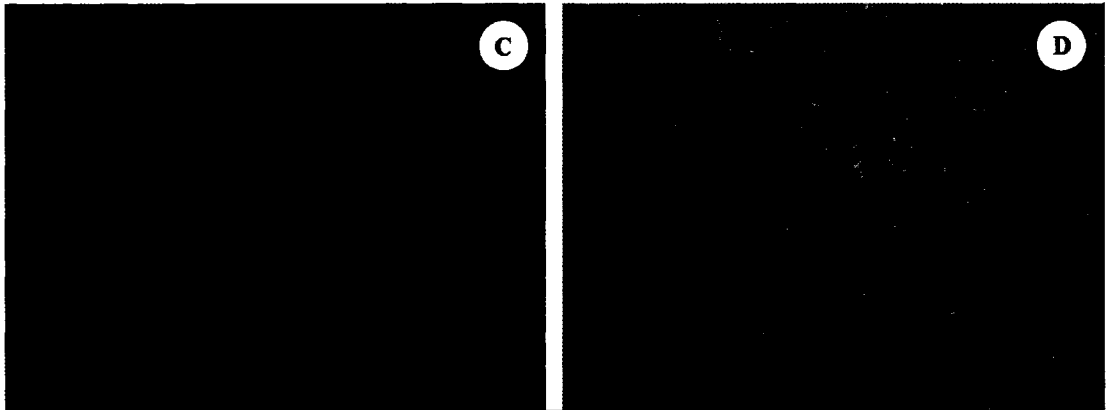
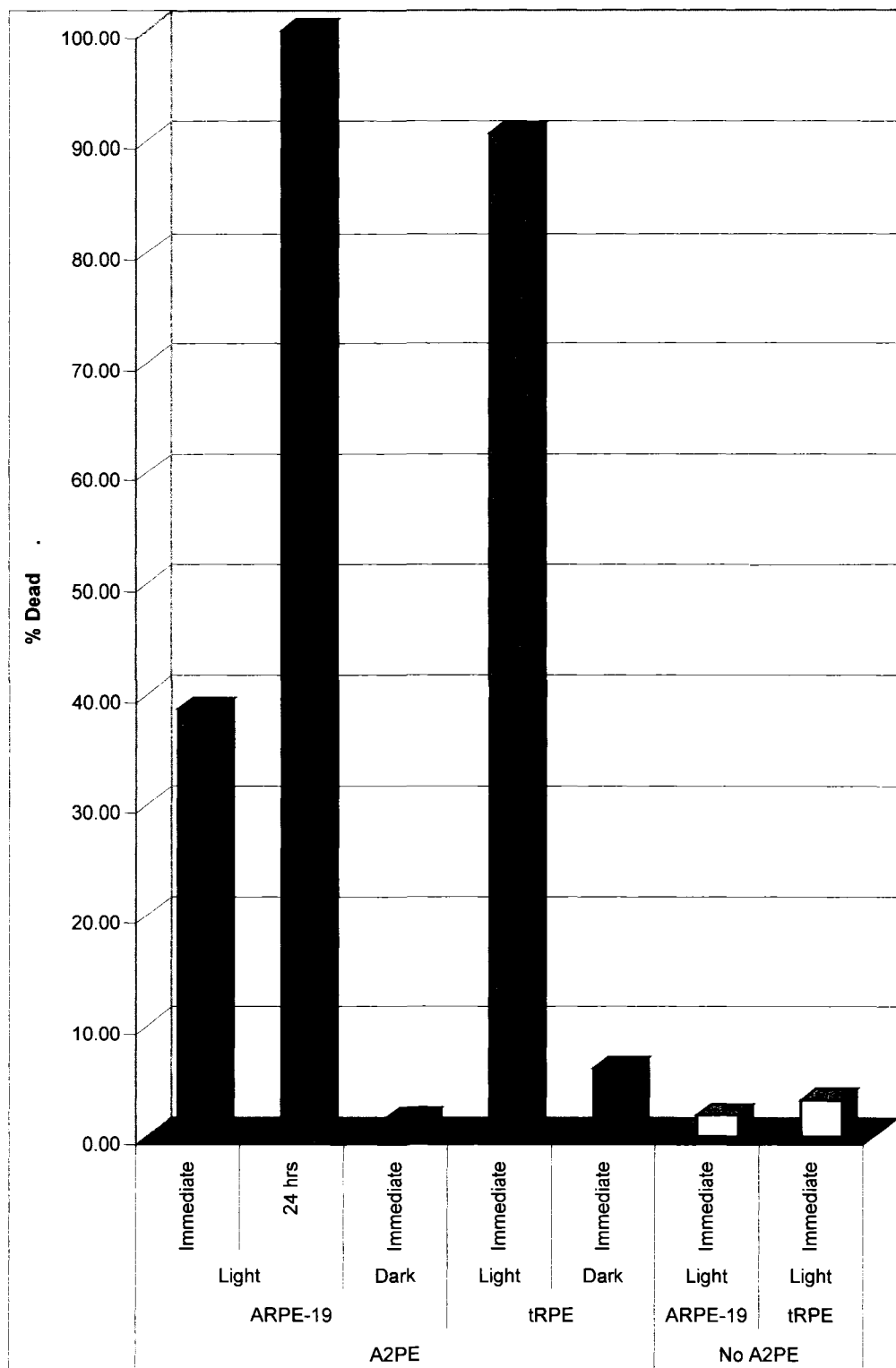


Figure 6.3: Cell death of cultures with or without A2PE under various irradiation times.



recover 24 hours after irradiation (blue bar). Under the conditions utilized for ARPE-19, both A2PE incorporation and irradiation with blue light cause a large number of cells to die. Cell death was not immediate for all of the cells, as seen by increase in death after allowing the cells to recover.

Apoptosis Analysis of A2PE-Fed Cells

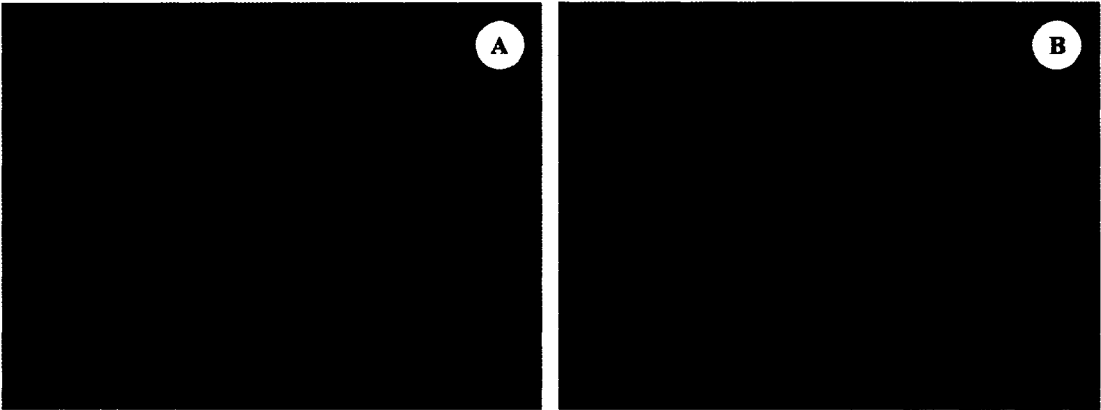
Because of the unusual increase in the number of dead cells after 24 hours, apoptosis was believed to be a potentiating factor. The mechanism of cell death was extremely important to determine in order to gain more insight into the progression of retinal diseases. For this purpose, the Annexin V/ PI kit was utilized to determine the number of cells that were dying by apoptosis versus necrosis. Irradiation of A2PE-fed RPE cells shows an intense green fluorescence in Panel 1 of Figure 6.4, whereas the control culture does not display the green or the red fluorescence (Panel 2).

The annexin V/ PI combination was also used to discriminate between classical signs of late apoptosis. Irradiated A2PE-fed cultures were allowed to recover for 24 hours prior to the assay. Cells that have taken up both dyes were considered in a stage of late apoptosis as shown in Panel 3 [254].

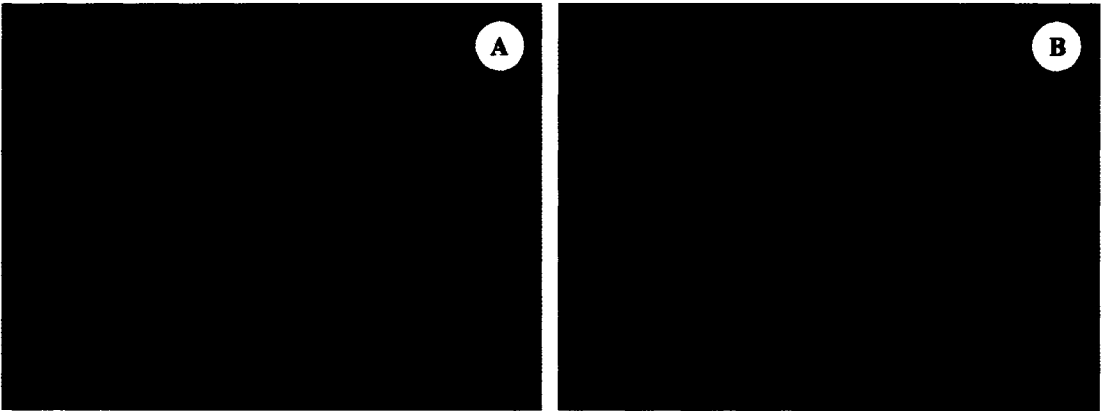
The photographs were scored based upon whether the cells were undergoing early apoptosis (green fluorescence only), late apoptosis (green and red fluorescence) or necrosis (red fluorescence only). Confirming earlier results with the Live/Dead assay, cultures that had incorporated A2PE and kept in the dark had virtually no cell death (Figure 6.5). Additionally, blue light exposure alone did not have a significant

Figure 6.4: Apoptosis photographs of RPE cells. A) FITC filter cube showing the fluorescence of annexin; B) TRITC filter cube showing the fluorescence of propidium iodide. Panel 1: A2PE-fed ARPE-19 cells irradiated with blue light for 6 hours. Panel 2: A2PE-fed ARPE-19 cells kept in the dark. Panel 3: A2PE-fed ARPE-19 cells irradiated with blue light for 6 hours and then allowed to sit for 24 hours prior to adding the fluorescent dyes. Cells that undergo apoptosis are characterized by the flipping of phosphatidylserine to the exterior, which allows the annexin V to bind and cause an intense green fluorescence (Exposures A). Conversely, dead cells do not flip the phosphatidylserine, but will allow the red fluorescent propidium iodide into the nucleus and intercalate with the DNA (Exposures B).

Panel 1



Panel 2



Panel 3

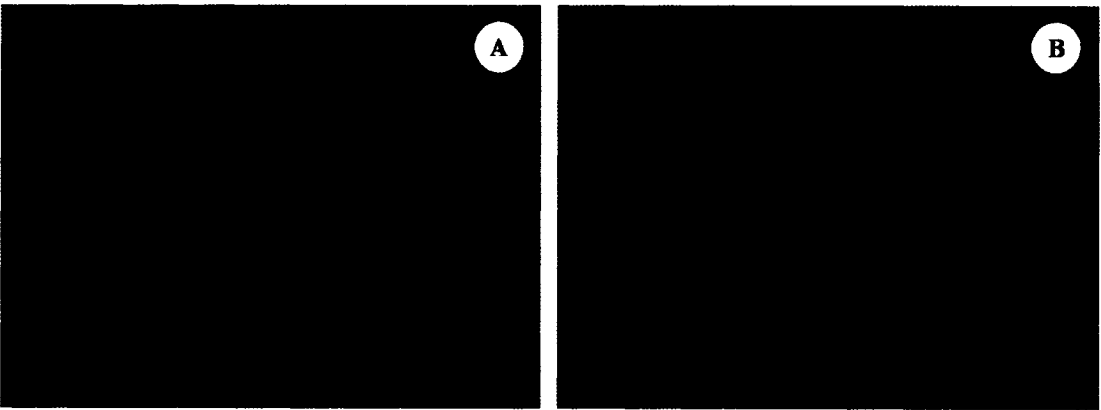
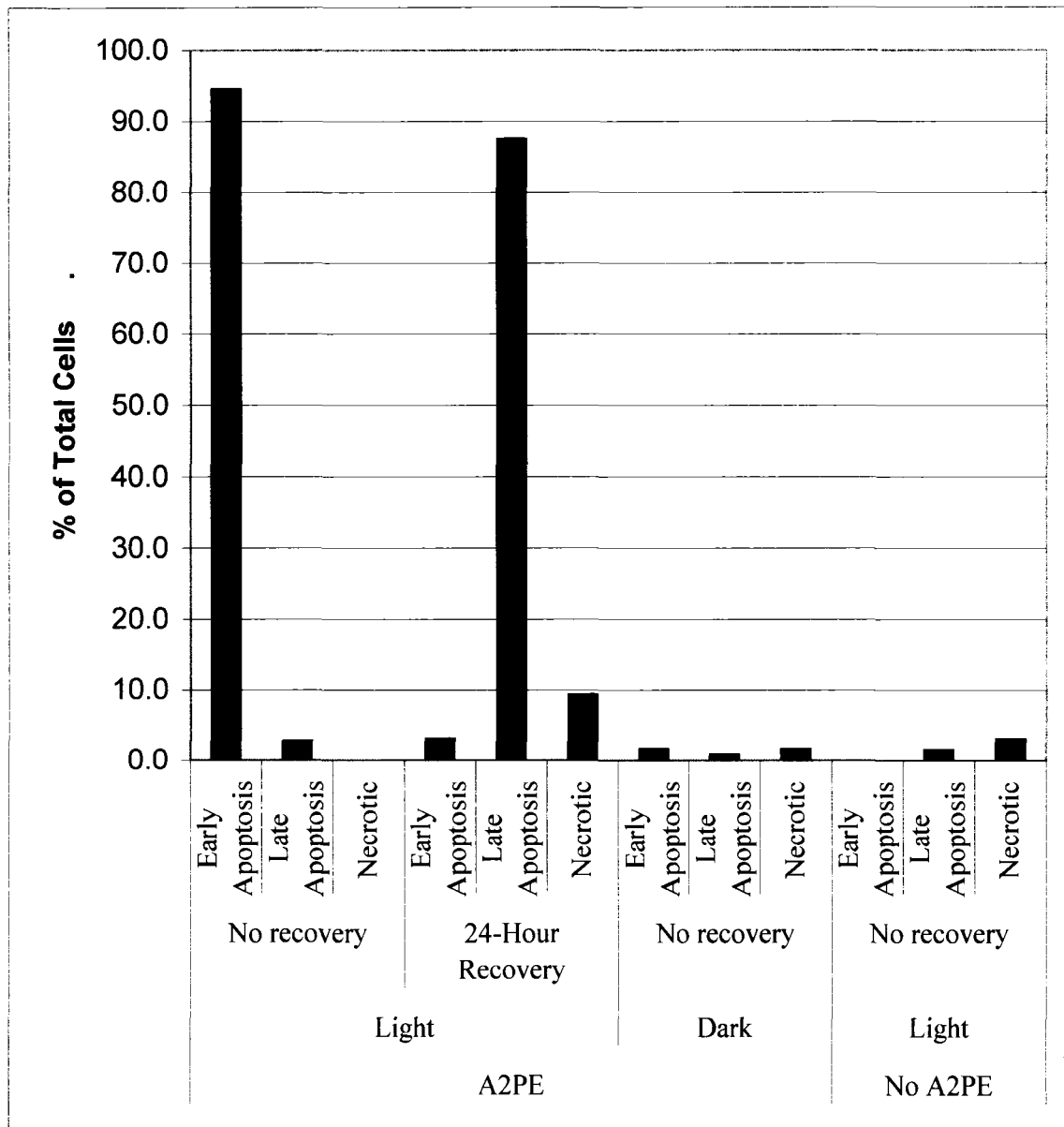


Figure 6.5: Types of cell death of cultures with or without A2PE under various irradiation times.

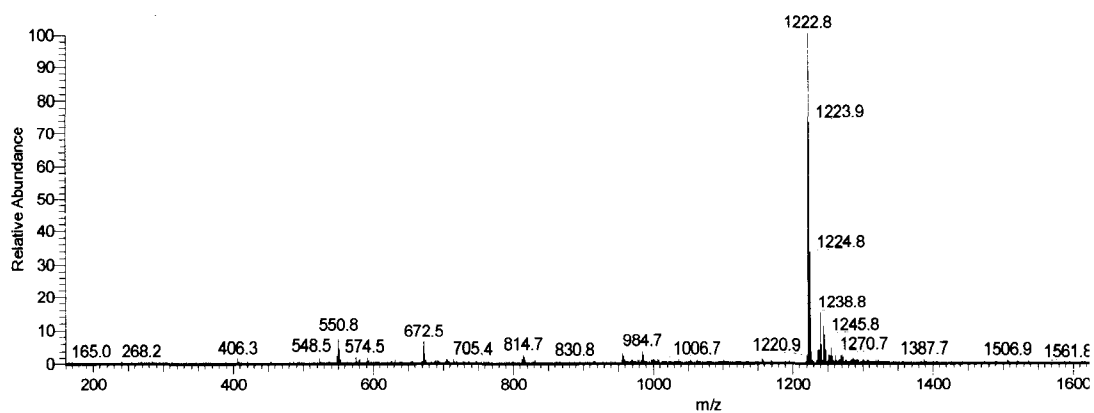
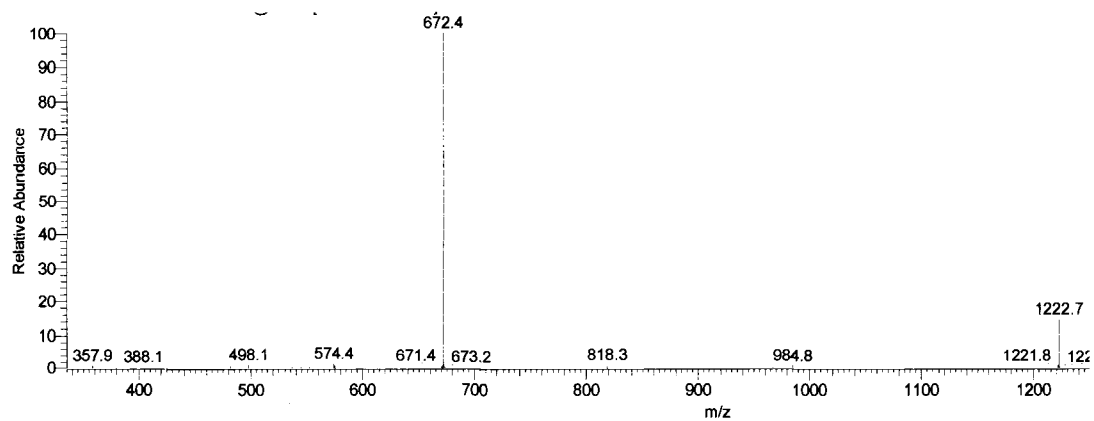
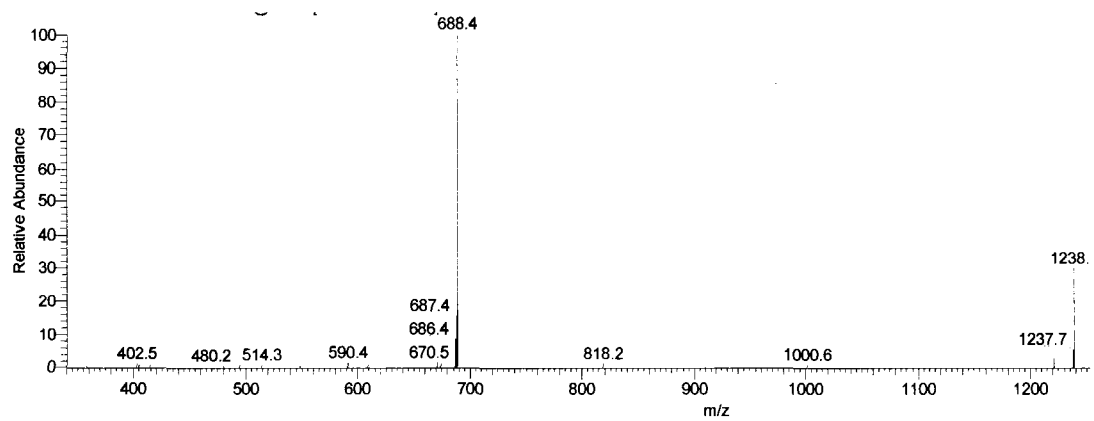


number of cells that had died. Conversely, in the cultures fed A2PE and irradiated with blue light, over 90% of the cells were undergoing classical signs of early apoptosis, and by 24 hours, they displayed classical signs of late apoptotic cells. A marginal number of the cells died by necrosis, but the death was not seen immediately and was not statistically different than the controls.

A2PE Analysis

The A2PE was analyzed by UV/Vis spectrophotometry and ESI-MS prior to feeding to the cells to determine the purity of the compound. This was also used as a base line to determine if A2PE undergoes changes during irradiation in the cell. The full mass spectrum for the 1222.8 m/z peak was predominant, with an ion count of 2.54×10^7 (Figure 6.6A). Additionally, a small peak at 1238.8 m/z was evident, which was indicative of oxidized A2PE by the increase of 16 amu. The MS/MS spectra, in Figure 6.6B, of the 1222.8 m/z peak showed a distinct 672.4 m/z peak using a collision energy of 32%, which corresponded to the A2E compound (592.4 m/z) with a phosphate group attached. The additional phosphate group added 80 amu (HPO_3^{-2}). No A2E peaks were present. The oxygenated species also yielded a single major product at 688.4 m/z using a collision energy of 31% (Figure 6.6C). This peak corresponded to the oxidized and phosphorylated A2E. Based upon the absorption and the MS data, the sample purity was mostly A2PE and very little, if any, of the starting materials, although there was a small amount of oxidized product.

Figure 6.6: ESI-MS spectra of A2PE suspended in methanol with 0.1% formic acid. A) Full MS spectrum; B) MS/MS spectrum for the 1222.8 m/z peak; C) MS/MS spectrum for the 1238.3 m/z peak.

A.**B.****C.**

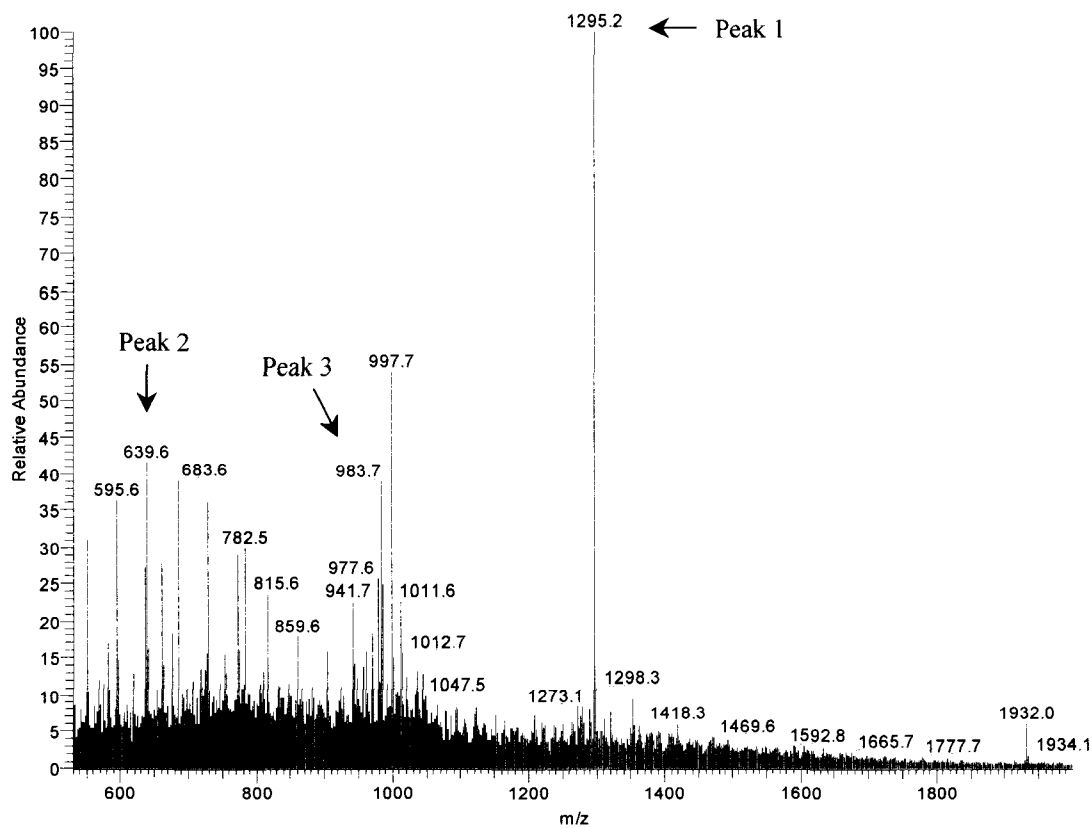
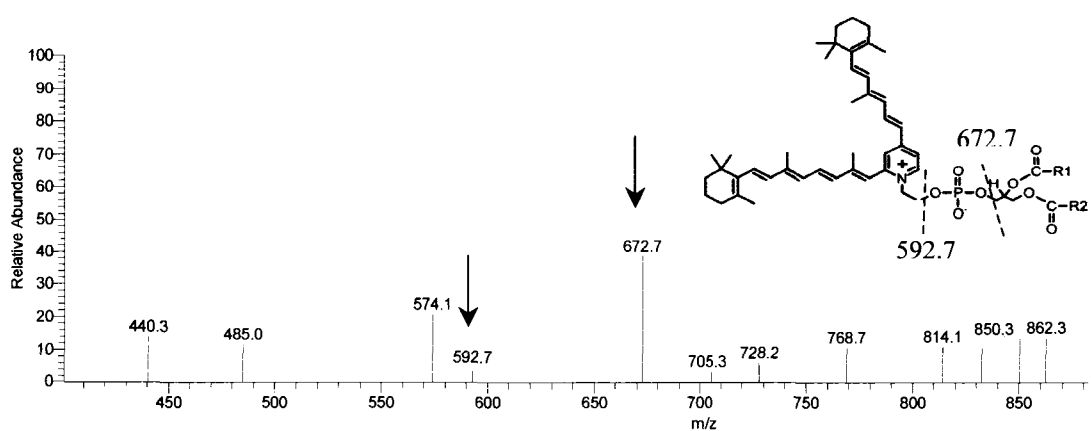
MS of A2PE-Fed Cells

Analysis for the presence of oxidized products of A2PE, and the presence of A2E, was performed by mass spectrometry following irradiation. Figure 6.7A depicts the full mass spectrum profile after direct injection of the organic soluble portion of the RPE cells. There are a number of components to this mixture, but the structures of several of the prominent peaks can be speculated. Peak 1 at m/z 1295.4 is likely to correspond to the known A2PE product with modified fatty acid chains (C22:6 and C16:0) [57, 255]. Peak 2 at 639.7 m/z has been observed before, in both A2E reaction mixtures and extracts of human lipofuscin [176, 177], and corresponds to A2E (592 m/z) that has been oxidized by the addition of three oxygens (48 amu). Finally, peak 3 at 983 m/z was analyzed by MS/MS with a collision energy of 36%. Figure 6.7B was the MS/MS spectrum of the 983 m/z peak. Two significant peaks at 592.7 m/z and 672.7 m/z correspond to A2E and A2E plus a phosphate, respectively. The presence of these two bands signifies that the m/z 983 in the full mass spectrum (Figure 6.7A) is a derivative of A2E. The other components were not subjected to further analysis.

Discussion

Cells that take up A2PE or are irradiated with blue light show limited cell death. Only the combination of feeding cells A2PE followed by irradiation results in a dramatic increase in cell death and apoptosis. An increase in cell death was seen

Figure 6.7: ESI-MS spectra of A2PE isolated from irradiated RPE cells. A) Full MS spectrum. B) MS/MS spectrum of the 983 m/z peak from the full MS spectrum.

A.**B.**

after 24 hours, and our analysis suggests that the primary mechanism of cell death was due to blue light irradiation of A2E-challenged cells was apoptosis. In addition, it was observed that the A2PE-fed tRPE cells were more sensitive to blue light than the ARPE-19 cell line. This indicates that the tRPE cell line may be a better model for retinal maculopathies when studying the damaging effects of blue light irradiation.

Since there have been no published studies on A2PE-fed RPE cells, results were compared to RPE cells fed A2E or human lipofuscin components. Experimentation with A2E *in vitro* and *in vivo* shows that the A2E can be highly oxidized, forming furanoid oxides on the cyclohexenyl rings [147]. Oxiranes have been suggested, but shown to be highly unlikely [147, 177, 178]. Additionally, A2PE has also been suggested to form epoxides [57, 255]. In the present study, three peaks have been characterized. A2PE that had been fed to RPE cells and subsequently irradiated with blue light was altered to form known compounds in lipofuscin. Based upon the analysis of peak 3, the alteration of the acyl fatty acid chain would be likely, since peroxidation of fatty acids has been shown to occur in the presence of reactive oxygen species [162].

The results obtained show that A2PE is cytotoxic to RPE cells only when combined with blue light irradiation, and the primary mechanism of cell death is apoptosis. In these cells, the A2PE is altered to form lipofuscin-like compounds that are found *in vivo*. The tRPE cell line has a higher rate of cell death than the established ARPE-19 cells, which indicates that the tRPE cell line may be a better model for studying maculopathies.

CHAPTER 7

CONCLUSIONS AND FUTURE WORK

ABCR

Much of the work on the structure of ABCR has been done on ABCR purified from isolated bovine rod outer segments [60, 122, 156] by immunoprecipitation, but there is much that is not known about the structural and functional aspects of the protein. Human cDNA has been transiently transfected into HEK cells, but there is no tag for isolation and it is not an inducible system.

Although biochemical analysis will be useful for understanding the protein, the insights may have limited relevance in a biological setting. Using the tightly regulated, inducible expression system as described in this dissertation, the protein can be studied both biochemically and in a cellular environment. So, experiments can be performed with and without mifipristone induction to compare their cellular responses.

Additional constructs were made and cloned in cells in order to incorporate a 6x histidine fusion tag, an enterokinase site and a GFP marker in the new protein. The 6x histidine tag allows the use of a Ni-NTA column which makes the isolation and purification of this protein less time consuming and expensive. The GFP marker

allows the fractions to be visualized and quantitated. The enterokinase site will allow extraneous amino acids, from the GFP and histidine tag, to be cut from the ABCR fusion protein so that the protein can also be studied biochemically in its native form. In this study, only portions of the ABCR construct were confirmed by sequencing. In the future the entire sequence of the ABCR portion of the plasmid needs to be performed to ensure that no mutations were incorporated.

Further confocal microscopy and electron microscopy are needed to determine the precise localization of the protein in CHO cells. Identification of the protein's location will aid in the isolation of the protein and help determine whether the ABCR can be easily separated from the plasma membrane as microsomes by free-flow electrophoresis without denaturing and renaturing the protein. Purified micelles can be utilized as a model for rod outer segments in a variety of biochemical experiments to understand the function of the protein. The same system can be utilized to determine the susceptibility of photodamage to ABCR in the presence of light.

The ABCR protein generated by the cells described in this dissertation and purified by the indicated techniques can be analyzed by mass spectrometry to determine its binding site and to build a model of the structure of the protein. Analysis by low-temperature photoaffinity labeling will yield information about the binding site [256, 257]. Hydrogen/deuterium exchange replaces the surface-exposed amino acids [258] to determine the overall structure of the protein.

tRPE

Cell culture is an important tool in the discovery of the mechanisms of pathogenesis of human diseases. A primary concern is whether the conclusions obtained using cell culture are indicative of the *in vivo* state. The tRPE cell line behaves like primary RPE cells based upon morphological characteristics, mRNA expression and immunocytochemistry. The cells are immortal, but not transformed. Additionally, they have the ability to ingest melanosomes. Using the experimental culture conditions, the tRPE cells were observed to behave as a polarized epithelium that retains the ability to form a quiescent monolayer of cells. Various aspects of the tRPE cells have been analyzed in comparison to the established ARPE-19 cell line and primary bovine RPE cells, and they were found to exhibit the defining RPE cell characteristics. Thus, the tRPE appears to be a valuable new tool for the study of ocular diseases such as macular degeneration.

Experimentation to further characterize the tRPE cells could be enlightening. Determination of RPE polarity can be further established by growth of the tRPE on BCE-ECM in microporous tissue culture filter inserts. Scanning electron micrographs of confluent RPE cells should show basal infoldings and apical microvilli when fed rod outer segments [64].

Cytotoxicity

Experimentation *in vitro* and *ex vivo* has shown lipofuscin to form a variety of reactive oxygen species (ROS') including hydrogen peroxide, singlet oxygen and superoxide anion [164-166]. Because of the difficulty in isolating lipofuscin and the lack of donor eyes, many researchers have utilized A2E in research, since it has been shown to be the primary fluorophore and can be produced *de novo*. A2PE can also be produced synthetically and is more representative of what RPE cells phagocytize in the eye.

RPE cells were challenged with A2PE and irradiated with blue light. This compound clearly sensitized the model RPE cells to blue light, and after irradiation, extensive cell death was noted. Using Annexin V/ PI kit, the mechanism of damage was determined to be primarily apoptosis. Unchallenged cells that were irradiated, or A2PE-fed cells kept in the dark, had virtually no cell death. The tRPE cells are slightly more photosensitive than the ARPE-19 cells, but react in a similar manner as the established cell line. This difference may be a benefit in that the tRPE cells closely resemble late stages of retinal maculopathies.

Chloroform extracts of cells fed A2PE and subsequently irradiated were analyzed in comparison to the initial A2PE. The disappearance of the major A2PE peak and emergence of several additional peaks suggested that the A2PE in irradiated cells was altered to produce known lipofuscin components. These results suggest that future studies may be possible in which the effects of A2PE can be determined on

melanin-repigmented tRPE cells.

Conclusions

Two tools have been developed to test the hypothesis that mutations in the ABCR protein cause an increase in lipofuscin compounds, which results in RPE cell death. The first is the production of a functional ABCR protein in an expression system, which allows isolation of the protein for biochemical analysis and examination of the protein in a cellular environment. Further studies will address how mutations affect the transport of its ligand. Additionally, a novel RPE cell line has been isolated which behaves like primary cells under the conditions previously described in Chapter 5.

The accumulation of A2PE is a result of mutations in ABCR in Stargardt's patients and in *abcr*^{-/-} mice. When this compound is fed to RPE cells, it is phototoxic and produces known lipofuscin compounds. Accordingly, the tRPE cells are a useful model for determining the effects of A2PE damage caused by mutations in ABCR.

REFERENCES

- 1 Allikmets, R., Shroyer, N. F., Singh, N., Seddon, J. M., Lewis, R. A., Bernstein, P. S., et al. (1997). Mutation of the Stargardt Disease Gene (ABCR) in Age-Related Macular Degeneration. *Science*. **277**, 1805-1807.
- 2 Sun, H. and Nathans, J. (2001). The Challenge of Macular Degeneration. *Scientific America*. 69-75.
- 3 Tsunenari, T., Sun, H., Williams, J., Cahill, H., Smallwood, P., Yau, K. W. and Nathans, J. (2003). Structure-Function Analysis of the Bestrophin Family of Anion Channels. *J. Biol. Chem.* **278**, 41114-41125.
- 4 Rattner, A., Sun, H. and Nathans, J. (1999). Molecular Genetics of Human Retinal Disease. *Ann. Rev. Genet.* **33**, 89-131.
- 5 <http://www.terrymen.demon.co.uk/eyepix/fundus.jpg>.
- 6 <http://www.macular-degeneration.org>.
- 7 Young, R. W. (1994). The Family of Sunlight-Related Eye Diseases. *Optometry Vision Sci.* **71**, 125-144.
- 8 Klein, R., Klein, B. K. and Linton, K. P. (1992). Prevalence of Age-Related Maculopathy. *Ophthalmol.* **99**, 933-943.
- 9 The Eye Diseases Prevalence Research Group. (2004). Prevalence of Age-Related Macular Degeneration in the United States. *Arch. Ophthalmol.* **122**, 564-572.
- 10 Chiu, C. J. and Taylor, A. (2007). Nutritional Antioxidants and Age-Related Cataract and Maculopathy. *Exp. Eye Res.* **84**, 229-245.
- 11 Hawkins, B. S., Bird, A., Klein, R. and West, S. K. (1999). Epidemiology of Age-Related Macular Degeneration. *Mol. Vis.* **5**, 26-34.
- 12 www.goodhope.org.uk/departments/eyedept.

- 13 Algvere, P. V. and Seregard, S. (2002). Age-Related Maculopathy: Pathogenetic Features and New Treatment Modalities. *Acta. Ophthalmol. Scand.* **80**, 136-143.
- 14 Guidry, C., Medeiros, N. E. and Curcio, C. C. (2002). Phenotypic Variation of Retinal Pigment Epithelium in Age-Related Macular Degeneration. *Invest. Ophthalmol. Vis. Sci.* **43**, 267-273.
- 15 Yates, J. W. and Morre, A. T. (2000). Genetic Susceptibility to Age-Related Macular Degeneration. *J. Med. Genet.* **37**, 83-87.
- 16 Sarks, J. P., Sarks, S. H. and Killingsworth, M. C. (1988). Evolution of Geographic Atrophy of the Retinal Pigment Epithelium. *Eye.* **2**, 552-577.
- 17 Marcus, D. M. and Camp, M. W. (1998). Age-Related Macular Degeneration. *Sci. and Med.* **5**, 10-17.
- 18 Campochiaro, P. A., Soloway, P., Ryan, S. J. and Miller, J. W. (1999). The Pathogenesis of Choroidal Neovascularization in Patients with Age-Related Macular Degeneration. *Mol. Vis.* **5**, 34-46.
- 19 Schmidt, S., Saunders, A. M., DeLaPaz, M. A., Postel, E. A., Heinis, R. M., Agarwal, A., et al. (2000). Association of the Apolipoprotein E Gene with Age-Related Macular Degeneration: Possible Effect Modification by Family History, Age and Gender. *Mol. Vis.* **6**, 287-293.
- 20 Macular Photocoagulation Study Group. (1991). Argon Laser Photocoagulation for Neovascular Maculopathy: Five-year Results from Randomized Clinical Trials. *Arch. Ophthalmol.* **109**, 1109-1114.
- 21 Adamis, A. P., Shima, D. T., Tolentino, M. J., Gragoudas, E. S., Ferra, N., Folkman, J., et al. (1996). Inhibition of Vascular Endothelial Growth Factor Prevents Retinal Ischemia-Associated Iris Neovascularization in a Nonhuman Primate. *Arch. Ophthalmol.* **114**, 66-71.
- 22 Stargardt, K. B. (1909). Über familiäre, progressive Degeneration in der Makulagegend des Auges. *Albrecht von Graefes Archiv für Ophthalmologie.* **71**, 534-550.
- 23 Fishman, G. A., Farbman, J. S. and Alexander, K. R. (1991). Delayed Rod Dark Adaptation in Patients with Stargardt's Disease. *Ophthalmol.* **98**, 957-962.

- 24 Stone, E. M., Webster, A. R., Vandeburgh, K., Streb, L. M., Hockey, R. R., Lotery, A. J. and Sheffield, V. C. (1998). Allelic Variation in ABCR Associated with Stargardt Disease but Not Age-Related Macular Degeneration. *Nat. Genet.* **20**, 328-329.
- 25 Papermaster, D. S., Schneider, B. G., Zorn, M. A. and Kraehenbuhl, J. P. (1978). Immunocytochemical Localization of a Large Intrinsic Membrane Protein to the Incisures and Margins of Frog Rod Outer Segment Disks. *J. Cell. Biol.* **78**, 415-425.
- 26 Sun, H., Smallwood, P. M. and Nathans, J. (2000). Biochemical Defects in ABCR Protein Variants Associated with Human Retinopathies. *Nat. Genet.* **26**, 242-246.
- 27 Birnback, C. D., Jarvelainen, M., Possin, D. E. and Milam, A. H. (1994). Histopathology and Immunocytochemistry of the Neurosensory Retina in Fundus Flavimaculatus. *Ophthalmol.* **101**, 1211-1219.
- 28 Hadden, O. B. and Grass, J. M. (1976). Fundus Flavimaculatus and Stargardt's Disease. *Am. J. Ophthalmol.* **82**, 527-539.
- 29 Armstrong, J. D., Meyer, D., Xu, S. and Elfervig, J. L. (1998). Long-Term Follow-Up of Stargardt's Disease and Fundus Flavimaculatus. *Ophthalmol.* **105**, 448-458.
- 30 Shroyer, N. F., Lewis, R. A., Yatsenko, A. N., Wensel, T. G. and Lupski, J. R. (2001). Cosegregation and Functional Analysis of Mutant ABCR (ABCA4) Alleles in Families That Manifest Both Stargardt Disease and Age-Related Macular Degeneration. *Hum. Mol. Genet.* **10**, 2671-2678.
- 31 Allikmets, R. (2000). The International ABCR Screening Consortium. Further Evidence for an Association of ABCR Alleles with Age-Related Macular Degeneration. *Am. J. Hum. Genet.* **67**, 487-491.
- 32 Dorey, C. K., Wu, G., Ebenstein, D., Garsd, A. and Weiter, J. J. (1989). Cell Loss in the Aging Retina-Relationship to Lipofuscin Accumulation and Macular Degeneration. *Invest. Ophthalmol. Vis. Sci.* **30**, 1691-1699.
- 33 Delori, F. C., Goger, D. G. and Dorey, C. K. (2001). Age-Related Accumulation and Spatial Distribution of Lipofuscin in RPE of Normal Subjects. *Invest. Ophthalmol. Vis. Sci.* **42**, 1855-1866.

- 34 Mata, N. L., Tzekov, R. T., Liu, X., Weng, J., Birch, D. G. and Travis, G. H. (2001). Delayed Dark-Adaptation and Lipofuscin Accumulation in *abcr*^{+/-} Mice: Implications for Involvement of ABCR in Age-Related Macular Degeneration. *Invest. Ophthalmol. Vis. Sci.* **42**, 1685-1690.
- 35 Kennedy, B. N., Goldflam, S., Chang, M. A., Campochiaro, P., Davis, A. A., Zack, D. J. and Crabb, J. W. (1998). Transcriptional Regulation of Cellular Retinaldehyde-Binding Protein in the Retinal Pigment Epithelium. *J. Biol. Chem.* **273**, 5591-5598.
- 36 Maugeri, A., Klevering, B. J., Rohrschneider, K., Blankenagel, A., Brunner, H. G., Deutman, A. F., et al. (2000). Mutations in the ABCA4 (ABCR) Gene are the Major Cause of Autosomal Recessive Cone-Rod Dystrophy. *Am. J. Hum. Genet.* **6**, 960-966.
- 37 Shroyer, N. F., Lewis, R. A., Yatsenko, A. and Lupiski, J. R. (2001). Null Missense ABCR (ABCA4) Mutations in a Family with Stargardt Disease and Retinitis Pigmentosa. *Invest. Ophthalmol. Vis. Sci.* **42**, 2757-2761.
- 38 Marmorstein, A. D., Marmorstein, L. Y., Rayborn, M., Wang, X., Hollyfield, J. G. and Petrukhin, K. (2000). Bestrophin, the Product of the Best Vitelliform Macular Dystrophy Gene (VMD2), Localizes to the Basolateral Plasma Membrane of the Retinal Pigment Epithelium. *Proc. Nat. Acad. Sci.* **97**, 12758-12763.
- 39 Chong, N. H., Alexander, R. A., Gin, T., Bird, A. C. and Luthert, P. J. (2000). TIMP-3, Collagen, and Elastin Immunohistochemistry and Histopathology of Sorsby's Fundus Dystrophy. *Invest. Ophthalmol. Vis. Sci.* **41**, 898-902.
- 40 Kamei, M. and Hollyfield, J. G. (1999). TIMP-3 in Bruch's Membrane: Changes During Aging and in Age-Related Macular Degeneration. *Invest. Ophthalmol. Vis. Sci.* **40**, 2367-2375.
- 41 Dillon, J., Zheng, L., Merriam, J. C. and Gaillard, E. R. (2004). Transmission of Light to the Aging Human Retina: Possible Implication for Age-Related Macular Degeneration. *Exp. Eye Res.* **79**, 753-759.
- 42 Dillon, J., Zheng, L., Merriam, J. C. and Gaillard, E. R. (1999). The Optical Properties of the Anterior Segment of the Eye: Implications for Cortical Cataract. *Exp. Eye Res.* **68**, 785-795.
- 43 Voke, J. (1999). Radiation Effects on the Eye: Part 3b-- Ocular Effects of Ultraviolet Radiation. *Optometry Today.* **1**, 37-41.

- 44 Gaillard, E. R., Zheng, L., Merriam, J. C. and Dillon, J. (2000). Age-Related Changes in the Absorption Characteristics of the Primate Lens. *Invest. Ophthalmol. Vis. Sci.* **41**, 1454-1459.
- 45 Feeney-Burns, L., Hilderbrand, E. S. and Eldridge, G. S. (1984). Aging Human RPE: Morphometric Analysis of Macular, Equatorial and Peripheral Cells. *Invest. Ophthalmol. Vis. Sci.* **25**, 195-200.
- 46 Polyak, S. L. (1941). *The Retina*. University of Chicago Press: Chicago.
- 47 Kolb, H. (1991). *Principles and Practices of Clinical Electrophysiology of Vision*. (Henkenlively, J.R. and Arden, G. B., Eds.). Pp. 22-52. Mosby Year Book Inc.: St. Louis, MO.
- 48 Shaban, H. and Richter, C. (2002). A2E and Blue Light in the Retina: The Paradigm of Age-Related Macular Degeneration. *Biol. Chem.* **383**, 537-545.
- 49 Marshall, J. (1985). Radiation and the Ageing Eye. *Ophthalmol. Physiol. Opt.* **5**, 241-263.
- 50 Ahnelt, P. K., Kolb, H. and Pflug, R. (1987). Identification of a Subtype of Cone Photoreceptor, Likely to be Blue Sensitive, in the Human Retina. *J. Comp. Neurol.* **255**, 18-34.
- 51 Young, R. W. (1996). Visual Cells and the Concept of Renewal. *Invest. Ophthalmol.* **15**, 700-725.
- 52 Mariani, A. P., Kolb, H. and Nelson, R. (1984). Dopamine-Containing Amacrine Cells of Rhesus Monkey Parallel Rods in Spatial Distribution. *Brain Res.* **322**, 1-7.
- 53 Marshall, J. (1977). The Retinal Receptors and the Pigment Epithelium. In *Scientific Foundations of Ophthalmology*. (Perkins, E.S. and Hill, D.W., Eds.). Pp. 8-17. William Heineman: London.
- 54 Young, R. W. (1967). The Renewel of Photoreceptor Cell Outer Segments. *J. Cell. Biol.* **33**, 61-72.
- 55 LaVail, M. M. (1976). Rod Outer Segment Disc Shedding in Rat Retina: Relationship to Cyclic Lighting. *Science.* **194**, 1071-1074.

- 56 Wihlmark, U., Wrigstad, A., Roberg, K., Nilsson, S. G. and Brunk, U. T. (1997). Lipofuscin Accumulation in Cultured Retinal Pigment Epithelial Cells Causes Enhanced Sensitivity to Blue Light Irradiation. *Free Rad. Biol. and Med.* **22**, 1229-1234.
- 57 Liu, J., Itagaki, Y., Ben-Shabat, S., Nakanishi, K. and Sparrow, J. R. (2000). The Biosynthesis of A2E, a Fluorophore of Aging Retina, Involves the Formation of the Precursor, A2-PE, in the Photoreceptor Outer Segment Membrane. *J. Biol. Chem.* **275**, 29354-29360.
- 58 Yeagle, P. L., Alderfer, J. L. and Albert, A. D. (1996). Structural Determination of the Fourth Cytoplasmic Loop and Carboxy-terminal Domain of Bovine Rhodopsin. *Mol. Vis.* **2**, 12-20.
- 59 Azarian, S. M. and Travis, G. H. (1997). The Photoreceptor Rim Protein is an ABC Transporter Encoded by the Gene for Recessive Stargardt's Disease (ABCR). *FEBS Leters.* **409**, 247-252.
- 60 Illing, M., Molday, L. L. and Molday, R. S. (1997). The 220-kDa Rim Protein of Retinal Rod Outer Segments Is a Member of the ABC Transporter Superfamily. *J. Biol. Chem.* **272**, 10303-10310.
- 61 Sarna, T. (1992). Properties and Function of the Ocular Melanin--A Photobiophysical View. *J. Photochem. Photobiol.* **12**, 215-258.
- 62 Jeffery, G. (1998). The Retinal Pigment Epithelium as a Developmental Regulator of the Neural Retina. *Eye.* **12**, 499-503.
- 63 Libby, R. T., Brunken, W. J. and Hunter, D. D. (2000). Roles of the Extracellular Matrix in Retinal Development and Maintenance. *Results and Problems in Cell Differentiation.* **31**, 115-140.
- 64 Marmorstein, A. D., Finnemann, S. C., Bonilha, V. and Rodriguez-Boulan, E. (1998). Morphogenesis of the Retinal Pigment Epithelium: Toward Understanding Retinal Degenerative Diseases. *Ann. NY. Acad. Sci.* **857**, 1-12.
- 65 Bok, D. (1993). The Retinal Pigment Epithelium: A Versatile Partner in Vision. *J. Cell Sci.* **17**, 189-195.
- 66 Ho, T. C. and Del Priore, L. V. (1997). Reattachment of Cultured Human Retinal Pigment Epithelium to Extracellular Matrix and Human Bruch's Membrane. *Invest. Ophthalmol. Vis. Sci.* **38**, 1110-1118.

- 67 Turksen, K., Opas, M. and Kalnins, V. I. (1989). Cytoskeleton, Adhesion and Extracellular Matrix of Fetal Human Retinal Pigmented Epithelial Cells in Culture. *Ophthalmic. Res.* **21**, 56-66.
- 68 Campochiaro, P. A., Jerdan, J. A. and Glaser, B. M. (1986). The Extracellular Matrix of Human Retinal Pigment Epithelial Cells In Vivo and its Synthesis In Vitro. *Invest. Ophthalmol. Vis. Sci.* **27**, 1615-1621.
- 69 Marmorstein, A. D. (2001). The Polarity of the Retinal Pigment Epithelium. *Traffic.* **2**, 867-872.
- 70 Finnemann, S. C., Bonilha, V. L., Marmorstein, A. D. and Rodriguez-Boulan, E. (1997). Phagocytosis of Rod Outer Segments by Retinal Pigment Epithelial Cells Requires Alpha-V-Beta-5 Integrin for Binding but Not for Internalization. *Proc. Nat. Acad. Sci.* **94**, 12932-12937.
- 71 Ward, D. A. and Barnhill, M. A. (1997). Extracellular Matrix Promotes Differentiation of Retinal Pigment Epithelium. *In Vitro Cell. Dev. Biol.* **33**, 588-591.
- 72 Hu, J. and Bok, D. (2001). A Cell Culture Medium that Supports the Differentiation of Human Retinal Pigment Epithelium Into Functionally Polarized Monolayers. *Mol. Vis.* **7**, 14-19.
- 73 Prota, G. (2000). Melanins, Melanogenesis and Melanocytes: Looking at Their Functional Significance from the Chemist's Viewpoint. *Pigment Cell Res.* **13**, 283-293.
- 74 Schraermeyer, U., Peters, S. E., Thumann, G., Kociok, N. and Heimann, K. (1999). Melanin Granules of Retinal Pigment Epithelium are Connected with the Lysosomal Degradation Pathway. *Exp. Eye Res.* **68**, 237-245.
- 75 Ancans, J., Tobin, D. J., Hoogduijn, M. J., Smit, N. P., Wakamatsu, K. and Thody, A. J. (2001). Melanosomal pH Controls Rate of Melanogenesis, Eumelanin/Phaeomelanin Ratio and Melanosome Maturation in Melanocytes and Melanoma Cells. *Exp. Cell Res.* **268**, 26-35.
- 76 Winder, A., Kobayashi, T., Tsukamoto, K., Urabe, K., Aroca, P., Kameyama, K. and Hearing, V. J. (1994). The Tyrosinase Gene Family--Interactions of Melanogenic Proteins to Regulate Melanogenesis. *Cellular and Mol. Biol. Res.* **40**, 613-626.
- 77 Sharma, S., Wagh, S. and Govindarajan, R. (2002). Melanosomal Proteins--Role in Melanin Polymerization. *Pigment Cell Res.* **15**, 127-133.

- 78 Wagh, S., Ramaiah, A., Subramanian, R. and Govindarajan, R. (2000). Melanosomal Proteins Promote Melanin Polymerization. *Pigment Cell Res.* **13**, 442-448.
- 79 Kobayashi, T., Vieira, W. D., Potterf, B., Sakai, C. and Imokawa, G. (1995). Modulation of Melanogenic Protein Expression During the Switch from Eumelanogenesis to Pheomelanogenesis. *J. Cell Sci.* **108**, 2301-2309.
- 80 Feeney-Burns, L. and Mixon, R. N. (1978). Development of Amelanotic Retinal Pigment Epithelium in Eyes with a Tapetum Lucidum: Melanosome Autophagy and Termination of Melanogenesis. *Dev. Biol.* **72**, 73-88.
- 81 Carr, R. E. and Siegel, I. M. (1979). The Retinal Pigment Epithelium in Ocular Albinism: In *The Retinal Pigment Epithelium*. (Zinn, K. M. and Marmor, M. F., Eds.). Pp. 413-423. Harvard University Press: Cambridge, Massachusetts.
- 82 Schrearmeyer, U. (1993). Does Melanin Turnover Occur in the Eyes of Adult Vertebrates? *Pigment Cell Res.* **6**, 193-204.
- 83 Cockell, C. S. and Knowland, J. (1999). Ultraviolet Radiation Screening Compounds. *Biol. Rev.* **74**, 311-345.
- 84 Mizutani, U., Massalski, T. B., McGinness, J. E. and Corry, P. M. (1976). Low Temperature Specific Heat Anomalies in Melanins and Tumor Melanosomes. *Nature.* **259**, 505-507.
- 85 Wang, Z., Dillon, J. and Gaillard, E. R. (2006). Antioxidant Properties of Melanin in Retinal Pigment Epithelial Cells. *Photochem. Photobiol.* **82**, 474-479.
- 86 Weiter, J. J., Delori, F. C., Wing, G. L. and Fitch, K. A. (1986). Retinal Pigment Epithelium Lipofuscin and Melanin and Choroidal Melanin in Human Eyes. *Invest. Ophthalmol.* **27**, 1063-1067.
- 87 Sarna, T., Burke, J. M., Korytowski, W., Rozanowska, M., Skumatz, C. M., Zareba, A. and Zareba, M. (2003). Loss of Melanin from Human RPE with Aging: Possible Role of Melanin Photooxidation. *Exp. Eye Res.* **76**, 89-98.
- 88 Sheedlo, H. J., Li, L., Fan, W. and Turner, J. E. (1995). Retinal Pigment Epithelial Cell Support of Photoreceptor Survival In Vitro. *In Vitro Cell. Dev. Biol.* **31**, 330-333.

- 89 Robinson, S. R. and Hendrickson, A. (1995). Shifting Relationships Between Photoreceptors and Pigment Epithelial Cells in Monkey Retina: Implications for the Development of Retinal Topology. *Vision Neurosci.* **12**, 767-778.
- 90 Rapaport, D. H., Rakic, P., Yasamura, D. and LaVail, M. M. (1988). Genesis of the Retinal Pigment Epithelium in the Macaque Monkey. *J. Comp. Neurol.* **269**, 479-505.
- 91 Hall, M. O. and Abrams, T. A. (1991). The Phagocytosis of ROS by RPE Cells is Not Inhibited by Mannose-Containing Ligands. *Exp. Eye Res.* 167-170.
- 92 Young, R. W. and Bok, D. (1970). Autoradiographic Studies on the Metabolism of the Retinal Pigment Epithelium. *Invest. Ophthalmol.* **9**, 524-536.
- 93 Hu, D. N., Del Monte, M. A., Liu, S. and Maumenee, I. H. (1982). Morphology, Phagocytosis, and Vitamin A Metabolism of Cultured Human Retinal Pigment Epithelium. *Birth Defects: Original Article Series.* **18**, 67-79.
- 94 Xue, L., Gollapali, D. R., Maiti, P., Jahng, W. J. and Rando, R. R. (2004). A Palmitoylation Switch Mechanism in the Regulation of the Visual Cycle. *Cell.* **117**, 761-771.
- 95 Miceli, M. V., Liles, M. R. and Newsome, D. A. (1994). Evaluation of Oxidative Processes in Human Pigment Epithelial Cells Associated with Retinal Outer Segment Phagocytosis. *Exp. Cell Res.* **214**, 242-249.
- 96 Bok, D. and Hall, M. O. (1971). The Role of the Pigment Epithelium in the Etiology of Inherited Retinal Dystrophy in the Rat. *J. Cell. Biol.* **49**, 664-682.
- 97 Sundelin, S., Wihlmark, U., Nilsson, S. G. and Brunk, U. T. (1998). Lipofuscin Accumulation in Cultured Retinal Pigment Epithelial Cells Reduces Their Phagocytic Capacity. *Curr. Eye Res.* **17**, 851-857.
- 98 Feeney-Burns, L. and Ellersieck, M. R. (1985). Age-Related Changes in the Ultrastructure of Bruch's Membrane. *Am. J. Ophthalmol.* **100**, 686-697.
- 99 Wang, H., Van Patten, Y., Sugino, I. K. and Zarbin, M. A. (2006). Migration and Proliferation of Retinal Pigment Epithelium on Extracellular Matrix Ligands. *J. Rehab. Res. Dev.* **43**, 713-722.

- 100 Tezel, T. H. and Del Priore, L. V. (1997). Reattachment to a Substrate Prevents Apoptosis of Human Retinal Pigment Epithelium. *Graefe's Arch. Clin. Exp. Ophthalmol.* **235**, 41-47.
- 101 Ruoslahti, E. (1997). Stretching is Good for a Cell. *Science.* **276**, 1345-1346.
- 102 Clark, E. A. and Brugge, J. S. (1995). Integrins and Signal Transduction Pathways: The Road Taken. *Science.* **268**, 233-239.
- 103 Gullapalli, V. K., Sugino, I. K., Van Patten, Y. V., Shah, S. and Zarbin, M. A. (2004). Retinal Pigment Epithelium Resurfacing of Aged Submacular Human Bruch's Membrane. *Trans. Am. Ophthalmol. Soc.* **102**, 123-138.
- 104 Tezel, T. H. and Del Priore, L. V. (1999). Repopulation of Different Layers of Host Human Bruch's Membrane by Retinal Pigment Epithelial Cell Grafts. *Invest. Ophthalmol. Vis. Sci.* **40**, 767-774.
- 105 Tezel, T. H., Kaplan, H. J. and Del Priore, L. V. (1999). Fate of Human Retinal Pigment Epithelial Cells Seeded onto Layers of Human Bruch's Membrane. *Invest. Ophthalmol. Vis. Sci.* **40**, 467-476.
- 106 Ho, T. C., Del Priore, L. V. and Kaplan, H. J. (1997). Tissue Culture of Retinal Pigment Epithelium Following Isolation with a Gelatin Matrix Technique. *Exp. Eye Res.* **64**, 133-139.
- 107 Sakai, N., Decatur, J., Nakanishi, K. and Eldred, G. E. (1996). Ocular Age Pigment 'A2-E': An Unprecedented Pyridinium Bisretinoid. *J. Am. Chem. Soc.* **118**, 1559-1560.
- 108 Burns, R. P. and Feeney-Burns, L. (1980). Clinicomorphologic Correlations of Drusen of Bruch's Membrane. *Trans. Am. Ophthalmol. Soc.* **78**, 206-223.
- 109 Hageman, G. S. and Mullins, R. F. (1999). Molecular Composition of Drusen as Related to Substructural Phenotype. *Mol. Vis.* **5**, 28-45.
- 110 Chen, C. S., Mrksich, M., Huang, S., Whitesides, G. M. and Ingber, D. E. (1997). Geometric Control of Cell Life and Death. *Science.* **276**, 1425-1428.
- 111 Alm, A. and Bill, A. (1973). Ocular and Optic Nerve Blood Flow at Normal and Increased Intraocular Pressures in Monkeys (*Macaca irus*): A Study with Radioactively Labeled Microspheres Including Flow Determination of Brain and Some Other Tissues. *Exp. Eye Res.* **15**, 15-29.

- 112 Alizadeh, M., Wada, M., Gelfman, C. M., Handa, J. T. and Hjelmeland, L. M. (2001). Downregulation of Differentiation Specific Gene Expression by Oxidative Stress in ARPE-19 Cells. *Invest. Ophthalmol. Vis. Sci.* **42**, 2706-2713.
- 113 Winkler, B. S., Boulton, M. E., Gottsch, J. D. and Sternberg, P. (1999). Oxidative Damage and Age-Related Macular Degeneration. *Mol. Vis.* **5**, 32-51.
- 114 Luty, G., Grunwald, J., Majji, A. B., Uyama, M. and Yoneya, S. (1999). Changes in Choriocapillaris and Retinal Pigment Epithelium (RPE) in Age-Related Macular Degeneration. *Mol. Vis.* **5**, 1-4.
- 115 Rando, R. R. (2001). The Biochemistry of the Visual Cycle. *Chem. Rev.* **101**, 1881-1896.
- 116 Vogel, R. <http://www.biophysik.uni-freiburg.de/Reiner/main.html>.
- 117 Hargrave, P. A., McDowell, J. H., Curtis, D. R., Wang, J. K., Juszczak, E., Fong, S. L., et al. (1983). The Structure of Bovine Rhodopsin. *Biophys. Struct. Mech.* **9**, 235-244.
- 118 Khorana, H. G. (2000). Molecular Biology of Light Transduction by the Mammalian Photoreceptor, Rhodopsin. *J. Biomol. Struct. Des.* **11**, 1-16.
- 119 Ebrey, T. and Koutalos, Y. (2001). Vertebrate Photoreceptors. *Prog. Retinal Eye Res.* **20**, 49-94.
- 120 Crouch, R. K., Chander, G. J., Wiggert, B. and Pepperberg, D. R. (1996). Retinoids and the Visual Process. *Photochem. Photobiol.* **64**, 613-621.
- 121 Wang, Z., Keller, L. M., Dillon, J. and Gaillard, E. R. (2006). Oxidation of A2E Results in the Formation of Highly Reactive Aldehydes and Ketones. *Photochem. Photobiol.* **82**, 1251-1257.
- 122 Beharry, S., Zhong, M. and Molday, R. S. (2004). N-Retinylidene-phosphatidylethanolamine is the Preferred Retinoid Substrate for the Photoreceptor-Specific ABC Transporter ABCA4 (ABCR). *J. Biol. Chem.* **279**, 53972-53979.
- 123 Sun, H. and Nathans, J. (2001). Mechanistic Studies of ABCR, The ABC Transporter in Photoreceptor Outer Segments Responsible for Autosomal Recessive Stargardt Disease. *J. Bioenergetics and Biomembranes.* **33**, 523-530.

- 124 <http://www.answers.com/topic/visual-cycle>.
- 125 Bavik, C. O., Busch, C. and Eriksson, U. (1992). Characterization of a Plasma Retinol-Binding Protein Membrane Receptor Expressed in the Retinal Pigment Epithelium. *J. Biol. Chem.* **267**, 23035-23042.
- 126 Mata, N. L., Moghrabi, W. N., Lee, J. S., Bui, T. V., Radu, R. A., Horwitz, J. and Travis, G. H. (2004). RPE65 is a Retinyl Ester Binding Protein That Presents Insoluble Substrate to the Isomerase in Retinal Pigment Epithelial Cells. *J. Biol. Chem.* **279**, 635-643.
- 127 Katz, M. L. and Redmond, T. M. (2001). Effect of RPE65 Knockout on Accumulation of Lipofuscin Fluorophores in the Retinal Pigment Epithelium. *Invest. Ophthalmol. Vis. Sci.* **42**, 3023-3030.
- 128 Redmond, T. M., Poliakov, E., Yu, S., Tsai, J. Y., Lu, Z. and Gentleman, S. (2005). Mutation of Key Residues of RPE65 Abolishes its Enzymatic Role as Isomerohydrolase in the Visual Cycle. *Proc. Nat. Acad. Sci.* **102**, 13657-16363.
- 129 Simon, A., Hellman, U., Wernsted, C. and Eriksson, U. (1995). The Retinal Pigment Epithelial-Specific 11-cis Retinol Dehydrogenase Belongs to the Family of Short Chain Alcohol Dehydrogenases. *J. Biol. Chem.* **270**, 1107-1112.
- 130 Nickerson, J. M., Li, G. R., Lin, Z. Y., Takizawa, N., Si, J. S. and Gross, E. A. (1998). Structure-Function Relationships in the Four Repeats of Human Interphotoreceptor Retinoid-Binding Protein (IRBP). *Mol. Vis.* **4**, 33-54.
- 131 Nakano, M. and Gotoh, S. (1992). Accumulation of Cardiac Lipofuscin in the Aging Canine. *J. Gerontol.* **47**, 126-129.
- 132 Terman, A. and Brunk, U. T. (1998). Lipofuscin: Mechanisms of Formation and Increase with Age. *APMIS.* **106**, 265-276.
- 133 Porta, E. A. (2002). Pigments in Aging: An Overview. *Ann. NY. Acad. Sci.* **95**, 57-65.
- 134 Terman, A. (2001). Garbage Catastrophe Theory of Aging: Imperfect Removal of Oxidative Damage? *Redox Rep.* **6**, 15-26.
- 135 Moore, T. and Wang, Y. L. (1947). Formation of Fluorescent Pigment in Vitamin E Deficiency. *Br. J. Nut.* **1**, 53-64.

- 136 Wihlmark, U., Wrigstad, A., Roberg, K., Brunk, U. T. and Nilsson, S. G. (1996). Lipofuscin Formation in Cultured Retinal Pigment Epithelial Cells Exposed to Photoreceptor Outer Segment Material Under Different Oxygen Concentrations. *APMIS*. **104**, 265-271.
- 137 Brunk, U. T. and Terman, A. (2002). Lipofuscin: Mechanisms of Age-Related Accumulation and Influence on Cell Function. *Free Rad. Biol. and Med.* **33**, 611-619.
- 138 Katz, M. L., Drea, C. M. and Robison, W. G. (1986). Relationship Between Dietary Retinol and Lipofuscin in the Retinal Pigment Epithelium. *Mech. Ageing Dev.* **35**, 291-305.
- 139 Eldred, G. E. and Katz, M. L. (1988). Fluorophores of the Human Retinal Pigment Epithelium: Separation and Spectral Characterization. *Exp. Eye Res.* **47**, 71-86.
- 140 Eldred, G. E. and Lasky, M. R. (1993). Retinal Age Pigments Generated by Self-Assembling Lysosomotropic Detergents. *Nature*. **361**, 724-726.
- 141 Parish, C. A., Hashimoto, M., Nakanishi, K., Dillon, J. and Sparrow, J. (1998). Isolation and One-Step Preparation of A2E and iso-A2A, Fluorophores From Human Retinal Pigment Epithelium. *Proc. Nat. Acad. Sci.* **95**, 14609-14613.
- 142 Radu, R. A., Mata, N. L. and Nusowitz, S. (2003). Treatment with Isotretinoin Inhibits Lipofuscin Accumulation in a Mouse Model of Recessive Stargardt's Macular Degeneration. *Proc. Nat. Acad. Sci.* **100**, 4742-4744.
- 143 Harper, W. S. and Gaillard, E. R. (2003). A Photochemical Study of (E,E,E,E)-2-[9-(2-hydroxyethyl)imino-3,7-dimethyl-1,3,5,7-decatrien-1-yl]-1,3,3-trimethylcyclohexene, a Derivative of All-trans-Retinal and Ethanolamine. *Photochem. Photobiol.* **78**, 298-305.
- 144 Weng, J., Mata, N. L., Azarian, S. M., Tzekov, R. T., Birch, D. G. and Travis, G. H. (1999). Insights into the Function of Rim Protein in Photoreceptors and Etiology of Stargardt's Disease from the Phenotype in abcr Knockout Mice. *Cell*. **98**, 13-23.
- 145 Mata, N. L., Weng, J. and Travis, G. H. (2000). Biosynthesis of a Major Lipofuscin Fluorophore in Mice and Humans with ABCR-Mediated Retinal and Macular Degeneration. *Proc. Nat. Acad. Sci.* **97**, 7154-7159.

- 146 Warburton, S., Southwick, K., Hardman, R. M., Secret, A. M., Grow, R. K., Xin, H., et al. (2005). Examining the Proteins of Functional Retinal Lipofuscin Using Proteomic Analysis as a Guide for Understanding Origin. *Mol. Vis.* **11**, 1122-1134.
- 147 Dillon, J., Wang, Z., Avalle, L. B. and Gaillard, E. R. (2004). The Photochemical Oxidation of A2E results in the Formation of a 5,8,5',8'-bis-furanoid Oxide. *Exp. Eye Res.* **79**, 537-542.
- 148 Kagan, V. E., Shvedova, A. A. and Novikov, K. N. (1978). On the Participation of Phospholipases in the Repair of Photoreceptor Membranes After Lipid Peroxidation. *Biophysik.* **23**, 279-282.
- 149 Feeney-Burns, L., Berman, E. R. and Rothman, H. (1980). Lipofuscin of Human Retinal Pigment Epithelium. *Am. J. Ophthalmol.* **90**, 783-791.
- 150 Feeney, L. and Berman, E. R. (1976). Oxygen Toxicity: Membrane Damage by Free Radicals. *Invest. Ophthalmol.* **15**, 789-792.
- 151 Feeney-Burns, L. (1980). The Pigments of the Retinal Pigment Epithelium. *Curr. Top. Eye. Res.* **2**, 119-178.
- 152 Bungert, S., Molday, L. L. and Molday, R. S. (2001). Membrane Topology of the ATP Binding Cassette Transporter ABCR and Its Relationship to ABC1 and Related ABCA Transporters. *J. Biol. Chem.* **276**, 23539-23546.
- 153 Suarez, T., Biswas, S. B. and Biswas, E. E. (2002). Biochemical Defects in Retina-specific Human ATP Binding Cassette Transporter Nucleotide Binding Domain 1 Mutants Associated with Macular Degeneration. *J. Biol. Chem.* **277**, 21759-21767.
- 154 Dean, M., Rzhetsky, A. and Allikmets, R. (2001). The Human ATP-Binding Cassette (ABC) Transporter Superfamily. *Genome Res.* **11**, 1156-1166.
- 155 Molday, L. L., Rabin, A. R. and Molday, R. S. (2000). ABCR Expression in Foveal Cone Photoreceptors and its Role in Stargardt Macular Dystrophy. *Nat. Genet.* **25**, 257-258.
- 156 Sun, H., Molday, R. S. and Nathans, J. (1999). Retinal Stimulates ATP Hydrolysis by Purified and Reconstituted ABCR, the Photoreceptor-Specific ATP-Binding Cassette Transporter Responsible for Stargardt Disease. *J. Biol. Chem.* **274**, 8269-8281.

- 157 Harlan, J. B., Weidenthal, D. T. and Green, W. R. (1997). Histological Study of a Shielded Macula. *Retina*. **17**, 232-238.
- 158 Grimm, C., Wenzel, A., Hafezi, F. and Reme, C. E. (2000). Gene Expression in the Mouse Retina: The Effect of Damaging Light. *Mol. Vis.* **6**, 252-260.
- 159 Katz, M. L. and Edred, G. E. (1989). Retinal Light Damage Reduces Autofluorescent Pigment Deposition in the Retinal Pigment Epithelium. *Invest. Ophthalmol. Vis. Sci.* **30**, 37-43.
- 160 Shigenaga, M. K., Hagen, T. M. and Ames, B. N. (1994). Oxidative Damage and Mitochondrial Decay in Aging. *Proc. Nat. Acad. Sci.* **91**, 10771-10778.
- 161 Beatty, S., Koh, H. H., Phil, M., Henson, D. and Boulton, M. (2000). The Role of Oxidative Stress in the Pathogenesis of Age-Related Macular Degeneration. *Surv. Ophthalmol.* **45**, 115-134.
- 162 Wright, A., Hawkins, C. L. and Davies, M. J. (2003). Photooxidation of Cells Generates Long-Lived Intracellular Protein Peroxides. *Free Rad. Biol. Med.* **34**, 637-647.
- 163 Sun, H. and Nathans, J. (2001). ABCR, the ATP-binding Cassette Transporter Responsible for Stargardt Macular Dystrophy, Is an Efficient Target of All-trans-retinal-mediated Photooxidative Damage In Vitro. *J. Biol. Chem.* **15**, 11766-11774.
- 164 Gaillard, E. R., Atherton, S. J., Eldred, G. and Dillon, J. (1995). Photophysical Studies on Human Retinal Lipofuscin. *Photochem. Photobiol.* **61**, 448-453.
- 165 Boulton, M., Dontsov, A., Jarvis-Evans, J., Ostrovsky, M. and Svistunenko, D. (1993). Lipofuscin is a Photoinducible Free Radical Generator. *J. Photochem. Photobiol.* **19**, 210-204.
- 166 Rozanowska, M., Wessels, J., Boulton, M., Burke, J. M., Rodgers, M. A., Truscott, T. G. and Sarna, T. (1998). Blue Light-Induced Singlet Oxygen Generation by Retinal Lipofuscin in Non-Polar Media. *Free Rad. Biol. Med.* **24**, 1107-1112.
- 167 Sparrow, J. R., Zhou, J., Ben-Shabat, S., Vollmer, H., Itagaki, Y. and Nakanishi, N. (2002). Involvement of Oxidative Mechanisms in Blue-Light-Induced Damage to A2E-Laden RPE. *Invest. Ophthalmol. Vis. Sci.* **43**, 12222-12227.

- 168 Sparrow, J. R., Zhou, J. and Cai, B. (2003). DNA is a Target of the Photodynamic Effects Elicited in A2E-Laden RPE by Blue-Light Illumination. *Invest. Ophthalmol. Vis. Sci.* **44**, 2245-2251.
- 169 Suter, M., Reme, C., Grimm, C., Wenzel, A., Jaattela, M., Esser, P., et al. (2000). Age-Related Macular Degeneration: The Lipofuscin Component N-Retinyl-N-Retinylidene Ethanolamine Detaches Proapoptotic Proteins from Mitochondria and Induces Apoptosis in Mammalian Retinal Pigment Epithelial Cells. *J. Biol. Chem.* **275**, 39625-39630.
- 170 Sparrow, J. R. and Cai, B. (2001). Blue Light-Induced Apoptosis of A2E-Containing RPE: Involvement of Caspase-3 and Protection by Bcl-2. *Invest. Ophthalmol. Vis. Sci.* **42**, 1356-1362.
- 171 Schutt, F., Davies, S., Kopitz, J., Holz, F. G. and Boulton, M. E. (2000). Photodamage to Human RPE Cells by A2-E, a Retinoid Component of Lipofuscin. *Invest. Ophthalmol. Vis. Sci.* **41**, 2303-2308.
- 172 Finnemann, S. C., Leung, L. W. and Rodriguez-Boulan, E. (2002). The Lipofuscin Component A2E Selectively Inhibits Phagolysosomal Degradation of Photoreceptor Phospholipid by the Retinal Pigment Epithelium. *Proc. Nat. Acad. Sci.* **99**, 3842-3847.
- 173 Schutt, F., Bergmann, M., Holz, F. G. and Kopitz, J. (2002). Isolation of Intact Lysosomes From Human RPE Cells and Effects of A2-E on the Integrity of the Lysosomal and Other Cellular Membranes. *Graefe's Arch. Clin. Exp. Ophthalmol.* **240**, 983-988.
- 174 De, S. and Sakmar, T. P. (2002). Interaction of A2E with Model Membranes. Implications to the Pathogenesis of Age-Related Macular Degeneration. *J. Gen. Physiol.* **120**, 147-157.
- 175 Gaillard, E. R., Avalle, L. B., Keller, L. M., Wang, Z., Reszka, K. J. and Dillon, J. P. (2004). A Mechanistic Study of the Photooxidation of A2E, a Component of Human Retinal Lipofuscin. *Exp. Eye Res.* **79**, 313-319.
- 176 Avalle, L. B., Wang, Z., Dillon, J. P. and Gaillard, E. R. (2004). Observation of A2E Oxidation Products in Human Retinal Lipofuscin. *Exp. Eye Res.* **78**, 895-898.
- 177 Radu, R. A., Mata, N. L., Bagla, A. and Travis, G. H. (2004). Light Exposure Stimulates Formation of A2E Oxiranes in a Mouse Model of Stargardt's Macular Degeneration. *Proc. Nat. Acad. Sci.* **100**, 5928-5933.

- 178 Ben-Shabat, S., Itagaki, Y., Jockusch, S., Sparrow, J. R., Turro, N. J. and Nakanishi, K. (2002). Formation of a Nonaoxirane from A2E, a Lipofuscin Fluorophore Related to Macular Degeneration, and Evidence of Singlet Oxygen Involvement. *Agnew. Chem. Int. Ed.* **41**, 814-817.
- 179 Dayhaw-Barker, P. (2002). Retinal Pigment Epithelium Melanin and Ocular Toxicity. *Int. J. Toxicology.* **21**, 451-454.
- 180 Dontsov, A. E., Glickman, R. D. and Ostrovsky, M. A. (1999). Retinal Pigment Epithelium Pigment Granules Stimulate the Photo-Oxidation of Unsaturated Fatty Acids. *Free Rad. Biol. and Med.* **26**, 1436-1446.
- 181 Warburton, S., Davis, W. E., Southwick, K., Xin, H., Woolley, A. T., Burton, G. F. and Thulin, C. D. (2007). Proteomic and Phototoxic Characterization of Melanolipofuscin: Correlation to Disease and Model for its Origin. *Mol. Vis.* **13**, 318-329.
- 182 Feeney-Burns, L. and Eldred, G. E. (1983). The Fate of the Phagosome: Conversion to 'Age Pigment' and Impact in Human Retinal Pigment Epithelium. *Trans. Ophthalmol. Soc. UK.* **103**, 416-421.
- 183 Feeney-Burns, L., Burns, R. P. and Gao, C. L. (1990). Age-Related Macular Changes in Humans Over 90 Years Old. *Am. J. Ophthalmol.* **109**, 265-278.
- 184 Korytowski, W., Pilas, B., Sarna, T. and Kalyanaraman, B. (1987). Photoinduced Generation of Hydrogen Peroxide and Hydroxyl Radicals in Melanins. *Photochem. Photobiol.* **45**, 185-190.
- 185 Kayatz, P., Thumann, G., Luther, T. T., Jordan, J. F., Bartz-Schmidt, K. U., Esser, P. J. and Schraermeyer, U. (2001). Oxidation Causes Melanin Fluorescence. *Invest. Ophthalmol. Vis. Sci.* **42**, 241-246.
- 186 Gaillard, E. R. *Mechanistic Studies of Photooxidative Damage to the Human Eye.* ORC#14.
- 187 Sambrook, J., Fritsch, E. F. and Manaitis, T. (2001). *Molecular Cloning: A Laboratory Manual.* **2**, Pp. 1.32, 1.74-1.84, A2, E3-E4. Cold Spring Harbor Press.: Cold Spring Harbor, New York.
- 188 (11/2002). *Growth and Maintenance of GeneSwitch Cell Lines.* Invitrogen. #25-0341.
- 189 (07/2004). *Lipofectamine 2000 Technical Brief.* Invitrogen.

- 190 (09/2004). *Amicon Ultra-4 Centrifugal Filter Devices: User Guide*. Millipore.
- 191 (02/2003). *Ni-NTA Spin Handbook*. Qiagen. 20-23.
- 192 (12/2003). *HisProbe-HRP Instruction Manual*. Pierce Biotechnology, Inc. #0674.1.
- 193 (01/2006). *SuperSignal West Femto Maximum Sensitivity Substrate*. Pierce Biotechnology, Inc. # 0738.
- 194 (01/2006). *Restore Western Blot Stripping Buffer*. Pierce Biotechnology, Inc. # 0887.1.
- 195 (2004). *Protein Blotting Handbook*. Millipore. #TP001EN00.
- 196 Chang, C. W., Roque, R. S., Defoe, D. M. and Caldwell, R. B. (1991). An Improved Method for Isolation and Culture of Pigment Epithelial Cells from Rat Retina. *Curr. Eye Res.* **10**, 1081-1086.
- 197 Campochiaro, P. A. and Hackett, S. F. (1993). Corneal Endothelial Cell Matrix Promotes Expression of Differentiated Features of Retinal Pigmented Epithelial Cells: Implication of Laminin and Basic Fibroblast Growth Factor as Active Components. *Exp. Eye Res.* **57**, 539-547.
- 198 *BD Matrigel Basement Matrix--Product Specification Sheet*. BD Biosciences.
- 199 MacDonald, R. J., Swift, G. H., Przybyla, A. E. and Chirgwin, J. M. (1987). Isolation of RNA Using Guanidinium Salts. *Meth. Enzymol.* **152**, 219-227.
- 200 (05/2002). *Oligotex Handbook*. Qiagen.17-44.
- 201 (04/1999). *Sensiscript Reverse Transcriptase Handbook*. Qiagen. 9-15.
- 202 (11/2002). *HotStarTaq PCR Handbook*. Qiagen. 10-19.
- 203 Znoiko, S. L., Crouch, R. K., Moiseyev, G. and Ma, J. X. (2002). Identification of the RPE65 Protein in Mammalian Cone Photoreceptors. *Invest. Ophthalmol. Vis. Sci.* **43**, 1604-1609.
- 204 Griffiths, T. D. and Carpenter, J. G. (1979). Premature Chromosome Condensation following X Irradiation of Mammalian Cells: Expression Time and Dose-Response. *Radiation Res.* **79**, 187-202.

- 205 Hopwood, L. E. and Tolmach, L. J. (1971). Deficient DNA Synthesis and Mitotic Death in X-Irradiated HeLa Cells. *Radiation Res.* **46**, 70-84.
- 206 (1993). *KODAK Products for Light Microscope Autoradiography*. Eastman Kodak Company. #**KP101268a**.
- 207 Boulton, M. and Marshall, J. (1985). Repigmentation of Human Retinal Pigment Epithelial Cells In Vitro. *Exp. Eye Res.* **41**, 209-218.
- 208 Avalle, L. B. Personal Communication. .
- 209 (10/2005). *LIVE/DEAD Viability/Cytotoxicity Kit for Mammalian Cells*. Molecular Probes-Invitrogen. #**MP 03224**.
- 210 (01/2005). *Vybrant Apoptosis Assay Kit #2*. Molecular Probes-Invitrogen. #**MP 13241**.
- 211 Allikmets, R., Gerrard, B., Hutchinson, A. and Dean, M. (1996). Characterization of the Human ABC Superfamily: Isolation and Mapping of 21 New Genes Using the Expressed Sequence Tags Database. *Hum. Mol. Genet.* **5**, 1649-1655.
- 212 Klein, I., Sarkadi, B. and Varadi, A. (1999). An Inventory of the Human ABC Proteins. *Biochem. Biophys. Acta.* **161**, 237-262.
- 213 Dean, M. and Allikmets, R. (1995). Evolution of ATP-Binding Cassette Transporter Genes. *Curr. Opin. Genet. Dev.* **5**, 779-785.
- 214 Higgins, C. F. (1992). ABC Transporters: From Microorganisms to Man. *Ann. Rev. Cell. Biol.* **8**, 67-113.
- 215 http://www.expasy.ch/tools/pi_tool.html.
- 216 (05/2000). *pRK-5 Mammalian Expression Vector Technical Data Sheet*. BDPharMingen.
- 217 (08/2001). *Using Mifepristone: Technical Brief*. Invitrogen. #**25-0314D**.
- 218 Leach, B. S., Collawn, J. F. and Fish, W. W. (1980). Behavior of Glycopolypeptides with Empirical Molecular Weight Estimation Methods in Sodium Dodecyl Sulfate. *Biochemistry.* **19**, 5734-5741.
- 219 Morin, J. and Hastings, J. (1971). Energy Transfer in a Bioluminescent System. *J. Cell Physiol.* **77**, 313-318.

- 220 Prasher, D. C., Eckenrode, V. K., Ward, W., Prendergast, F. and Cormier, M. (1992). Primary Structure of the *Aequorea victoria* Green-Fluorescent Protein. *Gene*. **111**, 229-233.
- 221 Chalfie, M., Tu, Y., Euskirchen, G., Ward, W. and Prasher, D. (1994). Green Fluorescent Protein as a Marker for Gene Expression. *Science*. **263**, 802-805.
- 222 Cubitt, A. B., Heim, R., Adams, S. R., Boyde, A. E., Gross, L. A. and Tsien, R. Y. (1995). Understanding, Improving and Using Green Fluorescent Proteins. *Trends Biochem. Sci.* **20**, 448-455.
- 223 Cramer, A., Whitehorn, E., Tate, E. and Stemmer, P. (1996). Improved Green Fluorescent Protein by Molecular Evolution Using DNA Shuffling. *Nature Biotechnol.* **14**, 315-319.
- 224 Heim, R., Prasher, D. and Tsien, R. (1994). Wavelength Mutations and Posttranslational Autoxidation of Green Fluorescent Protein. *Proc. Natl. Acad. Sci.* **91**, 12501-12504.
- 225 Heim, R., Cubitt, A. and Tsien, R. (1995). Improved Green Fluorescence. *Nature*. **373**, 663-664.
- 226 Puchooa, D. (2004). Expression of Green Fluorescent Protein Gene in *Litchi* (*Litchi chinensis* Sonn.) Tissues. *J. Appl. Hort.* **6**, 11-15.
- 227 Bodnar, A. G., Ouellette, M., Frolkis, M., Holt, S. E., Chiu, C. P., Morin, G. B., et al. (1998). Extension of Life-Span by Introduction of Telomerase into Normal Human Cells. *Science*. **279**, 349-352.
- 228 Kanuga, N., Winton, H. L., Beauchene, L., Koman, A., Zerbib, A., Halford, S., et al. (2002). Characterization of Genetically Modified Human Retinal Pigment Epithelial Cells Developed for In Vitro and Transplantation Studies. *Invest. Ophthalmol. Vis. Sci.* **43**, 546-555.
- 229 Park, J. K., Kim, B. H., Han, Y. S. and Park, K. (2002). The Effect of Telomerase Expression on the Escape from M2 Crisis in Virus-transformed Human Retinal Pigment Epithelial Cells. *Exp. Mol. Med.* **34**, 107-113.
- 230 McLaren, M. J., Sasabe, T., Li, C. Y., Brown, M. B. and Inana, G. (1993). Spontaneously Arising Immortal Cell Line of Rat Retinal Pigmented Epithelial Cells. *Exp. Cell Res.* **204**, 311-320.

- 231 Rambhatla, L., Chiu, C. P., Glickman, R. D. and Rowe-Rendleman, C. (2002). In Vitro Differentiation Capacity of Telomerase Immortalized Human RPE Cells. *Invest. Ophthalmol. Vis. Sci.* **43**, 1622-1630.
- 232 Davis, A. A., Bernstein, P. S., Bok, D., Turner, J., Nachtigal, M. and Hunt, C. H. (1995). A Human Retinal Pigment Epithelial Cell Line That Retains Epithelial Characteristics After Prolonged Culture. *Invest. Ophthalmol. Vis. Sci.* **36**, 955-964.
- 233 Dunn, K. C., Aotaki-Keen, A. E., Putkey, F. R. and Hjelmeland, L. M. (1996). ARPE-19, A Human Retinal Pigment Epithelial Cell Line with Differentiated Properties. *Exp. Eye Res.* **62**, 155-169.
- 234 www.atcc.org. **CRL-3202**.
- 235 Kim, K. S., Tezel, T. H. and Del Priore, L. V. (1998). Minimum Number of Adult Human Retinal Pigment Epithelial Cells Required to Establish a Confluent Monolayer In Vitro. *Curr. Eye Res.* **17**, 962-969.
- 236 Ma, J. X., Zhang, J., Othersen, K. L., Moiseyev, G., Ablonczy, Z., Redmond, T. M., et al. (2001). Expression, Purification and MALDI Analysis of RPE65. *Invest. Ophthalmol. Vis. Sci.* **42**, 1429-1435.
- 237 Rose, M. T., Aso, H., Yonekura, S., Komatsu, T., Hagino, A., Ozutsumi, K. and Obara, Y. (2002). In Vitro Differentiation of a Cloned Bovine Mammary Epithelial Cell. *J. Dairy Res.* **69**, 345-355.
- 238 Tezel, T. H. and Del Priore, L. V. (1998). Serum-Free Media for Culturing and Serial-Passaging of Adult Human Retinal Pigment Epithelium. *Exp. Eye Res.* **66**, 807-815.
- 239 Hamel, C. P., Tsilou, E., Pfeiffer, B. A., Hooks, J. J., Detrick, R. and Redmond, T. M. (1993). Molecular Cloning and Expression of RPE65, A Novel Retinal Pigment Epithelium-Specific Microsomal Protein That is Post-Transcriptionally Regulated In Vitro. *J. Biol. Chem.* **268**, 15751-15757.
- 240 Alge, C. S., Suppmann, S., Priglinger, S. G., Neubauer, A. S., May, C. A., Hauck, S., et al. (2003). Comparative Proteome Analysis of Native Differentiated and Cultured Dedifferentiated Human RPE Cells. *Invest. Ophthalmol. Vis. Sci.* **44**, 3629-3641.
- 241 Kaida, M., Cao, F., Skumatz, C. B., Irving, P. E. and Burke, J. M. (2000). Time at Confluence for Human RPE Cells: Effects on the Adherens Junction and In Vitro Wound Closure. *Invest. Ophthalmol. Vis. Sci.* **41**, 3215-3224.

- 242 Ban, Y. and Rizzolo, L. J. (1997). A Culture Model of Development Reveals Multiple Properties of RPE Tight Junctions. *Mol. Vis.* **3**, 1-9.
- 243 Van der Velden, L. A., Schaafsma, H. E., Manni, J. J., Ramaekers, F. C. and Kuijpers, W. (1993). Cytokeratin Expression in Normal and (Pre)Malignant Head and Neck Epithelia: An Overview. *Head and Neck.* **15**, 133-146.
- 244 Bonnet, A., Thevenon, S., Claro, F., Gautier, M. and Hayes, H. (2001). Cytogenetic Comparison Between Vietnamese Sika Deer and Cattle: R-Banded Karyotypes and FISH Mapping. *Chromosome Research.* **9**, 673-687.
- 245 Pihan, G. and Doxsey, S. J. (2003). Mutations and Aneuploidy: Co-conspirators in Cancer? *Cancer Cell.* **4**, 89-94.
- 246 McCormick, J. J. and Maher, V. M. (1989). Malignant Transformation of Mammalian Cells in Culture, Including Human Cells. *Env. Mol Mutagenesis.* **14**, 105-113.
- 247 Stoker, M. G. and Rubin, H. (1967). Density-Dependent Inhibition of Cell Growth in Culture. *Nature.* **215**, 171-172.
- 248 Katz, M. L. and Robinson, W. G. (1985). Nutritional Influences on Autooxidation, Lipofuscin Accumulation and Aging: In *Free Radicals, Aging and Degenerative Diseases.* (Johnson, J.E., Walford, R. Harman, D. and Miquel, J., Eds.). Pp. 211-259. Alan R. Liss: New York.
- 249 Spaide, R. F. (2003). Fundus Autofluorescence and Age-Related Macular Degeneration. *Ophthalmol.* **110**, 392-399.
- 250 Eldred, G. E. (1987). Questioning the Nature of the Fluorophores in Age Pigments. *Adv. Biosci.* **64**, 23-36.
- 251 Pawlak, A., Rozanowska, M., Zareba, M., Lamb, L. E., Simon, J. D. and Sarna, T. (2002). Action Spectra for the Photoconsumption of Oxygen by Human Ocular Lipofuscin and Lipofuscin Extracts. *Arch. Biochem. Biophys.* **403**, 59-62.
- 252 Ragauskaite, L., Heckathorn, R. C. and Gaillard, E. R. (2001). Environmental Effects on the Photochemistry of A2-E, a Component of Human Retinal Lipofuscin. *Photochem. Photobiol.* **74**, 483-488.

- 253 Lamb, L. E., Ye, T., Haralampus-Grynawski, N., Williams, T. R., Pawlak, A., Sama, T. and Simon, J. D. (2001). The Primary Photophysical Properties of A2E in Solution. *J. Phys. Chem.* **105**, 11507-11512.
- 254 Barrett, K. L., Willingham, J. M., Garvin, A. J. and Willingham, M. C. (2001). Advances in Cytochemical Methods for Detection of Apoptosis. *J. Histochemistry and Cytochemistry.* **49**, 821-832.
- 255 Ben-Shabat, S., Parish, C. A., Vollmer, H. R., Itagaki, Y., Fishkin, N., Nakanishi, K. and Sparrow, J. R. (2002). Biosynthetic Studies of A2E, a Major Fluorophore of Retinal Pigment Epithelial Lipofuscin. *J. Biol. Chem.* **277**, 7183-7190.
- 256 Suoto, M. L., Borhan, B. and Nakanishi, K. (2000). Low-Temperature Photoaffinity Labeling of Rhodopsin and Intermediates Along Transduction Pathways. *Meth. Enzymol.* **316**, 425-435.
- 257 Schoneich, C. (2005). Mass Spectrometry in Aging Research. *Mass Spectrometry Reviews.* **24**, 701-708.
- 258 Chance, M. R., Sclavi, B., Woodson, S. A. and Brenowitz, M. (1997). Examining the Conformational Dynamics of Macromolecules with Time-Resolved Synchrotron X-Ray 'Footprinting.' *Structure.* **5**, 865-869.

APPENDIX

MISCELLANEOUS FIGURES

Figure A.1: Blast II alignment of the plasmid sequence (**bold**) compared to the expected sequence of pGene/ABCR/ENT/V5/His.

cccacccccagaatagaatgacacactactcagacaatgcgatgcaatttcctcatttta
 |||
 cccacccccagaatagaatgacacactactcagacaatgcgatgcaatttcctcatttta

ttaggaaaggacagtgggagtggcaccttccagggtcaaggaaggcacgggggaggggca
 |||
 ttaggaaaggacagtgggagtggcaccttccagggtcaaggaaggcacgggggaggggca

aacaacagatggctggcaactagaaggcacagtgcaggctgatcagcgggtttaaactca
 |||
 aacaacagatggctggcaactagaaggcacagtgcaggctgatcagcgggtttaaactca

atggtgatggtgatgatgaccggtacgcgtagaatcgagaccgaggagaggggttagggat
 |||
 atggtgatggtgatgatgaccggtacgcgtagaatcgagaccgaggagaggggttagggat

aggcttacctcgaatgggtgacctcgagcggccgctttatcatcatcatcctgggcttg
 |||
 aggcttacctcgaatgggtgacctcgagcggccgctttatcatcatcatcctgggcttg

tcgactggctccagcagctcgagggtgcagagggaggtcatgactttcagtctgctgtt
 |||
 tcgactggctccagcagctcgagggtgcagagggaggtcatgactttcagtctgctgtt

agcaaaatttacaacacctgggtccagtggtctgtgtgactgagtactcctcgatgag
 |||
 agcaaaatttacaacacctgggtccagtggtctgtgtgactgagtactcctcgatgag

caggctgtccttgtgggagaggaggagctggaagatcctcgccagggaggaggaggagac
 |||
 caggctgtccttgtgggagaggaggagctggaagatcctcgccagggaggaggaggagac

ctggaactggagcatgtttagtgacctctcctctgcacactgcctgggaagtccccctg
 |||
 ctggaactggagcatgtttagtgacctctcctctgcacactgcctgggaagtccccctg

gaagaactgctccacaggggttcagggtcaggaagcaggtcntccttcggggatttgatctt
 |||
 gaagaactgctccacaggggttcagggtcaggaagcaggtcgtccttcggggatttgatctt

cnttgtgacnntagcncctcc
 | ||||| || ||||| |||||
 cattgtgacgatatagccatctcc

Figure A.2: MACAW alignment comparing the sequenced nucleotides to the expected sequence. Alignment was using the sequences with the primers EGFP-F (Seq1), EGFP-R (Seq2), EGFP-SF (Seq3), EGFP-SR (Seq4) to the expected sequence of pGene/ABCR/ENT/RSGFP/His (pGene).

pGene TATCGTCACAATGAAGATCAAATCCCCGAAGGACGACCTGCTTCCTGACCTGAACCCTGT
 Seq1
 Seq2
 Seq3
 Seq4 TATCGTCACAATGAAGATCAAATCCCCGAAGGACGACATGCTTCCTGACCTGAACCCTGT

pGene GGAGCAGTTCTTCCAGGGGAACTTCCCAGGCAGTGTGCAGAGGGAGAGGCACTACAACAT
 Seq1
 Seq2
 Seq3
 Seq4 GGAGCAGTTCTTCCAGGGGAACTTCCCAGGCAGTGTGCAGAGGGAGAGGCACTACAACAT

pGene GCTCCAGTTCCAGGTCTCCTCCTCCTCCCTGGCGAGGATCTTCCAGCTCCTCCTCTCCCA
 Seq1
 Seq2
 Seq3
 Seq4 GCTCCAGTTCCAGGTCTCCTCCTCCTCCCTGGCGAGGATCTTCCAGCTCCTCCTCTCCCA

pGene CAAGGACAGCCTGCTCATCGAGGAGTACTCAGTCACACAGACCACACTGGACCAGGTGTT
 Seq1
 Seq2
 Seq3
 Seq4 CAAGGACAGCCTGCTCATCGAGGAGTACTCAGTCACACAGACCACACTGGACCAGGTGTT

pGene TGTAATTTTTGCTAAACAGCAGACTGAAAGTCATGACCTCCCTCTGCACCCTCGAGCTGC
 Seq1
 Seq2
 Seq3
 Seq4 TGTAATTTTTGCTAAACAGCAGACTGAAAGTCATGACCTCCCTCTGCACCCTCGAGCTGC

pGene TGGAGCCAGTCGACAAGCCCAGGATGATGATGATAAAGCGGCCGCAAGTAAAGGAGAAGA
 Seq1 TGGAGCCAGTTAACAAGCC ACGATGAAGAATATAAAGGGGCCCCAGGTAAGGAGAAGA
 Seq2
 Seq3
 Seq4 TGGAGCCAGTCGACAAGCCCAGGATGATGATGATAAAGCGGCCGCAAGTAAAGGAGAAGA

pGene ACTTTTCACTGGAGTTG TCCCAATTCTTG TTGAATTAGATGG TGATGTTAATGGG C
 Seq1 ACTTTTCACTGGAGGTGGTCCCAATTCTTGTTGAATTAGATGGGTGATGTTAATGGGGC
 Seq2 TTCTTG TTGAATTAGATGG TGATGTTAATGGG C
 Seq3
 Seq4 ACTTTTCACTGGAGTTG TCCCAATTCTTG TTGAATTAGATGG TGATGTTAATGGG C

pGene ACAAATTTTCTGTCA GTGGAGAGGGTGAAGGTGATGCAACATACGGAAAACCTTACCCTT
 Seq1 ACAAATTTTCTGTCAAGTGGAGAGGGTGAAGGTGATGCAACATACGGAAAACCTTACCCTT
 Seq2 ACAAATTTTCTGTCA GTGGAGAGGGTGAAGGTGATGCAACATACGGAAAACCTTACCCTT
 Seq3
 Seq4 ACAAATTTTCTGTCA GTGGAGAGGGTGAAGGTGATGCAACATACGGAAAACCTTACCCTT

pGene AAATTTATTTGCACTACTGGAAAACCTACCTGTTCCATGGCCAACACTTGTCACTACTTTC
 Seq1 ACATTTATTTGCACTACTGGAAAACCTACCTGTTCCATGGCCCACACTTGTCACTACTTTC
 Seq2 AAATTTATTTGCACTACTGGAAAACCTACCTGTTCCATGGCCAACACTTGTCACTACTTTC
 Seq3
 Seq4 AAATTTATTTGCACTACTGGAAAACCTACCTGTTCCATGGCCAACACTTGTCACTACTTTC

pGene ACTTATGGTGTTC AATGCTTTTCAAGATACCCAGATCATATGAAGCGGCACGACTTCTTC
 Seq1 ACTTATGGTGTTC AATGCTTTTCAAGATACCCAGATCATATGAAGCGGCACGACTTCTTC
 Seq2 ACTTATGGTGTTC AATGCTTTTCAAGATACCCAGATCATATGAAGCGGCACGACTTCTTC
 Seq3
 Seq4 ACTTATGGTGTTC AATGCTTTTCAAGATACCCAGATCATATGAAGCGGCACGACTTCTTC

pGene AAGAGCGCCATGCCTGAGGGATACGTGCAGGAGAGGACCATCTCTTTCAAGGACGACGGG
 Seq1 AAGAGCGCCATGCCTGAGGGATACGTGCAGGAGAGGACCATCTCTTTCAAGGACGACGGG
 Seq2 AAGAGCGCCATGCCTGAGGGATACGTGCAGGAGAGGACCATCTCTTTCAAGGACGACGGG
 Seq3
 Seq4 AAGAGCGCCATGCCTGAGGGATACGTGCAGGAGAGGACCATCTCTTT

pGene AACTACAAGACACGTGCTGAAGTCAAGTTTGAGGGAGACACCCCTCGTCAACAGGATCGAG
 Seq1 AACTACAAGACACGTGCTGAAGTCAAGTTTGAGGGAGACACCCCTCGTCAACAGGATCGAG
 Seq2 AACTACAAGACACGTGCTGAAGTCAAGTTTGAGGGAGACACCCCTCGTCAACAGGATCGAG
 Seq3
 Seq4

pGene CTTAAGGGAATCGATTTCAAGGAGGACGGAAACATCCTCGGCCACAAGTTGGAATACAAC
 Seq1 CTTAAGGGAATCGATTTCAAGGAGGACGGAAACATCCTCGGCCACAAGTTGGAATACAAC
 Seq2 CTTAAGGGAATCGATTTCAAGGAGGACGGAAACATCCTCGGCCACAAGTAGGAATACAAC
 Seq3 GAAACATCCTCGGCCACAAGTTGGAATACAAC
 Seq4

pGene TACAAC TCCACAACGTATACATCACGGCAGACAAAACAAAAGAA TGAATCAAAGCTAAC
 Seq1 TACAAC TCCACAACGTATACATCACGGCAGACAAAACAAAAGAA TGAATCAAAGCTAAC
 Seq2 TACAAC TCCACAACGTATACATCACGGCAGACAAAACAAAAGAA TGAATCAAAGCTAAC
 Seq3 TACAAC TCCACAACGTATACATCACGGCAGACAAAACAAAAGAA TGAATCAAAGCTAAC
 Seq4

pGene TTCAAAAT TAGACACAACAT TGAAGATGGAAGCGTTCAACTAGCAGACCAT TATCAACAA
 Seq1 TTCAAAAT TAGACACAACAT TGAAGATGGAAGCGTTCAACTAGCAGACCAT TATCAACAA
 Seq2 TTCAAAAT TAGACACAACAT TGAAGATGGAAGCGTTCAACTAGCAGACCAT TATCAACAA
 Seq3 TTCAAAAT TAGACACAACAT TGAAGATGGAAGCGTTCAACTAGCAGACCAT TATCAACAA
 Seq4

pGene AATACTCCAAT TGGCGATGGCCCTGTCTTTTACCAGACAACCAT TACCTGTCCACACAA
 Seq1 AATACTCCAAT TGGCGATGGCCCTGTCTTTTACCAGACAACCAT TACCTGTCCACACAA
 Seq2 AATACTCCAAT TGGCGATGGCCCTGTCTTTTACCAGACAACCAT TACCTGTCCACACAA
 Seq3 AATACTCCAAT TGGCGATGGCCCTGTCTTTTACCAGACAACCAT TACCTGTCCACACAA
 Seq4

pGene TCTGCCC TTTCGAAAGATCCCAACGAAAAGAGAGACCACATGG TCCTTCTTGAGTTTG
 Seq1 TCTGCCC TTTCGAAAGATCCCAACGAAAAGAGAGACCACATGG TCCTTCTTGAGTTTG
 Seq2 TCTGCCCATATCGAAAGATCCCAACGAAAAGAGAGAACACATGGGTCCTTCTTGAGTTTG
 Seq3 TCTGCCC TTTCGAAAGATCCCAACGAAAAGAGAGACCACATGG TCCTTCTTGAGTTTG
 Seq4

pGene TAACAGCTGCTGGGATTACACATGGCATGGATGAACTATACAAAACCGGTCATCATCACC
 Seq1 TAACA
 Seq2 TAACAGCTGCTGGGA TACACATGCCATGAATGACCAATAC AAACCGGTCATCATCA C
 Seq3 TAACAGCTGCTGGGATTACACATGCCATGGATGAACTATACAAAACCGGTCATCATCACC
 Seq4

pGene ATCACCATTGAGTTTAAACCCGCTGATCAGCCTCGACTGTGCCTTCTAGTTGCCAGCCAT
 Seq1
 Seq2 ATC CCATTGA ATTAACCCCGCTGATCA CCCCAGCTGTGCCT
 Seq3 ATCACCATTGAGTTTAAACCCGCTGATCAGCCTCGACTGTGCCTTCTAGTTGCCAGCCAT
 Seq4

pGene CTGTTGTTTGCCCTCCCCCGTGCCTTCCCTTGACCCTGGAAGGTGCCACTCCCAGTCC
 Seq1
 Seq2
 Seq3 CTGTTGTTTGCCCTCCCCCGTGCCTTCCCTTGACCCTGGAAGGTGCCACTCCCAGTCC
 Seq4

pGene TTTCTAATAAAATGAGGAAATGCATCGCATTGTCTGAGTAGGTGTCATTCTATTCTGG
 Seq1
 Seq2
 Seq3 TTTCTAATAAAATGAGGAAATGCATCGCATTGTCTGAGTAGGTGTCATTCTATTCTGG
 Seq4

pGene GGGGTGGGG TGGGGCAGGACAGCAAGGGGG AGGATTGGGAAGACAATAGCAGGCATGC
 Seq1
 Seq2
 Seq3 GGGGTGGGGGTGGGGCAGGACAGCAAGGGGGGAAGATTGGGAAGACAATAGCAGGCATGC
 Seq4

pGene TGGGGATGCGGTGGGCTCTATGGCTTCTGAGGCGGAAAGAACCAGCTGGGGCTCTAGGGG
 Seq1
 Seq2
 Seq3 TGGGGATGCGGTGGGCTCTATGGCTTCTGAGGCGGAAAGAAC AGCTGGGGCTCTAGGGG
 Seq4

pGene GTATCCCCACGCGCCCTGTAGCGGCGCATTAAAGCGCGGC GGGT
 Seq1
 Seq2
 Seq3 GTATCCCCACGCGCCCTGTAGCGGCGCATTAAAGCGGCGCGGGT
 Seq4